PTEP

Prog. Theor. Exp. Phys. **2020**, 05A103 (68 pages)
DOI: 10.1093/ptep/ptaa120

Overview of KAGRA: KAGRA science

KAGRA Collaboration

T. Akutsu[1,2], M. Ando[1,3,4], K. Arai[5], Y. Arai[5], S. Araki[6], A. Araya[7], N. Aritomi[3], H. Asada[8], Y. Aso[9,10], S. Bae[11], Y. Bae[12], L. Baiotti[13], R. Bajpai[14], M. A. Barton[1], K. Cannon[4], Z. Cao[15], E. Capocasa[1], M. Chan[16], C. Chen[17,18], K. Chen[19], Y. Chen[18], C.-Y. Chiang[20], H. Chu[19], Y.-K. Chu[20], S. Eguchi[16], Y. Enomoto[3], R. Flaminio[1,21], Y. Fujii[22], F. Fujikawa[23], M. Fukunaga[5], M. Fukushima[2], D. Gao[24], G. Ge[24], S. Ha[25], A. Hagiwara[5,26], S. Haino[20], W.-B. Han[27], K. Hasegawa[5], K. Hattori[28], H. Hayakawa[29], K. Hayama[16], Y. Himemoto[30], Y. Hiranuma[31], N. Hirata[1], E. Hirose[5], Z. Hong[32], B. H. Hsieh[5], C.-Z. Huang[32], H.-Y. Huang[20], P. Huang[24], Y. Huang[20], Y.-C. Huang[18], D. C. Y. Hui[33], S. Ide[34], B. Ikenoue[2], S. Imam[32], K. Inayoshi[35], Y. Inoue[19], K. Ioka[36], K. Ito[37], Y. Itoh[38,39], K. Izumi[40], C. Jeon[41], H.-B. Jin[42,43], K. Jung[25], P. Jung[29], K. Kaihotsu[37], T. Kajita[44], M. Kakizaki[28], M. Kamiizumi[29], N. Kanda[38,39], G. Kang[11], K. Kashiyama[4], K. Kawaguchi[5], N. Kawai[45], T. Kawasaki[3], C. Kim[41], J. Kim[46], J. C. Kim[47], W. S. Kim[12], Y.-M. Kim[25], N. Kimura[26], N. Kita[3], H. Kitazawa[37], Y. Kojima[48], K. Kokeyama[29], K. Komori[3], A. K. H. Kong[18], K. Kotake[16], C. Kozakai[9], R. Kozu[49], R. Kumar[50], J. Kume[4], C. Kuo[19], H.-S. Kuo[32], Y. Kuromiya[37], S. Kuroyanagi[51], K. Kusayanagi[45], K. Kwak[25], H. K. Lee[52], H. W. Lee[47], R. Lee[18], M. Leonardi[1], K. L. Li[18], T. G. F. Li[73], C.-Y. Lin[53], F.-K. Lin[20], F.-L. Lin[32], H. L. Lin[19], L. C.-C. Lin[25], G. C. Liu[17], L.-W. Luo[20], E. Majorana[54], M. Marchio[1], Y. Michimura[3], N. Mio[55], O. Miyakawa[29], A. Miyamoto[38], Y. Miyazaki[3], K. Miyo[29], S. Miyoki[29], Y. Mori[37], S. Morisaki[5], Y. Moriwaki[28], K. Nagano[40], S. Nagano[56], K. Nakamura[1], H. Nakano[57], M. Nakano[5,28], R. Nakashima[45], Y. Nakayama[28], T. Narikawa[5], L. Naticchioni[54], R. Negishi[31], L. Nguyen Quynh[58], W.-T. Ni[24,42,59], A. Nishizawa[4,*], S. Nozaki[28], Y. Obuchi[2], W. Ogaki[5], J. J. Oh[12], K. Oh[33], S. H. Oh[12], M. Ohashi[29], N. Ohishi[9], M. Ohkawa[23], H. Ohta[4], Y. Okutani[34], K. Okutomi[29], K. Oohara[31], C. P. Ooi[3], S. Oshino[29], S. Otabe[45], K. Pan[18], H. Pang[19], A. Parisi[17], J. Park[1], F. E. Peña Arellano[29], I. Pinto[60], N. Sago[61], S. Saito[2], Y. Saito[29], K. Sakai[62], Y. Sakai[31], Y. Sakuno[16], S. Sato[63], T. Sato[23], T. Sawada[38], T. Sekiguchi[4], Y. Sekiguchi[64], L. Shao[35], S. Shibagaki[16], R. Shimizu[2], T. Shimoda[3], K. Shimode[29], H. Shinkai[65], T. Shishido[10], A. Shoda[1], K. Somiya[45], E. J. Son[12], H. Sotani[66], R. Sugimoto[37,40], J. Suresh[5], T. Suzuki[23], T. Suzuki[5], H. Tagoshi[5], H. Takahashi[67], R. Takahashi[1], A. Takamori[7], S. Takano[3], H. Takeda[3], M. Takeda[38], H. Tanaka[68], K. Tanaka[38], K. Tanaka[68], T. Tanaka[5], T. Tanaka[69], S. Tanioka[1,10], E. N. Tapia San Martin[1], S. Telada[70], T. Tomaru[1], Y. Tomigami[38], T. Tomura[29], F. Travasso[71,72], L. Trozzo[29], T. Tsang[73], J.-S. Tsao[32], K. Tsubono[3], S. Tsuchida[38], D. Tsuna[4], T. Tsutsui[4], T. Tsuzuki[2], D. Tuyenbayev[20], N. Uchikata[5], T. Uchiyama[29], A. Ueda[26], T. Uehara[74,75], K. Ueno[4], G. Ueshima[67], F. Uraguchi[2], T. Ushiba[5], M. H. P. M. van Putten[76], H. Vocca[72], J. Wang[24], T. Washimi[1], C. Wu[18], H. Wu[18], S. Wu[18], W.-R. Xu[32], T. Yamada[68], K. Yamamoto[28], K. Yamamoto[68], T. Yamamoto[29], K. Yamashita[28], R. Yamazaki[34], Y. Yang[77], K. Yokogawa[37], J. Yokoyama[4,3], T. Yokozawa[29], T. Yoshioka[37], H. Yuzurihara[5], S. Zeidler[78], M. Zhan[24], H. Zhang[32], Y. Zhao[1], and Z.-H. Zhu[15]

[1] *Gravitational Wave Science Project, National Astronomical Observatory of Japan (NAOJ), Mitaka City, Tokyo 181-8588, Japan*

[2]*Advanced Technology Center, National Astronomical Observatory of Japan (NAOJ), Mitaka City, Tokyo 181-8588, Japan*
[3]*Department of Physics, The University of Tokyo, Bunkyo-ku, Tokyo 113-0033, Japan*
[4]*Research Center for the Early Universe (RESCEU), The University of Tokyo, Bunkyo-ku, Tokyo 113-0033, Japan*
[5]*Institute for Cosmic Ray Research (ICRR), KAGRA Observatory, The University of Tokyo, Kashiwa City, Chiba 277-8582, Japan*
[6]*Accelerator Laboratory, High Energy Accelerator Research Organization (KEK), Tsukuba City, Ibaraki 305-0801, Japan*
[7]*Earthquake Research Institute, The University of Tokyo, Bunkyo-ku, Tokyo 113-0032, Japan*
[8]*Department of Mathematics and Physics, Hirosaki University, Hirosaki City, Aomori 036-8561, Japan*
[9]*Kamioka Branch, National Astronomical Observatory of Japan (NAOJ), Kamioka-cho, Hida City, Gifu 506-1205, Japan*
[10]*The Graduate University for Advanced Studies (SOKENDAI), Mitaka City, Tokyo 181-8588, Japan*
[11]*Korea Institute of Science and Technology Information (KISTI), Yuseong-gu, Daejeon 34141, Korea*
[12]*National Institute for Mathematical Sciences, Daejeon 34047, Korea*
[13]*International College, Osaka University, Toyonaka City, Osaka 560-0043, Japan*
[14]*School of High Energy Accelerator Science, The Graduate University for Advanced Studies (SOKENDAI), Tsukuba City, Ibaraki 305-0801, Japan*
[15]*Department of Astronomy, Beijing Normal University, Beijing 100875, China*
[16]*Department of Applied Physics, Fukuoka University, Jonan, Fukuoka City, Fukuoka 814-0180, Japan*
[17]*Department of Physics, Tamkang University, Danshui Dist., New Taipei City 25137, Taiwan*
[18]*Department of Physics and Institute of Astronomy, National Tsing Hua University, Hsinchu 30013, Taiwan*
[19]*Department of Physics, Center for High Energy and High Field Physics, National Central University, Zhongli District, Taoyuan City 32001, Taiwan*
[20]*Institute of Physics, Academia Sinica, Nankang, Taipei 11529, Taiwan*
[21]*Université Grenoble Alpes, Laboratoire d'Annecy de Physique des Particules (LAPP), Université Savoie Mont Blanc, CNRS/IN2P3, F-74941 Annecy, France*
[22]*Department of Astronomy, The University of Tokyo, Mitaka City, Tokyo 181-8588, Japan*
[23]*Faculty of Engineering, Niigata University, Nishi-ku, Niigata City, Niigata 950-2181, Japan*
[24]*State Key Laboratory of Magnetic Resonance and Atomic and Molecular Physics, Innovation Academy for Precision Measurement Science and Technology (APM), Chinese Academy of Sciences, Xiao Hong Shan, Wuhan 430071, China*
[25]*Department of Physics, School of Natural Science, Ulsan National Institute of Science and Technology (UNIST), Ulsan 44919, Korea*
[26]*Applied Research Laboratory, High Energy Accelerator Research Organization (KEK), Tsukuba City, Ibaraki 305-0801, Japan*
[27]*Chinese Academy of Sciences, Shanghai Astronomical Observatory, Shanghai 200030, China*
[28]*Faculty of Science, University of Toyama, Toyama City, Toyama 930-8555, Japan*
[29]*Institute for Cosmic Ray Research (ICRR), KAGRA Observatory, The University of Tokyo, Kamioka-cho, Hida City, Gifu 506-1205, Japan*
[30]*College of Industrial Technology, Nihon University, Narashino City, Chiba 275-8575, Japan*
[31]*Graduate School of Science and Technology, Niigata University, Nishi-ku, Niigata City, Niigata 950-2181, Japan*
[32]*Department of Physics, National Taiwan Normal University, Sec. 4, Taipei 116, Taiwan*
[33]*Astronomy & Space Science, Chungnam National University, 9 Daehak-ro, Yuseong-gu, Daejeon 34134, Korea, Korea*
[34]*Department of Physics and Mathematics, Aoyama Gakuin University, Sagamihara City, Kanagawa 252-5258, Japan*
[35]*Kavli Institute for Astronomy and Astrophysics, Peking University, Yiheyuan Road 5, Haidian District, Beijing 100871, China*
[36]*Yukawa Institute for Theoretical Physics (YITP), Kyoto University, Sakyou-ku, Kyoto City, Kyoto 606-8502, Japan*
[37]*Graduate School of Science and Engineering, University of Toyama, Toyama City, Toyama 930-8555, Japan*

[38]*Department of Physics, Graduate School of Science, Osaka City University, Sumiyoshi-ku, Osaka City, Osaka 558-8585, Japan*
[39]*Nambu Yoichiro Institute of Theoretical and Experimental Physics (NITEP), Osaka City University, Sumiyoshi-ku, Osaka City, Osaka 558-8585, Japan*
[40]*Institute of Space and Astronautical Science (JAXA), Chuo-ku, Sagamihara City, Kanagawa 252-0222, Japan*
[41]*Department of Physics, Ewha Womans University, Seodaemun-gu, Seoul 03760, Korea*
[42]*National Astronomical Observatories, Chinese Academic of Sciences, 20A Datun Road, Chaoyang District, Beijing, China*
[43]*School of Astronomy and Space Science, University of Chinese Academy of Sciences, 20A Datun Road, Chaoyang District, Beijing, China*
[44]*Institute for Cosmic Ray Research (ICRR), The University of Tokyo, Kashiwa City, Chiba 277-8582, Japan*
[45]*Graduate School of Science and Technology, Tokyo Institute of Technology, Meguro-ku, Tokyo 152-8551, Japan*
[46]*Department of Physics, Myongji University, Yongin 17058, Korea*
[47]*Department of Computer Simulation, Inje University, Gimhae, Gyeongsangnam-do 50834, Korea*
[48]*Department of Physical Science, Hiroshima University, Higashihiroshima City, Hiroshima 903-0213, Japan*
[49]*Institute for Cosmic Ray Research (ICRR), Research Center for Cosmic Neutrinos (RCCN), The University of Tokyo, Kamioka-cho, Hida City, Gifu 506-1205, Japan*
[50]*California Institute of Technology, Pasadena, CA 91125, USA*
[51]*Institute for Advanced Research, Nagoya University, Furocho, Chikusa-ku, Nagoya City, Aichi 464-8602, Japan*
[52]*Department of Physics, Hanyang University, Seoul 133-791, Korea*
[53]*National Center for High-performance computing, National Applied Research Laboratories, Hsinchu Science Park, Hsinchu City 30076, Taiwan*
[54]*Istituto Nazionale di Fisica Nucleare (INFN), Sapienza University, Roma 00185, Italy*
[55]*Institute for Photon Science and Technology, The University of Tokyo, Bunkyo-ku, Tokyo 113-8656, Japan*
[56]*The Applied Electromagnetic Research Institute, National Institute of Information and Communications Technology (NICT), Koganei City, Tokyo 184-8795, Japan*
[57]*Faculty of Law, Ryukoku University, Fushimi-ku, Kyoto City, Kyoto 612-8577, Japan*
[58]*Department of Physics, University of Notre Dame, Notre Dame, IN 46556, USA*
[59]*Department of Physics, National Tsing Hua University, Hsinchu 30013, Taiwan*
[60]*Department of Engineering, University of Sannio, Benevento 82100, Italy*
[61]*Faculty of Arts and Science, Kyushu University, Nishi-ku, Fukuoka City, Fukuoka 819-0395, Japan*
[62]*Department of Electronic Control Engineering, National Institute of Technology, Nagaoka College, Nagaoka City, Niigata 940-8532, Japan*
[63]*Graduate School of Science and Engineering, Hosei University, Koganei City, Tokyo 184-8584, Japan*
[64]*Faculty of Science, Toho University, Funabashi City, Chiba 274-8510, Japan*
[65]*Faculty of Information Science and Technology, Osaka Institute of Technology, Hirakata City, Osaka 573-0196, Japan*
[66]*iTHEMS (Interdisciplinary Theoretical and Mathematical Sciences Program), The Institute of Physical and Chemical Research (RIKEN), Wako, Saitama 351-0198, Japan*
[67]*Department of Information and Management Systems Engineering, Nagaoka University of Technology, Nagaoka City, Niigata 940-2188, Japan*
[68]*Institute for Cosmic Ray Research (ICRR), Research Center for Cosmic Neutrinos (RCCN), The University of Tokyo, Kashiwa City, Chiba 277-8582, Japan*
[69]*Department of Physics, Kyoto University, Sakyou-ku, Kyoto City, Kyoto 606-8502, Japan*
[70]*National Metrology Institute of Japan, National Institute of Advanced Industrial Science and Technology, Tsukuba City, Ibaraki 305-8568, Japan*
[71]*University of Camerino, via Madonna delle Carderi 9, 62032 Camerino (MC), Italy*
[72]*Istituto Nazionale di Fisica Nucleare, University of Perugia, Perugia 06123, Italy*
[73]*Faculty of Science, Department of Physics, The Chinese University of Hong Kong, Shatin, N.T., Hong Kong*
[74]*Department of Communications, National Defense Academy of Japan, Yokosuka City, Kanagawa 239-8686, Japan*
[75]*Department of Physics, University of Florida, Gainesville, FL 32611, USA*
[76]*Department of Physics and Astronomy, Sejong University, Gwangjin-gu, Seoul 143-747, Korea*
[77]*Department of Electrophysics, National Chiao Tung University, 101 Univ. Street, Hsinchu, Taiwan*
[78]*Department of Physics, Rikkyo University, Toshima-ku, Tokyo 171-8501, Japan*
*Email: anishi@resceu.s.u-tokyo.ac.jp

Received April 12, 2020; Revised July 31, 2020; Accepted July 31, 2020; Published Month 00, 0000

KAGRA is a newly build gravitational wave observatory, a laser interferometer with 3 km arm length, located in Kamioka, Gifu, Japan. In this paper, one of a series of articles featuring KAGRA, we discuss the science targets of KAGRA projects, considering not only the baseline KAGRA (current design) but also its future upgrade candidates (KAGRA+) for the near to middle term (∼5 years).

Subject Index E02

1. Introduction

Advanced LIGO (aLIGO) [1] and advanced Virgo (AdV) [2] have detected gravitational waves (GWs) from 10 mergers of binary black holes (BBHs) [3] and one merger of binary neutron stars (BNSs) [4] in the O1 and O2 observing run[1]. The observations of these GW events have broadened many science opportunities: the astrophysical formation scenarios of BBH and BNS, the emission mechanisms of short gamma-ray bursts (sGRBs) and the following electromagnetic (EM) counterparts associated with BNS mergers, the equation of state (EOS) of a neutron star (NS), measurement of the Hubble constant, the tests of gravity, the no-hair theorem of a black hole (BH) and so on. In addition to these topics studied based on the observational data, there are still several sources of GWs to be observed in the future with ground-based detectors, such as those from supernovae, isolated NSs, intermediate-mass BHs, and the early Universe.

It is planned that the instruments of the current ground-based detectors, aLIGO and AdV, will start to be upgraded around 2024 right after the O4 observation ends to improve their sensitivities (called A+ [5] and AdV+ [6], respectively) [7]. KAGRA [8] will also be upgraded in the same term as aLIGO and AdV, though a concrete upgrade plan has not yet been decided officially. In this paper, one of a series of articles featuring KAGRA, we review the scientific cases available with the second-generation ground-based detectors, including aLIGO, AdV, and the baseline KAGRA (bKAGRA), and their future upgrades, A+, AdV+, and KAGRA+, respectively, and discuss KAGRA's scientific contributions to the global detector networks composed of the detectors above. Since the official design of KAGRA+ has not been decided yet, we consider four possible upgrade options for the near to middle term (∼5 years): one focused on low frequencies (∼ 10–50 Hz, LF), one focused on high frequencies (∼ 300 Hz–5 kHz, HF), one using heavier mirrors to improve the middle frequencies (∼ 50–300 Hz, 40 kg), and one injecting frequency-dependent squeezing for broadband improvement (FDSQZ)[2]. In addition to these, we also consider a slightly optimistic case in which technologies for four KAGRA+ upgrades are combined (called Combined). The noise curves of bKAGRA and its upgrade candidates are shown in Fig. 1. More details on the concrete plans and technological aspects are discussed in a companion paper in the series [9].

[1] More GWs have been detected in the O3 observing run, but as of 27 July 2020 have not been published yet.

[2] We divide the frequencies into three ranges: low, middle, and high, depending on the shape of the noise curves in Fig. 1.

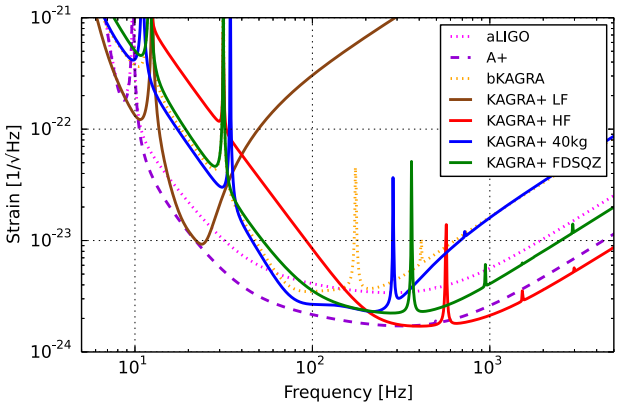

Fig. 1. Sensitivity curves for bKAGRA and upgrade candidates for KAGRA+. Sensitivity curves for aLIGO, A+, and bKAGRA are shown for comparison [10].

2. Stellar-mass binary black holes

2.1. Formation scenarios

2.1.1. Scientific objective

The existence of massive stellar-mass BBH provides us with new insight about the formation pathways of such heavy compact binaries [11,12]. Since massive stars likely lose their masses by stellar winds driven by metal lines, dust, and pulsations of the stellar surface, heavy BHs with masses of $\gtrsim 20\ M_\odot$ are not expected to be left as remnants at the end of the lifetime of massive stars with metallicity of the solar value [13]. In fact, the masses of the BHs that have ever been observed in EM waves (e.g., X-ray binaries) are significantly lower than those detected in GWs [3]. This fact motivates us to explore the astrophysical origin of such massive stellar-mass BBH populations in low-metallicity environments (below 50% of solar metallicity or possibly less) [13]. So far, a number of authors have proposed formation channels: the evolution of low-metallicity isolated binaries in the field [14–17], dynamical processes in dense cluster systems (globular clusters, nuclear stellar clusters, or compact gaseous disks in active galactic nuclei) [18–24], massive stars formed in extremely low-metallicity gas in the high-redshift Universe (Population III stars, hereafter Pop III stars) [25–28], etc. As an alternative non-astrophysical possibility, a primordial BH (PBH) population in the extremely early Universe (e.g., originating from phase transitions, a temporary softening in the EOS, quantum fluctuations) has been attracting attention [29,30] (see Ref. [31] for a review).

2.1.2. Observations and measurements

In order to reveal the astrophysical origin of stellar-mass BBHs detected by LIGO and Virgo, we need to explore the properties of coalescing BBHs, depending on their formation pathway and environment in which they form. In particular, the effective spin parameters of a BBH $\chi_{\rm eff}$ (the dimensionless spin components aligned or anti-aligned with the orbital angular momentum) are expected to be useful to discriminate the evolution models [32,33]. In the field binary scenario, concerning binaries formed in a galactic plane, tidal torque exerted on two stars (or one star and one BH) in a close binary transports the orbital angular momentum into stellar spins, resulting in $\chi_{\rm eff} \gtrsim 0$. Since tidal synchronization occurs as quickly as $\dot{\Omega} \propto (R_\star/a)^6$, a binary with a short GW coalescence timescale (i.e., a small orbital separation) would be significantly spun to $\chi_{\rm eff} \sim 1$. Since BBH populations formed at high redshift have a long GW coalescence timescale, their BBHs are hardly affected by tidal torque [34]. The underlying assumption is that the orbital angular momentum is not significantly

changed via natal kicks that newborn BHs could receive during the core collapse of their progenitors [35]. Although a strong natal kick $\gtrsim 500$ km s^{-1} is required to affect the effective spin parameter, observations of low-mass X-ray binaries show no evidence of such strong natal kicks of BHs (see, e.g., Ref. [36]).

On the other hand, in the dynamical formation scenario concerning binaries formed in dense stellar environments, the distribution of effective spin would be isotropic at $-1 \leq \chi_{\rm eff} \leq 1$, and negative values are allowed, unlike the isolated binary scenario, because the directions of stellar spins could be chosen randomly. As a robust result of the formation channel, the effective spin can have negative values at $-1 \lesssim \chi_{\rm eff} \lesssim 0$. Moreover, in the dynamical capture model, a small fraction of the binaries/BBHs could gain significantly high eccentricities ($e \gtrsim 0.1$), which will be imprinted in the GW waveform [19].

For PBHs formed in the early Universe (the radiation-dominated era), the spin is suppressed to $\chi_{\rm eff} \lesssim 0.4$ [37] or even smaller [38] because they are formed from the collapses of density inhomogeneities right after the cosmological horizon entry. However, if the early matter phase exists after inflation, the spin can be large [39]. Because of the uncertainty in the early-Universe scenario, it would be difficult to distinguish the PBH origin from astrophysical ones.

In addition to the BBH population within a detection horizon of $z \lesssim 0.2$, BBHs that coalesce at higher redshifts due to small initial separations are unresolved individually, but contribute to a GW background (GWB). The spectral shape of a GWB caused by compact binary mergers is characterized by a single-power law of $\Omega_{\rm GW} \propto f^{2/3}$ at lower frequencies ($f < f_0$), is flattened from it at $f \simeq f_0$, and has a cutoff at higher frequencies ($f > f_0$) [40]. Importantly, this result hardly depends on the merger history of the BBH population qualitatively. Therefore, a GWB produced from a low-redshift, relatively less massive BBH population is robustly given by $\Omega_{\rm GW} \propto f^{2/3}$ in the frequency range. This GWB signal could be detected by a future observing run O5 with aLIGO and AdV [41], as shown in Fig. 2. In fact, the spectral flattening occurs outside the GWB sensitive frequency range ($f_0 \gtrsim 100$ Hz). On the other hand, a GWB caused by merger events of the higher-redshift, massive

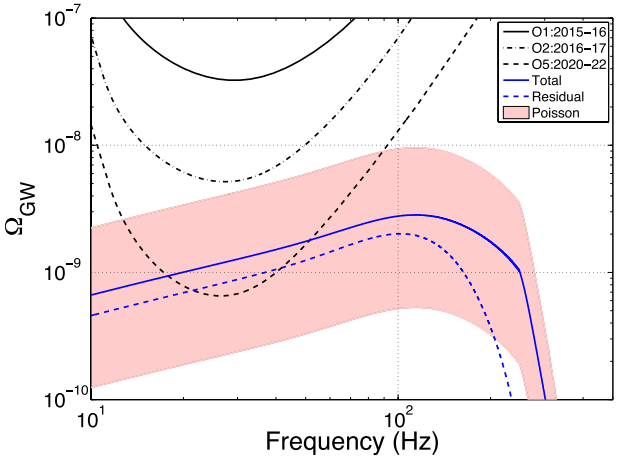

Fig. 2. Expected sensitivity of the network of aLIGO and AdV to a GWB from BBHs in the fiducial model in Ref. [41]. Energy density spectra are shown in blue (solid for the total background; dashed for the residual background, excluding resolved sources, assuming final aLIGO and AdV sensitivity). The pink shaded region, "Poisson", shows the 90% CL statistical uncertainty, propagated from the local rate measurement, on the total background. The black power-law integrated curves show the 1σ sensitivity of the network expected for the two first observing runs O1 and O2, and for 2 years at the design sensitivity in O5. Adapted from Ref. [41].

BBH population suggested by Pop III models is expected to be flattened at a lower frequency of $f_0 \simeq 30$ Hz [27], where LIGO/Virgo/KAGRA are the most sensitive. Detection of unique flattening at such low frequencies will indicate the existence of a high-chirp mass, high-redshift BBH population, which is consistent with a Pop III origin. A detailed study of the GWB would enable us to explore the properties of massive binary stars at higher redshift and in the epoch of cosmic reionization.

2.1.3. Future prospects

LIGO–Virgo's sensitivities during O1 and O2 have been proved to be efficient to detect stellar-mass BBHs with a mass range between $\mathcal{O}(1)$ and (100) [3]. The typical detection frequency of these stellar-mass BBHs is between 30 and 500 Hz. bKAGRA's sensitivity would be similar to aLIGO and AdV and we expect that the observable sample for bKAGRA would be similar to those listed in GWTC-1 [3], i.e., stellar-mass BBHs. The LIGO–Virgo–KAGRA (LVK) configuration would provide a better sky localization but without finding a host galaxy (via EM waves), it would be challenging to identify the location of a BBH (e.g., in a galactic disk or in a cluster).

Toward the upgrades of bKAGRA, we expect that improved sensitivity toward the lower frequencies would be useful to increase the signal-to-noise ratio (SNR) for BBH populations. More observation means better number statistics in event rate estimation and distributions for underlying properties such as BH mass distribution. Furthermore, by observing earlier inspiral phase signals available at lower frequencies, it will be possible to achieve better accuracy in parameter estimation for individual masses and spin parameters. For a BBH population with small masses, say total mass below 10 $M_\odot$, by improving the so-called "bucket" sensitivity around a few hundred Hz would be most effective to increase the detectability as well as the precision of parameter estimation.

From stellar-mass to supermassive populations, BHs are considered to have a broad mass spectrum. While a standard binary evolution scenario prefers a compact binary consisting of similar masses [42], some binaries may have mass ratios $1/q \equiv m_1/m_2$ much larger than 1, where m_1 is the primary mass and m_2 is the secondary mass of the binary. A dense stellar system is considered to be a factory generating compact binaries through dynamical interactions; see, e.g., Ref. [43]. However, a toy model for the dynamic formation scenario for compact binaries still prefers BBHs with $1/q < 3$; see, e.g., Ref. [23]. Unequal-mass BBHs with $1/q >$ a few are particularly interesting as the modulations in amplitude that are expected by the post-Newtonian formalism in the inspiral phase become significant. Higher multiple modes (with the existence of spin(s)) are also more important for binaries with large mass ratios than they are for equal-mass binaries [44]. Therefore, detections of unequal-mass binaries require an overall improvement in the detector sensitivity corresponding to the detection frequency band in the "bucket". Indeed, a recent event, GW190412, has provided us with evidence to support the detection of higher multiple modes and proved that a broader frequency band plays a crucial role in the detection [45].

In Table 1, we present the innermost stable circular orbit (ISCO) frequencies [46] corresponding to stellar-mass BBHs or BH–NS binaries with various masses. GW signals from binaries with total mass of $\mathcal{O}(10)$ $M_\odot$ or larger would be spanned between $f_{\rm low}$ of an interferometer and around the estimated $f_{\rm ISCO}$, assuming the duration of ringdown signals to be much shorter than inspiral signals. The actual detectability will depend on the sensitivity of the interferometer within the frequency range given for the binary.

In Tables 2 and 3, the measurement errors of the binary parameters for equal-mass BBHs with 30 $M_\odot$ and 10 $M_\odot$ at $z = 0.1$ are estimated with the Fisher information matrix. We assume detector networks composed of A+, AdV+, and bKAGRA or KAGRA+ (LF, HF, 40 kg, FDSQZ, or combined).

Table 1. The ISCO frequencies for compact binary mergers with different mass components consisting of NSs and/or stellar-mass BHs. We assume no spin for BHs; i.e., $f_{\rm ISCO,gw} = (6^{3/2}\pi m_{\rm tot})^{-1}$. The entries are sorted by the total mass of a binary.

m_1 ($M_\odot$)	m_2 ($M_\odot$)	$m_{\rm tot}$ ($M_\odot$)	$1/q = m_1/m_2$ ($M_\odot$)	$f_{\rm ISCO,gw}$ (Hz)
1.4	1.4	2.8	1	1574
5	1.4	6.4	3.6	1001
10	1.4	11.4	7.1	387
10	10	20	1	220
30	10	40	3	110
40	30	70	1.3	63

Table 2. SNR, median errors of the mass ratio in units of 10^{-4}, the effective spin $\chi_{\rm eff}$ in units of 10^{-3}, the luminosity distance in %, the inclination angle in %, and the sky localization area in deg^2 for a $30\,M_\odot$ BBH. The BBHs are at a distance of $z = 0.1$. 2G denotes the detector network composed of the second-generation detectors, aLIGO at Hanford and Livingston, AdV, and bKAGRA. The networks bKAGRA, LF, HF, 40 kg, FDSQZ, and Combined are composed of A+, AdV+, and bKAGRA or KAGRA+ (low frequency, high frequency, 40 kg, frequency-dependent squeezing, and combined), respectively.

quantities	2G	bKAGRA	LF	HF	40 kg	FDSQZ	Combined
SNR	44.4	76.4	75.5	76.0	81.2	81.5	89.5
$\Delta\log\eta$	9.13	5.62	5.83	5.60	5.15	5.23	4.61
$\Delta\chi_{\rm eff}$	15.6	9.75	9.41	9.58	9.35	9.13	8.59
$\Delta\log d_{\rm L}$	11.7	6.82	8.67	7.19	6.19	7.32	5.79
$\Delta\cos\iota$	8.89	4.92	6.35	5.60	4.68	5.25	4.36
$\Delta\Omega_{\rm S}$	0.805	0.300	0.648	0.263	0.243	0.219	0.169

Table 3. SNR and the median errors of parameter estimation for a $10\,M_\odot$ BBH as in Table 2.

quantities	2G	bKAGRA	LF	HF	40 kg	FDSQZ	Combined
SNR	19.8	32.4	31.6	34.2	34.9	33.9	36.7
$\Delta\log\eta$	24.2	14.9	15.2	13.2	13.9	13.7	12.6
$\Delta\chi_{\rm eff}$	9.48	6.02	5.73	5.83	5.75	5.87	5.62
$\Delta\log d_{\rm L}$	25.0	15.0	19.8	15.6	14.2	13.9	11.8
$\Delta\cos\iota$	19.1	10.7	13.7	12.5	10.8	10.1	8.55
$\Delta\Omega_{\rm S}$	1.96	0.821	1.44	0.404	0.654	0.487	0.451

The waveforms that we use are the spin-aligned inspiral–merger–ringdown waveform (PhenomD) for BBH. There are significant improvements from 2G detectors to 2.5G detectors (bKAGRA, LF, HF, 40 kg, FDSQZ, Combined) in the SNR and the errors, but this is not solely due to KAGRA's contribution. The upgrade of bKAGRA to KAGRA+ among A+ and AdV+ modestly enhances the SNR and the sensitivities to the binary parameters in the GW phase: the symmetric mass ratio η, the effective spin $\chi_{\rm eff}$, and the luminosity distance to a source $d_{\rm L}$. For the parameters in GW amplitude, the orbital inclination angle ι and the sky localization area $\Omega_{\rm S}$, the improvement of the errors is significant because the fourth detector is important to pin down the source direction and determine the other correlated parameters. The improvement factor depends on the configuration of the upgrade of KAGRA+. From the point of view of discriminating the formation scenarios, it would be better

for KAGRA to improve the detector sensitivity at both low and middle frequencies. In addition, in order to increase the detectability of BBH coalescences at higher redshifts such as Pop III star binaries and primordial BH binaries, it is important to increase the horizon distance for BBHs and analyze together with the data of a GWB measuring the spectral index and the spectral cutoff.

3. Intermediate-mass binary black holes

3.1. Formation scenarios

3.1.1. Scientific objective

The direct detections of GW emission have revealed the existence of massive BHs with masses of $\gtrsim$ 20–50 $M_\odot$, which are significantly heavier than those ever observed in X-ray binaries [3,11,13]. On the other hand, supermassive BHs of the order of 10^6–10^9 $M_\odot$ almost ubiquitously exist at the centers of galaxies and are believed to be one of the most essential components of galaxies. However, the existence of a (binary) BH population between the stellar-mass and supermassive regimes, i.e., $100 \lesssim M_{\rm BH}/M_\odot \lesssim 10^5$, has not been confirmed yet (though there are some candidates). The lack of such an intermediate-mass binary BH (IMBBH) population is one of the most intriguing unsolved puzzles in astrophysics. Detection of GWs from IMBBHs would be one of the best ways to probe their existence and physical nature.

3.1.2. Observations and measurements

A plausible formation pathway for IMBHs is runaway collisions of massive stars in dense stellar systems (e.g., globular clusters and/or nuclear stellar clusters) [47,48]. In a dense young star cluster, massive stars sink down to the center due to mass segregation and begin to physically collide. During the collision processes, the most massive one gains more masses and grows to a very massive star (VMS) in a runaway fashion, and thus an IMBH with a mass of $M_{\rm IMBH} \simeq 100$–10^4 $M_\odot$ is left after gravitational collapse of the VMS. Even after IMBH formation, stellar-mass BHs (SBHs) migrate to the central region and could form a binary system with the IMBH, the so-called intermediate mass-ratio inspirals (IMRIs) [49,50]. GW emission from such IMRI systems can be detected not only by space-borne GW observatories such as LISA but also by ground-based detectors whose configurations are specifically designed to reach a better sensitivity at lower frequencies (e.g., A+ or KAGRA LF). For $M_{\rm IMBH} \sim 100$–10^3 $M_\odot$ and $M_{\rm SBH} \sim 10$ $M_\odot$, GWs produced from the IMRIs can be detected up to a distance of a few Gpc [51]. Since IMRI systems are likely to have high eccentricities due to the formation process, the GW energy distribution is shifted to higher frequencies, increasing the SNR [52]. Although the IMRI coalescence rate is still highly uncertain, $R \simeq$ 1–30 events yr^{-1} would be expected from several theoretical studies [50,51]. In addition, Ref. [53] discussed the possibility that two IMBHs are formed in a massive dense cluster via runaway stellar collisions, and would form an IMBBH at a lower rate [49].

Alternatively, formation of VMSs in extremely low-metallicity environments (Pop III stars) can initiate IMBHs with masses of $\gtrsim 100$ $M_\odot$ [54]. Since a molecular cloud forming massive Pop III stars would be very unstable against its self-gravity, the cloud would be likely to fragment into massive clumps with $\gtrsim 10$ $M_\odot$ and leave a very massive binary system that will collapse into IMBBHs with $\sim 100 + 10$ $M_\odot$ [55–57]. Assuming a Salpeter-like initial stellar-mass function and the merger delay-time distribution to be $dN/dt \propto t^{-1}$, the merger event rate for such an IMBBH is inferred to be $\sim$ 0.1–1 Gpc^{-3} yr^{-1}, and thus $R \sim$ a few events yr^{-1} [25].

3.1.3. *Future prospects*

The possible target source that is detectable with ground-based detectors is IMRIs. See Sect. 3.2.

3.2. *Intermediate mass-ratio binaries*

3.2.1. *Scientific objective*

The existence of IMBHs in globular clusters is suggested both by observational evidence and theoretical prediction [58]. An IMBH in a globular cluster may capture a stellar-mass compact object surrounding it through some process (e.g., two-body relaxation), and may form an intermediate mass-ratio binary (IMRB) (where "intermediate" mass ratio means the range between the comparable mass ratio (~ 1) and extreme mass ratio ($\lesssim 10^{-4}$)).

The captured object in an IMRB orbits the IMBH many times during the inspiral phase before it plunges into the BH. Therefore, GW signals from IMRBs contain information on the geometry around the IMBHs, which can be used to test the general relativity in the strong field, e.g., the no-hair theorem of BHs and the tidal coupling between the central BH and the orbit of the captured object [59]. Also, if observations of IMRBs are accumulated, they may give a constraint on the event rate and population of IMBHs.

3.2.2. *Observations and measurements*

The GW waveform from the inspiral phase of an IMRB can be estimated in the stationary phase approximation by

$$\tilde{h}(f) = \mathcal{A} f^{-7/6} e^{i\Psi(f)}, \quad \mathcal{A} = \frac{1}{\sqrt{30}\pi^{2/3}} \frac{\mathcal{M}^{5/6}}{D_{\rm L}}, \tag{1}$$

where $\mathcal{M}$, $D_{\rm L}$, and $\Psi(f)$ are the redshifted chirp mass of the binary, the luminosity distance to the source, and the GW phase, respectively [60,61]. The black (solid, dashed, dotted) lines in Fig. 3 show the strain amplitude of GWs, $2\sqrt{f}|\tilde{h}|$, from IMRBs for three different cases, in which a BH with $10\,{\rm M}_\odot$ spirals into heavier BHs with masses of $10^2\,{\rm M}_\odot$, $10^3\,{\rm M}_\odot$, and $10^4\,{\rm M}_\odot$ (these masses include the redshift factors) and the same spin parameter of 0.7 at a luminosity distance of 100 Mpc. The inspiral phase ceases around a certain cutoff frequency, which corresponds to the frequency just before the plunge phase. For circular orbit cases, the cutoff is estimated by the frequency for an ISCO [46]. The ISCO frequency, $f_{\rm ISCO}$ mainly depends on the mass and spin of the central BH. If the mass decreases or the spin increases, the ISCO frequency becomes higher and the overlap with the sensitive band of ground-based detectors becomes larger.

After the inspiral phase, the orbit of the captured object changes to the plunge phase through the transition phase. The shift of the frequency during the transition is roughly estimated by $\Delta f/f_{\rm ISCO} \sim \eta^{2/5}$, where η is the mass ratio [62]. The plunge of the object to the central IMBH will induce ringdown GWs, whose frequency of the dominant mode is given by $f_{\rm RD} \sim 32.3\,{\rm Hz} \times (m_2/10^3{\rm M}_\odot)^{-1} g(\chi_2)$, where m_2 and χ_2 are the redshifted mass and spin of the IMBH and $g(\chi_2)$ shows the spin dependence (see Ref. [63] for details). Since the contribution from the transition phase and the ringdown phase is smaller than that from the inspiral phase, here we do not consider them (an analysis including the transition and ringdown is given in Ref. [64]).

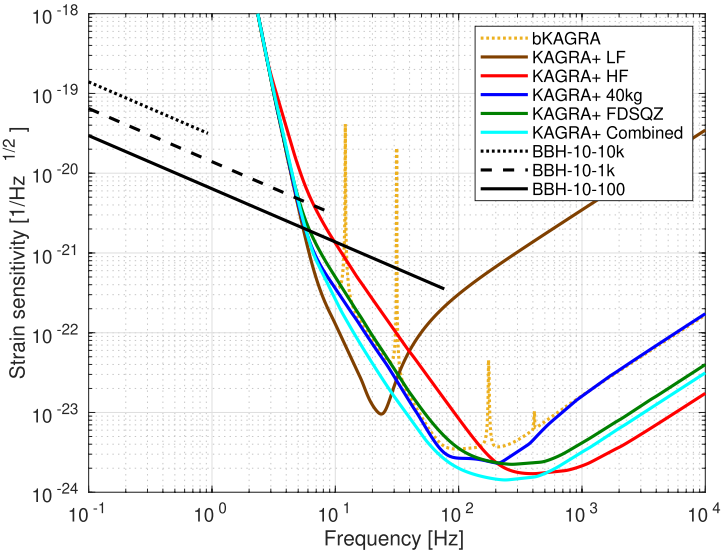

Fig. 3. The strain sensitivity of KAGRA and strain amplitude, $2\sqrt{f}|\tilde{h}|$, of GWs from IMRBs.

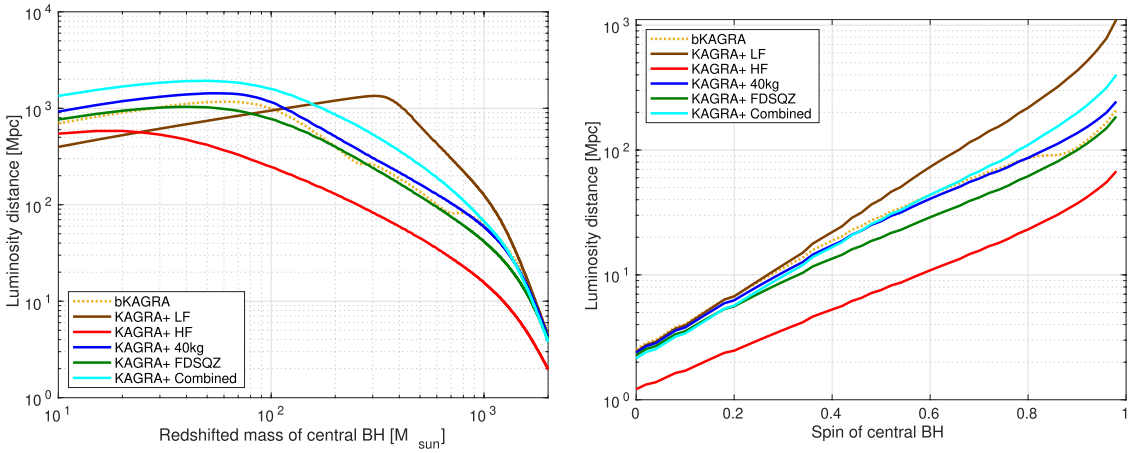

Fig. 4. The detectable luminosity distance of IMRIs.

3.2.3. Future prospects

Since IMRBs with the redshifted mass of 10^2–$10^4 M_\odot$ are expected to be GW sources in the 0.4–40 Hz band [65], some of them may be possible targets for the low-frequency band of ground-based detectors. To see the dependence of the detectability on the sensitivity in the lower band, here we consider the detectable luminosity distance $D_{\rm L}^{\rm detect}$ for the design sensitivity of bKAGRA and KAGRA+ in the same way as in Ref. [61]. The left panel in Fig. 4 shows the dependence of $D_{\rm L}^{\rm detect}$ on the redshifted mass of the central IMBH (m_2) with fixed spin parameter ($\chi_2 = 0.7$). The right panel shows the dependence of $D_{\rm L}^{\rm detect}$ on the spin parameter with fixed mass ($m_2 = 10^3 M_\odot$). In both figures, we fix the mass ($m_1 = 10 M_\odot$) and spin parameter ($\chi_1 = 0$) of the captured object, and the threshold of SNR $= 8$. For example, the values of $D_{\rm L}^{\rm detect}$ with $(m_1, m_2) = (10 M_\odot, 1000 M_\odot)$, $(\chi_1, \chi_2) = (0, 0.7)$, and SNR $= 8$ are given as 62, 126, 16, 59, 42, 67 Mpc for bKAGRA, LF, HF, 40 kg, FDSQZ, and Combined, respectively. From the figures, we find that the detectability of IMRBs with $\sim 300 M_\odot$ can be improved significantly by the LF, while it is difficult to detect IMRBs by the HF. To detect an event, the detection volume is a crucial quantity because it is roughly proportional

to the event rate. Using a detector network composed of two A+, AdV+, and bKAGRA or KAGRA+ (LF, HF, 40 kg, FDSQZ, and Combined), the improvement factors of the detection volume are LF 8.29, 40 kg 0.85, FDSQZ 0.30, HF 0.02, Combined 1.27 for a $10^3\,M_\odot$–$10\,M_\odot$ BBH with spin 0.7.

4. Neutron-star binaries

4.1. Binary evolution

4.1.1. Scientific objective

Formation scenarios of BNSs are similar to those of stellar-mass BBHs. One is based on the standard binary evolution in a galactic disk (see, e.g., Refs. [66,67]) and the other involves dynamical interactions in dense stellar environments such as globular clusters (see, e.g., Ref. [68]). By precision measurements of the NS masses and orbital parameters such as eccentricity by GW observations, it should be possible to shed light on the origin of BNS formation as pointed out many previous works on the BNS population, including Ref. [66]. Although the expected kick involved in the BNS formation is small [66], the role of the natal kick from a supernova explosion can be relatively more significant for the BNS formation than that of BBH formation. The evidence of the natal kick is observed in the known BNSs in our Galaxy, such as the Hulse–Taylor binary pulsar where the eccentricity is 0.67 [69]. Even though a binary's orbit could be significantly eccentric at the time of formation, the BNS orbit becomes circularized quite efficiently [70] and typical BNSs within the detection frequency band of KAGRA are expected to have eccentricities below 10^{-4}. Similar to BBHs, if there are eccentric NS binaries within the KAGRA frequency band, they are more likely to be formed through stellar interactions in dense stellar environments [20,23]. If eccentric binaries exist, measuring eccentricity would be one useful probe to distinguish the field population (formed by a standard binary evolution scenario) and the cluster population (formed by stellar interactions). We note that the measurement of eccentricity requires a much better sensitivity toward the lower-frequency band below 20 Hz; therefore it is more plausible that a third-generation detector may be better suited for searching for eccentric BNSs.

Another difference between NS and BH populations is the mass range. While the BH mass spectrum spans over nine orders of magnitudes, the NS mass range is narrow. For example, the NS mass range should depend on the formation mechanism but is estimated, assuming a Gaussian distribution, to be $1.33 \pm 0.09\,M_\odot$ for double NSs, $1.54 \pm 0.23\,M_\odot$ for recycled NSs, and $1.49 \pm 0.19\,M_\odot$ for slow pulsars, which are likely to be NSs right after their birth [71]. These are based on the known NS–pulsar binaries in our Galaxy before 2016 and do not include a possibly heavy NS recently discovered by GWs [72]. However, even if this is included, the mass range of NSs is much narrower than that of BHs, which is advantageous for the establishment of a template bank. In addition, spin distribution would be something to be compared between NS and BH populations. NS spin distribution for those in BNSs is not well constrained and we expect that GW observations would shed light on the NS spin distribution by parameter estimation.

4.1.2. Observations and measurements

As of early 2019, there were 15 BNSs known in the Galactic disk (see, e.g., Table 1 in Ref. [73]), where all systems consist of at least one active radio pulsar [74,75]. Eight of them are expected to merge within a Hubble time. Measurements of the binary orbital decay and other post-Keplerian parameters clearly showed the effects of gravitational radiation in these NS–pulsar binaries.

GW170817 is the first BNS discovered by GW observation. It is also the first extragalactic BNS. The binary is identified as a BNS based on mass estimation, where both m_1 and m_2 estimates are

consistent with the expected NS masses [76]. The detection of GW170817 also makes it possible to constrain the BNS merger rate. Considering the first and second observing runs, the merger rate solely based on GW observation is estimated to be 110–3840 $\mathrm{Gpc}^{-3}\,\mathrm{yr}^{-1}$ at the 90% confidence interval [3]. GW observation can observe extragalactic BNSs, which are not accessible with current radio telescopes. The GW and radio observations of BNSs would be complementary to reveal the underlying properties of BNSs.

In addition to the BNS population, GW observation would be able to provide rich information about NS interiors (see Sects. 4.2 and 4.3) or the formation of young NSs (see also Sects. 6.3 and 7.1) if late-inspiral, merger, or even ringdown phases are observed by future detectors.

4.1.3. Future prospects

In terms of an observation, improving sensitivities toward lower and higher frequencies has significant implications for understanding the astrophysics of BNSs. The typical chirp mass of a BNS is $\approx 1.13\,\mathrm{M}_\odot$ assuming $m_1 = m_2 = 1.3\,\mathrm{M}_\odot$. This implies that the frequencies of the merger and ringdown phases would be around 2 kHz where the current generation of GW detectors is not sensitive. However, the merger and ringdown phases of BNS coalescence would provide crucial hints to the remnant of the merger. On the other hand, the lower cutoff frequency of a detector is crucial to measure the early-inspiral phase.

The effects of improved detector sensitivity can be considered to be twofold: (a) At higher frequencies, better sensitivity would allows us to set stronger constraints for the NS EOS than aLIGO and AdV could do for GW170817 [77], not to mention improving the accuracy for the mass and spin parameters at higher post-Newtonian (PN) orders. Therefore, better sensitivities at high frequencies will be useful to have the observed sample of BNSs via GWs as complete as possible in the mass–spin parameter space. (b) Improved sensitivity toward lower frequencies below 20 Hz allows us to observe early-inspiral signals. This would be crucial to constrain the orbital eccentricity and determine the origin of the binary formation.

BH–NS binaries are expected to exist and their evolution would be similar to those of stellar-mass BBHs and BNSs. As mentioned above, as there are several parameters that need to be measured in order to discriminate the formation scenarios; with the Fisher information matrix we estimate the measurement errors of the binary parameters for a 10 $M_\odot$ BH–NS binary at $z = 0.06$ and those for a BNS at $z = 0.03$. The waveform that we use is the spin-aligned inspiral waveform up to 3.5PN in phase. The maximum frequency for the inspiral part is set to the ISCO frequency. We assume detector networks composed of A+, AdV+, and bKAGRA or KAGRA+ (LF, HF, 40 kg, FDSQZ, or combined). The measurement errors of the binary parameters are shown in Tables 4 and 5. There are significant improvements from 2G detectors to 2.5G detectors (bKAGRA, LF, HF, 40 kg, FDSQZ, Combined). But this is not solely due to KAGRA's contribution. The upgrade of bKAGRA to KAGRA+ among A+ and AdV+ modestly enhances the SNR and the sensitivities to the binary parameters in the GW phase: the symmetric mass ratio η, the effective spin χ_{eff}, and the luminosity distance to a source d_{L}. For the parameters in GW amplitude, the orbital inclination angle ι and the sky localization area Ω_{S}, the improvement in the errors is significant because the fourth detector is important for pinning down the source direction and determining the other correlated parameters. The improvement factor depends on the configuration of the upgrade of KAGRA+. From the point of view of discrimination of the formation scenarios, it would be better for KAGRA to improve the detector sensitivity at both low and middle frequencies.

Table 4. SNR, median errors of the symmetric mass ratio in units of 10^{-2}, the effective spin $\chi_{\rm eff}$ in units of 10^{-2}, the luminosity distance in %, the inclination angle in %, and the sky localization area in deg^2 for BH–NS binaries. The mass of an NS is 1.4 $M_\odot$. The distance of a 10 $M_\odot$ BH–NS is at $z = 0.06$. 2G denotes the detector network composed of the second-generation detectors, aLIGO at Hanford and Livingston, AdV, and bKAGRA. The networks bKAGRA, LF, HF, 40 kg, FDSQZ, and Combined are composed of A+, AdV+, and bKAGRA or KAGRA+ (low frequency, high frequency, 40 kg, frequency-dependent squeezing, and combined), respectively.

quantities	2G	bKAGRA	LF	HF	40 kg	FDSQZ	Combined
SNR	13.8	22.3	21.9	22.3	23.6	22.6	25.4
$\Delta \log \eta$	9.47	8.93	8.86	8.86	8.86	8.87	8.71
$\Delta \chi_{\rm eff}$	98.2	80.9	80.5	78.2	78.7	78.6	73.3
$\Delta \log d_{\rm L}$	42.6	24.6	27.0	26.7	22.0	22.8	20.8
$\Delta \cos \iota$	32.2	19.6	20.8	21.5	16.8	16.4	15.0
$\Delta\Omega_{\rm S}$	9.04	4.26	9.02	3.48	3.57	3.42	2.71

Table 5. SNR and the median errors of parameter estimation for a BNS at $z = 0.03$ as in Table 4.

quantities	2G	bKAGRA	LF	HF	40 kg	FDSQZ	Combined
SNR	14.8	22.9	23.6	24.1	24.5	24.3	27.7
$\Delta \log \eta$	8.50	5.91	5.48	5.64	5.76	5.74	5.18
$\Delta \chi_{\rm eff}$	5.65	3.96	3.67	3.79	3.87	3.87	3.49
$\Delta \log d_{\rm L}$	37.1	21.5	26.4	21.4	18.6	18.7	17.4
$\Delta \cos \iota$	30.1	15.2	18.2	17.1	14.3	13.7	13.8
$\Delta\Omega_{\rm S}$	3.14	1.60	2.39	0.80	1.28	1.05	0.790

4.2. Neutron-star equation of state and tidal deformation

4.2.1. Scientific objective

BNS mergers provide us with rich information to study nuclear astrophysics, since NSs consist of ultra-dense matter [78]. In the BNS system, an NS is deformed by the tidal field generated by the companion star in the late-inspiral stage [79–81]. The tidal deformability originating from the matter effect encodes the information of the NS EOS. Therefore, measurement of the tidal deformabilities from GWs of the BNS mergers provides information about nuclear physics [82–84]. In this section, we investigate the ability to measure the tidal deformability of NSs with current and future detector networks including bKAGRA and KAGRA+ in addition to A+ and AdV+.

4.2.2. Observations and measurements

During the late stages of the BNS inspiral, at the leading order, the induced quadrupole moment tensor Q_{ij} is proportional to the external tidal field tensor $\mathcal{E}_{ij}$ as $Q_{ij} = -\lambda \mathcal{E}_{ij}$. The information about the NS EOS can be quantified by the tidal deformability parameter $\lambda = (2/3)k_2 R^5/G$, where k_2 is the second Love number and R is the stellar radius [79,80]. The leading-order tidal contribution to the GW phase evolution appears through the binary tidal deformability [82]:

$$\tilde{\Lambda} = \frac{16}{13}\frac{(m_1 + 12m_2)m_1^4\Lambda_1 + (m_2 + 12m_1)m_2^4\Lambda_2}{(m_1 + m_2)^5}, \tag{2}$$

which is a mass-weighted linear combination of both component tidal parameters, where $\Lambda_{1,2}$ is the dimensionless tidal deformability parameter $\Lambda = G\lambda[c^2/(Gm)]^5$. It is first imprinted at relative 5PN order.

The first detection of a GW signal from a BNS system, GW170817 [4], provides an opportunity to extract information about NSs by measuring the tidal deformability. The LIGO–Virgo Collaboration has placed an upper bound on the tidal deformability of $\tilde{\Lambda} \leq 800$ when restricting the magnitude of the component spins [4] using the restricted `TF2` model [85,86] (this limit is later corrected to $\tilde{\Lambda} \leq 900$ in Ref. [76]). In Refs. [3,76], an updated analysis by the LIGO–Virgo Collaboration using a numerical-relativity (NR) calibrated waveform model, `NRTidal` [87] has been reported. By using EOS-insensitive relations among several properties of NSs [88], the constraints on $\tilde{\Lambda}$ can be improved [77] (but see also Ref. [89]). As found in Refs. [76,90], stiffer EOSs (large radii) yielding larger tidal deformabilities such as MS1 and MS1b [91] are disfavored by the data of GW170817. Independent analyses have also been done by assuming a common EOS for both NSs [92,93]. In Ref. [94], the authors indicate that there is a difference in estimates of $\tilde{\Lambda}$ for GW170817 between NR calibrated waveform models (the `KyotoTidal` and `NRTidalv2` models). Here, the `KyotoTidal` model is one of the NR calibrated waveform models of inspiraling BNSs [95,96] and the `NRTidalv2` model is an upgrade of the `NRTidal` model [97]. Several other studies have also derived constraints on the NS EOS by measuring tidal deformability from GW170817 [98–108]. A review of these and other results is available in Ref. [109].

4.2.3. Future prospects

In order to investigate the expected error in the measurement $\tilde{\Lambda}$, we use the Fisher matrix analysis with respect to the source parameters $\{\ln d_{\rm L}, t_c, \phi_c, \mathcal{M}, \eta, \tilde{\Lambda}\}$, where $d_{\rm L}$ is the luminosity distance, t_c and ϕ_c are the time and phase at coalescence, $\mathcal{M}$ is the chirp mass, and η is the symmetric mass ratio. We use the restricted `TF2_PNTidal` model, which employs the 3.5PN-order formula for the phase and only the Newtonian-order evolution for the amplitude as the point-particle part [85,86] and the 1PN-order (relative 5+1PN-order) tidal-part phase formula (see, e.g., Ref. [81]). We take the frequency range from 23 Hz to the ISCO frequency. Here, we consider a non-spinning binary for simplicity.

In Table 6, we show the fractional errors in the tidal deformability $\Delta\tilde{\Lambda}/\tilde{\Lambda}$ in the cases of some NS EOS models, using the inspiral PN waveform, the `TF2_PNTidal` model. We assume future detector networks including bKAGRA and KAGRA+ in addition to two A+ and AdV+. We assume a $1.35M_\odot$–$1.35M_\odot$ BNS located at a distance of 100 Mpc and study three different NS EOS models [110]: APR4 [111] ($\tilde{\Lambda} = 321.7$), SLy [112] ($\tilde{\Lambda} = 390.2$), and high-$\tilde{\Lambda}$ ($\tilde{\Lambda} = 1000$). In one example, for the SLy, the fractional errors on the tidal deformability are 0.069, 0.070, 0.061, 0.068, 0.067, and 0.062 for bKAGRA, LF, HF, 40 kg, FDSQZ, and Combined, respectively. We find that the measurement precision of the tidal deformability can be slightly improved for the HF, but not for the LF. We also present the fractional errors in the tidal deformability for the single detector case in Table 7 to see how much KAGRA can contribute to the global networks.

In Ref. [113], the authors have found a discrepancy in the tidal deformability of GW170817 between the Hanford and Livingston detectors of aLIGO. While the two distributions look consistent with each other and also consistent with what we would expect from noise realization, the Livingston data are not very useful for determining the tidal deformability of GW170817. Their results suggest that measurement of the tidal deformability by a third detector such as AdV or bKAGRA might be helpful in order to improve the constraint on the tidal deformability. In Ref. [94], their results indicate that the systematic error for the NR calibrated waveform models will be significant to measure $\tilde{\Lambda}$ from upcoming GW detections. It is necessary to improve current waveform models for the BNS mergers.

Table 6. The fractional errors in the tidal deformability $\Delta\tilde{\Lambda}/\tilde{\Lambda}$ for a $1.35M_{\odot}$–$1.35M_{\odot}$ BNS located at a distance of 100 Mpc for three different NS EOS models: APR4 ($\tilde{\Lambda} = 321.7$), SLy ($\tilde{\Lambda} = 390.2$), and high-$\tilde{\Lambda}$ ($\tilde{\Lambda} = 1000$). The networks bKAGRA, LF, HF, 40 kg, FDSQZ, and Combined are composed of A+, AdV+, and bKAGRA or KAGRA+ (low frequency, high frequency, 40 kg, frequency-dependent squeezing, and combined), respectively.

	bKAGRA	LF	HF	40 kg	FDSQZ	Combined
APR4 ($\tilde{\Lambda} = 321$)	0.834	0.0840	0.0735	0.0826	0.0795	0.0750
SLy ($\tilde{\Lambda} = 390$)	0.0689	0.0695	0.0608	0.0683	0.0658	0.0620
High-$\tilde{\Lambda}$ ($\tilde{\Lambda} = 1000$)	0.0276	0.0278	0.0244	0.0273	0.0263	0.0248
Network SNR	105	102	105	108	106	115

Table 7. The same results as in Table 6 but for a single detector.

Source	aLIGO	bKAGRA	LF	HF	40 kg	FDSQZ	Combined
APR4 ($\tilde{\Lambda} = 321$)	0.289	0.659	59.7	0.231	0.589	0.270	0.180
SLy ($\tilde{\Lambda} = 390$)	0.239	0.545	49.3	0.192	0.487	0.223	0.149
High-$\tilde{\Lambda}$ ($\tilde{\Lambda} = 1000$)	0.0939	0.217	19.3	0.796	0.194	0.0903	0.0598
SNR	33.9	26.7	12.4	27.4	35.4	31.4	53.9

4.3. Neutron-star remnants

4.3.1. Scientific objective

Investigating the evolution of the object that forms after the merger of a BNS system is more difficult, but also possibly rewarding (see Refs. [109,114,115] for recent reviews). In addition to the connection between such a merged object and ejecta powering the kilonova (which will be treated in detail in Sect. 11.1), strong interest in observations of the post-merger phase also comes from the fact that these would at some point yield information about the EOS of matter at densities higher (several times the nuclear density) than typical densities in inspiraling stars and also at much higher temperatures (up to $\sim$ 50 MeV).

Interestingly, the post-merger phase may be luminous in GW emission, perhaps more so than the preceding merger phase, but since post-merger GW frequencies are higher (from 1 to several kHz [115,118]), the SNR for current and projected detectors is smaller than the pre-merger phase. However, when analyzed in different ways, such GW emission gives us a novel opportunity to prove for a hypermassive NS (HMNS) in the immediate post-merger phase (see below in this subsection). Also gravitational collapse to a rotating BH, should it occur, opens an additional window to emission from a BH–torus system at relatively lower frequencies [116].

Theoretical estimates from numerical simulations of emission from the post-merger HMNS are less reliable than those of the inspiral, because such simulations are intrinsically more difficult to carry out accurately. This is due to the presence of strong shocks, turbulence, large magnetic fields, various physical instabilities, neutrino cooling, viscosity, and other microphysical effects. Currently there exist no reliable determinations of the phase of post-merger gravitational radiation, but only of its spectrum (see, e.g., Refs. [117–120]).

Measuring even just the main frequencies of the post-merger waveform from the putative HMNS may, however, give precious hints to the supranuclear EOS. It has been found, in fact, that the

frequencies of the main peaks of the post-merger power spectrum strongly correlate with properties (radius at a fiducial mass, compactness, tidal deformability, etc.) of a zero-temperature spherical equilibrium star (see, among others, Refs. [117–119,121] and, for applications, Refs. [120,122–124]). For example, finding the tidal deformability of the post-merger object to be very different from that estimated from the inspiral may hint at phase transitions in the high-density matter (see Ref. [109] for a review). A similar hint would be given by an abrupt change in the post-merger main frequency [125,126]. The complicated morphology of these post-merger signals makes constructing accurate templates challenging and thus matched filtering less efficient [120].

In addition to predictions on the GW spectrum, simulations also show, in most cases, delayed gravitational collapses to a rotating BH with dimensionless spin parameter $a/M \simeq 0.76$–0.84 [127], surrounded by a disk. Strong magnetic fields [128] and baryon-rich disk winds are also predicted, though with inferior accuracy, and they are prescient to kilonova light curves [129].

However, simulations cannot accurately predict the time of delay in gravitational collapse of the putative HMNS to a BH, representative of the lifetime of the HMNS initially supported against collapse by differential rotation. The lifetime of the HMNS may be measured in EM–GW observations. Furthermore, because of constraints in computational resources, simulations of post-merger BH–disk or torus systems are limited to tens of ms; see, e.g., Refs. [114,130]. Yet, rotating BHs provide a window to powerful emission over a secular Kelvin–Helmholtz timescale $\tau_{\rm KH} = E_J/L_H$, where $E_J = 2Mc^2 \sin^2(\lambda/4)$ ($\sin\lambda = a/M$) is the spin-energy in angular momentum J of a Kerr BH of mass M [131], c is the velocity of light and L_H is the total BH luminosity, most of which may be irradiating surrounding matter [132]. For gamma-ray bursts, canonical estimates show $\tau_{\rm KH}$ to be tens of seconds [116].

EM–GW observations promise to fill the missing links in our picture of BNS mergers, namely the lifetime of the HMNS in delayed gravitational collapse to a BH; see, e.g., Refs. [133,134]. If finite, continuing emission may extend over the lifetime of BH spin by $\tau_{\rm KH}$ above. For GW170817, if the HMNS experienced delayed collapse, the merger sequence

$$\mathrm{NS} + \mathrm{NS} \underset{a}{\rightarrow} \mathrm{HMNS} \underset{b}{\rightarrow} \mathrm{BH} + \mathrm{GW} + \mathrm{GRB170817A} + \mathrm{AT2017gfo} \tag{3}$$

offers a unique window to post-merger EM–GW emission powered by the energy reservoir E_J of the remnant compact object. Crucially, gravitational collapse b to a BH in the process (3) can increase E_J significantly above canonical bounds on the same at formation a of the progenitor HMNS [135] in the immediate aftermath of the merger.

In the following subsection, we will focus only on calorimetric studies of the post-merger object, leaving the other topics to the above-mentioned reviews [109,114,115].

4.3.2. Observations and measurements

Post-merger EM calorimetry on GRB170817A and the kilonova AT 2017gfo [136–139] show a combined post-merger energy in EM radiation limited to $\mathcal{E}_{\rm EM} \simeq 0.5\%\mathrm{M}_\odot c^2$. This output is well below the scale of total energy output in GW170817, and is insufficient to break the degeneracy between an HMNS or BH remnant.

Gravitational radiation provides a radically new opportunity to probe a transient source that, "if detected, promises to reveal the physical nature of the trigger" [140]. GW calorimetry builds on

earlier applications of indirect calorimetry to, notably, PSR1913+105 [141] and pulsar wind nebulae [142]. Power-excess methods [143,144] have thus far proven ineffective, however, by a threshold of $\mathcal{E}_{\rm gw} = 6.5\,{\rm M}_\odot c^2$ [145], given a total mass $M < 3{\rm M}_\odot$ of the BNS progenitor and hence the mass of its remnant compact object.

Independent EM and GW observations corroborate the process (3) with a lifetime $t_b - t_a$ of the HMNS of less than about one second [116,146]. In EM, the lifetime of the HMNS is inferred from an initially blue component in the kilonova AT 2017gfo [130,146–150], whereas the same is inferred from the time-of-onset t_s of post-merger GW-emission in time–frequency spectrograms produced by butterfly filtering, originally developed to identify broadband Kolmogorov spectra of light curves of long GRBs in the BeppoSAX catalog [151,152]. Application to the LIGO snippet of 2048 s of H1–L1 O2 data covering GW170817 serendipitously shows observational evidence of ~ 5 s post-merger gravitational radiation [153]. Subsequent signal injection experiments indicate an output $\mathcal{E}_{\rm gw} = (3.5 \pm 1)\%{\rm M}_\odot c^2$ in this extended emission [116]. Its time-of-onset $t_s < 1$ s post-merger falls in the 1.7 s gap between GW170817 and GRB170817A, satisfying causality at birth of a central engine of GRB170817A.

$\mathcal{E}_{\rm gw}$ exceeds the maximal spin-energy of an (HM)NS [135], yet it readily derives from E_J of a BH following gravitational collapse thereof at b in the process (3). Moreover, the aforementioned $\mathcal{E}_{\rm EM}$ is quantitatively consistent with model predictions of ultra-relativistic baryon-poor jets and baryon-rich disk winds from a BH–torus system, the size of which derives from the frequency of its GW emission [116].

At current detector sensitivities, witnessing the formation and evolution of the progenitor HMNS in the immediate aftermath of a merger is extremely challenging. Null results on GW170817 [154] are entirely consistent with the energetically moderate and relatively high-frequency (> 1kHz) spectra expected from numerical simulations [114].

4.3.3. Future prospects

Once the BH forms, it has no memory of its progenitor except for total mass and angular momentum. This suggests pursuing GW calorimetry in Eq. (3) to catastrophic events more generally, including mergers of an NS with a BH companion and nearby core-collapse supernovae (CCSNe), notably the progenitors of type Ib/c of long gamma-ray bursts (GRBs) [155]. While the latter is rare, the fraction of failed GRB supernovae that are nevertheless luminous in gravitational radiation may exceed the local GRB rate and hence the rate of mergers involving an NS; see, e.g., Ref. [151]. Blind all-sky butterfly searches may thus produce candidate signals with and without merger precursors from events within distances on a par with GW170817, which may be followed up by time-slide correlation analysis and optical–radio signals from existing transient surveys of the local Universe. It also appears opportune to consider directed searches for events in neighboring galaxies (see, e.g., Ref. [156]), notably M51 ($D \simeq 7$ Mpc) and M82 ($D \simeq 3.5$ Mpc), each offering about one radio-loud CCSN per decade. By their close proximity, these also appear to be of interest independent of any association with progenitors of GRBs [157,158].

For a planned KAGRA upgrade, the above suggests optimizing the broadband window of 50–1000 Hz to pursue GW calorimetry on extreme transient sources using modern heterogeneous computing, in multi-messenger approaches involving existing and planned high-energy missions such as THESEUS [159,160]. Jointly with LIGO and Virgo, KAGRA is expected to give us a window to modeled and unmodeled transient events out to tens of Mpc.

5. Accreting binaries

5.1. Continuous GWs from X-ray binaries

5.1.1. Scientific objective

There are several classes of continuous GWs (CWs). One major population of CW sources is systems involving a spinning NS that has an asymmetry with respect to its rotation axis [161]. Potential candidates include pulsars, NSs in supernova remnants, and NSs in binary systems. In particular, an accreting NS in a low-mass X-ray binary is a promising target. In this system, the central NS accretes materials from an orbiting late-type companion star. A finite quadrupole moment of an accreting NS can be possibly induced by various processes such as the laterally asymmetric distribution of accreted material and elastic strain in the crust as well as magnetic deformation [162].

Sco X–1 is the prime target for directed searches of CWs from X-ray binaries because it is the brightest persistent X-ray binary. The source is relatively nearby (~ 2.8 kpc) and its X-ray luminosity suggests that the source is accreting near the Eddington limit for an NS. If the torque-balance (i.e., balance between accretion-induced spin-up torque and the total spin-down torque due to gravitational and EM radiation) can be maintained in the binary system, Sco X–1 is a promising target for CW signals [163].

Current theoretical understanding of the torque-balance and spin-wandering effects of X-ray binaries is poor [163,164]. By combining CWs from X-ray binaries and multi-wavelength observations, we may track the evolution of spin torques and orbit, shedding light on disk dynamics and the maximum rotation frequency of an NS in a binary system [161].

No CW signal from X-ray binaries has been observed so far. During the LIGO S6 observing run, upper limits were estimated for Sco X–1 and XTE J1751–305 while the O1 observation of Sco X–1 yielded a null detection as well [165–167]. In the O2 observing run, by using a hidden Markov model (HMM) to track spin wandering, a more sensitive search for Sco X–1 was performed [168]. No evidence of CW can be found in the frequency range of 60–650 Hz. An upper limit (95% confidence) of $h \sim 3.5 \times 10^{-25}$ is placed at 194.6 Hz, which is the tightest constraint placed on this system so far [168].

5.1.2. Observations and measurements

CW signals from accreting X-ray binaries are extremely small compared to all known compact binary mergers. Assuming a torque-balance, the GW amplitude can be linked with the X-ray flux presumably associated with the accretion rate [163]:

$$h \approx 4 \times 10^{-27} \left(\frac{F_X}{10^{-8}\,\mathrm{erg\,cm^{-2}\,s^{-1}}} \right)^{1/2} \left(\frac{\nu_s}{300\,\mathrm{Hz}} \right)^{-1/2} \left(\frac{R}{10\,\mathrm{km}} \right)^{3/4} \left(\frac{M}{1.4\mathrm{M}_\odot} \right)^{-1/4}. \quad (4)$$

Sco X–1 is the brightest persistent X-ray binary ($F_X \sim 4 \times 10^{-7}$ erg cm^{-2} s^{-1}) and the expected GW signals are of the order of $h \sim 10^{-25}$ or smaller. To search for such a weak signal, we need to integrate the data over a long period of time. One major challenge for Sco X–1 is that the spin period is unknown. We therefore need to search for a broad range of frequencies. Moreover, because of the spin-wandering effect due to changing accretion rates onto the NS [164], it is difficult to integrate the signals with a long coherence time (hence better sensitivity). If we could discover the pulsation of Sco X–1 via X-ray observations in the future, it will narrow the parameter space, increasing our chances of achieving the first detection of CWs from an X-ray binary.

Apart from Sco X–1, there are other luminous X-ray binaries such as GX 5–1 and GX 349+2. However, their X-ray fluxes are at least an order of magnitude lower than that of Sco X–1, making them

even more difficult to detect with current GW detectors. Although Sco X–1 is still the only promising persistent X-ray binary for CW signals, we may detect CWs from a very luminous outburst of an NS X-ray binary in the future. For example, the X-ray outbursts from Cen X–4 were even brighter than Sco X–1 although they only lasted for about a month [169].

5.1.3. Future prospects

In order to optimize the search for CWs from X-ray binaries and Sco X–1 in particular, the best frequencies should be from a few tens of to a few hundred Hz. A stable (with high duty cycle) long-term (months to years) observing run is required to integrate the data for the weak signals of the order of $h \sim 10^{-25}$ or smaller. Unless we know the spin frequency of the NS from EM observations, we have to search for a large frequency range, implying a high demand for computation time. In any case, better computing algorithms have to be developed along with implementation of GPU computation in order to increase the detection efficiency [170,171]. If we define the SNR ratio averaged over relevant frequencies, we can quantitatively compare performances of various configurations of possible KAGRA upgrades. We define the ratio $r_{\alpha/\beta} \equiv r_\alpha / r_\beta$ for the configurations α and β where

$$r_\alpha \equiv \sqrt{\int_{f_{\rm low}}^{f_{\rm high}} \frac{1}{S_h^\alpha(f)} df}; \tag{5}$$

a similar equation holds for the β configuration. In the case of an accreting X-ray binary, for a typical frequency range between $f_{\rm low} = 30$ Hz and $f_{\rm high} = 200$ Hz, the SNR ratios of KAGRA+ to bKAGRA are LF 0.04, 40 kg 1.62, FDSQZ 1.38, HF 0.89, Combined 2.25.

Recently, a novel methodology of searching for CWs by deep learning has been proposed [172]. Since the CW is expected to be weak, it is necessary to integrate the data with a very long time span to result in SNR above the detection threshold. This poses a computational challenge to the traditional coherent matched-filtering search. First, it is difficult to apply such method to a data span longer than weeks. Moreover, as we do not know the spin period and period derivatives precisely, we have to perform a blind search in a large parameter space at the same time, which makes the problem more computationally demanding. On the other hand, once a deep learning network has been trained, prediction on any inputs can be executed very fast, which is very favorable for CW searches. Although the sensitivity of the first proof-of-principle deep learning CW search is far from being optimal [172], it does demonstrate an excellent ability in generalization. Further investigation of this methodology (e.g., exploring which network architecture is optimal for CW searches) could be fruitful.

6. Isolated neutron stars

6.1. Pulsar ellipticity

6.1.1. Scientific objective

GWs that last more than ~ 30 minutes, when we search for them using ground-based GW detectors, are susceptible to Doppler modulation due to the Earth spin and orbital motion. Those long-lasting GWs are called "continuous" GWs, or CWs.

Spinning stars with non-axisymmetric deformations may emit CWs. Pulsars may have such non-axisymmetric deformations and are good candidates for GW observatories. It is estimated that there are roughly $\sim 160\,000$ normal pulsars and $\sim 40\,000$ millisecond pulsars in our Galaxy. At the time

of writing this paper, the ATNF pulsar catalogue [74,75] includes $\sim$ 2800 pulsars, among which $\sim$ 480 pulsars ($\sim$ 17%) spin at more than 10 Hz. While $\sim$ 10% of pulsars are in binaries, the fraction increases to more than 57% when limited to pulsars with $f_{\rm spin} \geq 10$ Hz. The Square Kilometer Array (SKA) is expected to find many more pulsars in the near future [173].

A rapidly spinning NS may emit GWs (roughly) at its spin frequency $f_{\rm spin}$, 4/3, and/or twice its value, depending on emission mechanisms. If an NS emits at $\sim f_{\rm spin}$, it may mean that the NS is "wobbling" (freely precessing). Detection of "wobbling-mode" CWs gives information on interactions between the crust and fluid core of the NS. If an NS has a non-axisymmetric mass quadrupole deformation, it may emit CWs at $2f_{\rm spin}$. CW frequency can be different from twice the spin frequency estimated from an EM observation, if a component producing EM radiation does not completely couple with that producing GWs. We sometimes call the $2f_{\rm spin}$ mode "mountain mode". "Mountains" on a star may be due to, e.g., fossil deformations developed during NS formation supported by crustal strain and/or a strong magnetic field within the NS, or a thermal gradient (in the case of an accreting NS in a binary). If both GWs of the wobbling mode and the mountain mode are detected from a single NS, one may be able to determine its mass [174]. The r-mode may be unstable within a young NS and it may emit CWs at $\sim 4f_{\rm spin}/3$. Detection of "r-mode" CWs gives us information on the evolution history of the star, as the damping timescale depends on the interior temperature. See, e.g., Refs. [117,175,176], for recent reviews on the physics of possible mountain-mode, r-mode, and wobbling-mode CWs.

Due to the lack of space, we focus on isolated NSs that emit mountain-mode CWs in this section. The LIGO–Virgo Collaboration has been searching for mountain-mode CWs [177,178]. Readers are referred to Ref. [178] for a wobbling-mode CW search (or more generally, $m = 1$-mode CWs) and Ref. [179] for an r-mode search. Mountain-mode CWs typically last for more than the observation time T_0 ($\sim$ year). As such, the detectable CW amplitude h at frequency $f_{\rm gw}$ scales as

$$h = C\sqrt{\frac{S_h(f_{\rm gw})}{T_0}} \tag{6}$$

where C depends on the search method and a predefined threshold for detection. The LSC Bayesian time-domain search for known pulsars [177] adopts $C \simeq 10.8$, where "known" means that their timing solutions as well as their positions on the sky are known to sufficient accuracies and there is little, if any, need to search over parameter space in the search.

6.1.2. Observations and measurements

A mountain-mode CW depends on the strain amplitude h, GW frequency $f_{\rm gw}$, its higher-order time derivatives, direction to the source, inclination angle between the line of sight and the spin angular momentum, GW initial phase, and polarization angle. As a persistent source, a single detector can detect and locate a CW source. Since the detector beam pattern changes during the observation time, one can test general relativity (GR) by searching for CWs with non-tensorial polarizations [180]. GW frequency and its higher time derivatives together with h may tell us how the source loses its energy and spin angular momentum.

The amplitude h of the dominant mountain-mode CW depends on $\ell = m = 2$ mass quadrupole deformation Q_{22}, distance to the source r, and the GW frequency as

$$h \simeq 1.4 \times 10^{-27} \left(\frac{Q_{22}}{10^{38}\,{\rm g\,cm^2}}\right) \left(\frac{r}{1\,{\rm kpc}}\right)^{-1} \left(\frac{f_{\rm gw}}{100\,{\rm Hz}}\right)^2. \tag{7}$$

Q_{22} is related to the stellar ellipticity ϵ in the literature as $\epsilon \mathcal{I}_3 = \sqrt{8\pi/15} Q_{22}$ where $\mathcal{I}_3$ is the moment of inertia of the star with respect to its spin axis.

Roughly speaking, $Q_{22,\max} \propto \mu\sigma R^6/M$ where μ is the shear modulus, σ is the breaking strain of the crust, R is the stellar radius, and M is its mass. As it depends on the stellar radius and mass, the maximum possible $Q_{22,\max}$ depends on the EOS [181,182]. For a normal NS [183],

$$Q_{22,\max} \simeq 2.4 \times 10^{39}\,\mathrm{g\,cm^2} \left(\frac{\sigma}{0.1}\right) \left(\frac{R}{10\,\mathrm{km}}\right)^{6.26} \left(\frac{M}{1.4\mathrm{M}_\odot}\right)^{-1.2}. \tag{8}$$

If we find that some "NS" has Q_{22} much larger than $Q_{22,\max}$, it means that that particular star may not be a "normal NS" (or we do not understand "normal NSs" well enough to predict $Q_{22,\max}$).

Real NSs may have Q_{22} much smaller than $Q_{22,\max}$. The LIGO–Virgo Collaboration has reported upper limits on Q_{22} for more than 200 pulsars, many of which have already surpassed the theoretical upper limit significantly. For those pulsars, even if their GWs are detected, we may not be able to obtain information on the NS EOS from measurement of Q_{22}.

6.1.3. Future prospects

Figures of merit for isolated pulsar searches may be the h value given by Eq. (7) for possible Q_{22} values, and the so-called spin-down upper limit. Many pulsars show spin-downs that indicate the rate of loss of stellar rotational energy. Assuming that some of the rotational energy is radiated as GWs, we can estimate the maximum possible GW amplitude, called the spin-down upper limit on GW amplitude:

$$\begin{aligned} h_0^{\mathrm{sd}} &= \left(\frac{5\eta G \mathcal{I}_3 \dot{f}_{\mathrm{spin}}}{2c^3 f_{\mathrm{spin}} r^2}\right)^{1/2} \\ &\simeq 8.06 \times 10^{-19} \eta^{1/2} \left(\frac{\mathcal{I}_3}{10^{45}\,\mathrm{g\,cm^2}}\right)^{1/2} \left(\frac{r}{1\,\mathrm{kpc}}\right)^{-1} \sqrt{\frac{|(\dot{f}_{\mathrm{spin}}/\mathrm{Hz\,s^{-1}})|}{(f_{\mathrm{spin}}/\mathrm{Hz})}}; \end{aligned} \tag{9}$$

this equation assumes that 100η% of energy is radiated as GWs.

Figure 5 shows the detector sensitivity curves for the CW search (assuming one-year integration, coherent search) as well as the figures of merit for the pulsars that the LIGO–Virgo Collaboration has searched for using O2 data [178]. It is clear that KAGRA+ HF is more useful for the CW search.

Figure 6 shows the upper limits on Q_{22} that LIGO and Virgo obtained in their O2 search (stars), as well as possible upper limits that are expected by using various configurations of KAGRA+ for the same pulsars. The horizontal thick line indicates the theoretical maximum for Q_{22} for a normal NS. The LIGO–Virgo Collaboration has already exceeded $Q_{22,\max}$ at higher frequencies than $\sim$ 100Hz. KAGRA+ LF does not have any power to explore normal NS CWs.

It is possible to conduct unknown pulsar searches (e.g., all-sky search, wide-band frequency search). In this case, a possible figure of merit is the reach of a detector, which is shown for various detector configurations in Fig. 7, assuming coherent one-year integration (although it is impossible in practice to conduct a fully coherent unknown pulsar search due to computational resource limitations). This plot again shows that we may increase the chances of detection if we put more emphasis on higher frequencies.

We can quantitatively compare the performances of various configurations of possible KAGRA upgrades by introducing the gain in the SNR averaged over relevant frequencies. Namely, we define the ratio $r_{\alpha/\beta} \equiv r_\alpha/r_\beta$ for the configurations α and β where r_α is defined in Eq. (5) and a similar

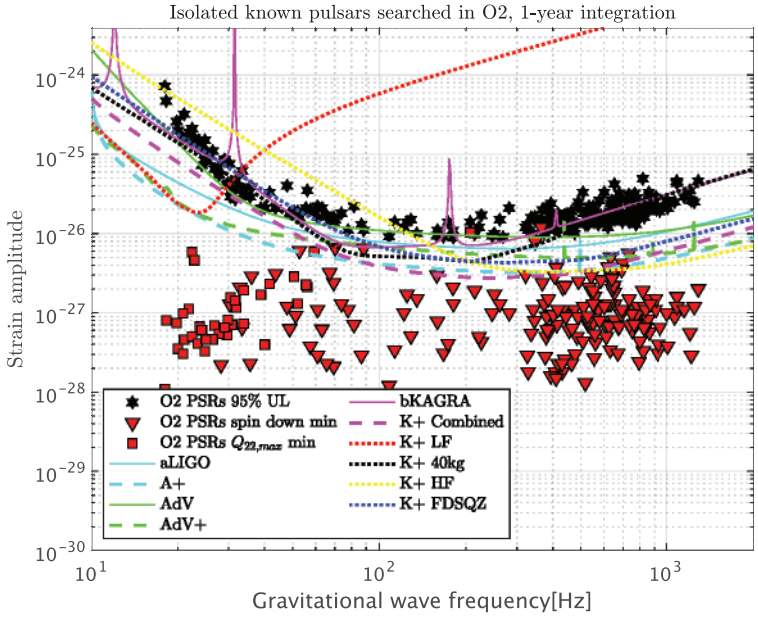

Fig. 5. The detector sensitivity curves as well as the figures of merit for the pulsars that the LIGO–Virgo Collaboration has searched for using O2 data [178]. The black stars are the 95% upper limits by the LIGO–Virgo O2 search. For each pulsar that the LIGO–Virgo Collaboration searched for using O2 data, the smaller of the spin-down upper limit or the upper limit assuming $Q_{22,\max}$ is plotted: if the spin-down upper limit is smaller for the pulsar, then an inverted triangle is plotted, if not, then a red box is plotted. Coherent one-year integration is assumed.

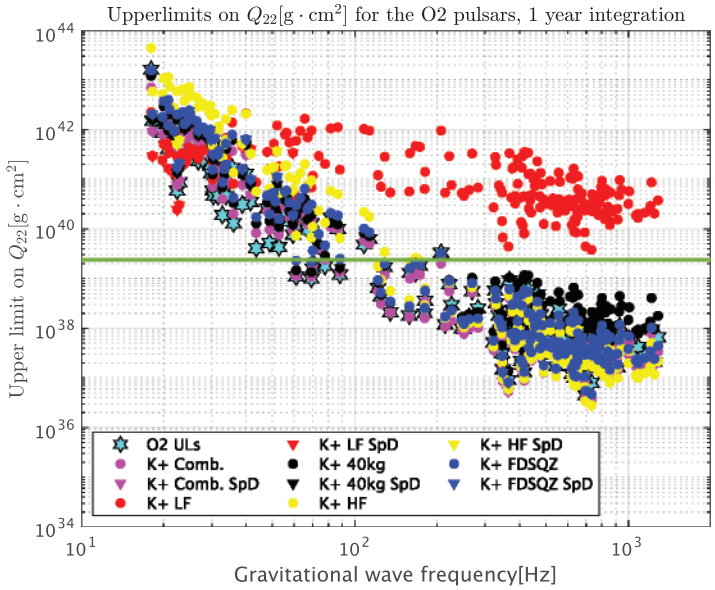

Fig. 6. The upper limits on Q_{22} that LIGO and Virgo obtained in their O2 search (stars) [178], as well as possible upper limits that are expected by using various configurations of KAGRA+ for the same pulsars. Coherent one-year integration is assumed. The horizontal thick line indicates the theoretical maximum for Q_{22} for a normal NS. LIGO and Virgo have already exceeded $Q_{22,\max}$ at higher frequencies than $\sim$ 100 Hz. KAGRA+ LF does not have any power to explore normal NS CWs.

AQ19

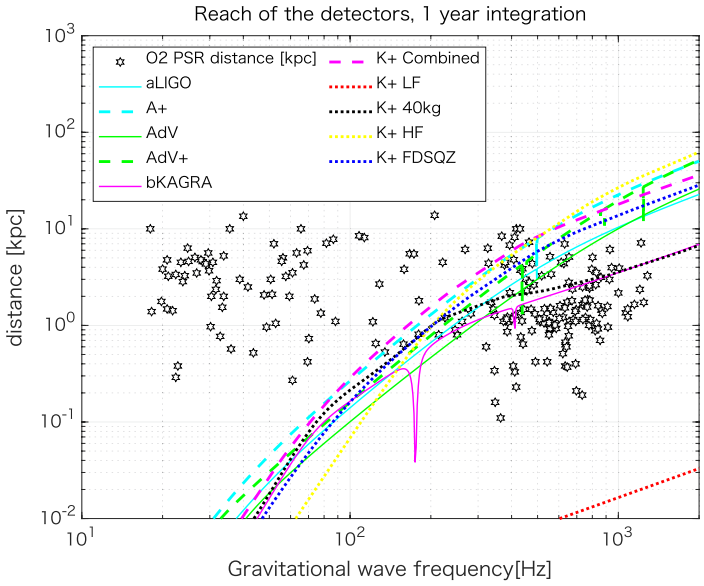

Fig. 7. Possible reaches of detectors of various configurations where $\epsilon = 10^{-7}$ (or $Q_{22} = 7.7 \times 10^{37}\mathrm{g\,cm^2}$) is assumed. Stars indicate the distances estimated for the pulsars that LIGO and Virgo has searched for using O2 data.

equation holds for the β configuration. In the case of a continuous wave search, we may be interested in the sensitivity at higher frequencies, say, $f_{\rm low} = 500$ Hz and $f_{\rm high} = 1$ kHz where the possible constraints on Q_{22} would be the tightest. For $\alpha =$ "KAGRA+" and $\beta =$ "bKAGRA", the $r_{\alpha/\beta}$ then are 1.04 ("40 kg"), 3.27 ("FDSQZ"), 5.89 ("HF"), and 4.53 ("Combined").

6.2. Magnetar flares and pulsar glitches

6.2.1. Scientific objective

Giant flares in soft gamma-ray repeaters (SGRs), which are a class of strongly magnetized NSs, so-called magnetars, have been observed: 5 March 1979 (SGR 0526-66); 27 August 1998 (SGR 1900+14); 27 December 2004 (SGR 1806-20). The event rate is quite low, but a huge amount of energy is known to be radiated in the EM X and gamma bands. For example, in the last SGR 1806-20 hyperflare, the peak luminosity was $10^{47}\,\mathrm{erg\,s^{-1}}$ and the total energy released in a spike within 1 second was estimated as 10^{46} erg [184]. Quasi-periodic oscillations were also observed in the burst tail. Their frequencies are 20–2000 Hz, and are identified by seismic modes excited in the magnetar flare. The (quasi-)periodic oscillations are separately discussed in Sect. 6.3. The properties and mechanisms of the flare are not certain at present, owing to the limited number of events. In particular, the energy carried by GWs is unclear. The theoretical estimate of GW energy associated with flares ranges from $\sim 10^{40}$ erg [185,186] to $\sim 10^{49}$ erg [187,188]. The dipole field strength derived by stellar spin and its time derivative are normally used for the energy deposited before a flare, but much stronger fields might be hidden inside. Thus, the problem will be solved only by actual observations due to many uncertain factors. Actually, the GW energy for the SGR 1806-20 hyperflare was limited by LIGO. At that time, one interferometer at Hanford was in operation. The upper limit on the GW amplitude is $5 \times 10^{-22}\ \mathrm{Hz^{-1/2}}$ and the GW energy is less than 8×10^{46} erg [189]. It is very important to make a similar argument for each flare observation.

Another interesting astrophysical event is the pulsar glitch. A sudden change in spin angular frequency is $\Delta\Omega/\Omega \sim 10^{-6}$ in a typical giant glitch and the rotation energy changes by $I\Omega^2/2 \times$

$\Delta\Omega/\Omega \sim 10^{41}$ erg as for a maximum value. The change is likely to be much smaller, since the rearrangement of stellar structure is partial in the transition.

6.2.2. Observations and measurements

These burst events will be probably first detected in EM signs, and GW signals should be carefully searched at the burst epoch. There is no reliable waveform, so that GW signals are identified by combinations of multiple detectors. The burst is a dynamical event on a timescale of milliseconds, and therefore a sharp peak in the kHz range is expected. Coincidence among different GW/EM detectors is crucial. The observational strategy of GW analysis may depend on the EM information. When quasi-periodic oscillation frequencies are identified in EM data, we should search for GW counterparts in the same frequency range. GW signals in LIGO O2 data [190] were searched for magnetar bursts, which are less-energetic events. Two software packages, X-Pipeline and STAMP, were used: Clusters of bright pixels above a threshold in each time–frequency map are searched in X-Pipeline, directional excess power due to arrival time delay between detectors in STAMP.

6.2.3. Future prospects

As for the future extension of bKAGRA, improvements in a higher-frequency band are favored for these events. If we fix the frequency of the signal to 1 kHz, the SNR ratios of KAGRA+ to bKAGRA at 1 kHz are 40 kg 1.03, FDSQZ 3.98, HF 7.47, Combined 5.01. However, it is not clear at present how to predict the detection level of meaningful signals by improvements. We will catch them or upper limits by chance, when bursts happen. Stable operation is desirable.

6.3. Stellar oscillations

6.3.1. Scientific objective

In order to observationally extract the properties of astronomical objects, asteroseismology is a very powerful technique, where one can get information about objects via their specific frequencies. This is similar to seismology in the Earth and helioseismology in the Sun. For this purpose, GWs provide the most suitable astronomical information, owing to their high permeability. In fact, several modes in GWs are expected to be radiated from compact objects [191], and each mode depends on different aspect of internal physics. The GWs have complex frequencies, because the GWs carry out the oscillation energy, where the real and imaginary parts correspond to the oscillation frequency and damping rate, respectively. So, by identifying the observed frequencies (and damping times) of GWs to the corresponding specific modes, one would get the physics behind the phenomena. In general, the GWs are classified into two families with their parity. The axial parity (toroidal) oscillations are incompressible oscillations, which do not involve density variation, while the polar parity (spheroidal) oscillations involve density variation and stellar deformation. Thus, from an observational point of view, polar-type oscillations are more important, although these are coupled with axial-type oscillations on the non-spherical background.

6.3.2. Observations and measurements

Some of the GWs from NSs are classified in the same way as the oscillations of the usual (Newtonian) stars. That is, the fundamental (f) and the pressure (p_i) modes are excited as acoustic oscillations of NSs, while the gravity (g_i) modes are excited by the buoyancy force due to the existence of the density discontinuity or composition gradients inside the star. The Rossby (r) modes are also excited by the Coriolis force in rotating stars, although they are axial parity oscillations. In addition to these

modes associated with the fluid motions, the oscillations related to the spacetime curvature are also excited, i.e., the so-called GW (w_i) modes, which can be discussed only in the relativistic framework. The typical frequencies of the f, p_1, g_1, and w_1 modes for standard NSs are around a few kHz, higher than 4–7 kHz, smaller than a hundred Hz, and around 10 kHz, respectively [191]. With these specific modes from the NSs, extraction of NS information via direct detection of GWs has been discussed.

A good example of GW asteroseismology may be the results shown by Andersson and Kokkotas [192,193], where they found universal relations for the frequencies of the f and w_1 modes as a function of the average density of the star and the compactness, respectively, almost independently of the EOS for NS matter. This is because the frequency of the f mode, which is an acoustic wave, should depend on the crossing time inside the star with the sound velocity, while the frequency of the w mode is strongly associated with the strength of the gravitational field. So, if one simultaneously detect, could two modes in GWs from the NS, one could get the average density and compactness of the source object, which tells us the NS mass and radius. On the other hand, g-mode GWs may tell us the existence of the density discontinuity due to the phase transition [194–197], or they may become more important in newborn NSs or proto-neutron stars (PNSs) [198–200]. The non-axisymmetric r-mode oscillations may also be interesting due to their instability against gravitational radiations [201,202]. That is, for the rapidly rotating case, the GW amplitude can exponentially increase due to the instability, which may become a detectable signal. Eventually, the GW amplitude would be suppressed via non-linear coupling [203]. We note that even the f-mode oscillations may become unstable in rapidly rotating relativistic NSs [204]. In any case, detection of GWs from an isolated (cold) NS may be quite difficult with the current GW detectors, because most of their frequencies are more than around kHz.

On the other hand, the detection of GWs from PNSs would be more likely if they are formed within our Galaxy. This is because, since the PNSs are initially less massive and have larger radii, i.e., their average density is smaller than that of cold NSs, one can expect the frequency of f-mode GWs to be smaller than the typical one for cold NSs. In practice, the f-mode frequency of PNSs is around a few hundred Hz in the early phase after core-bounce [205]. However, studies of asteroseismology in PNSs are very few, unlike in cold NSs. This is because of the difficulty of providing background models. That is, cold NSs can be constructed with the zero-temperature EOS, i.e., the relation between energy density and pressure, while one has to consider the distribution of the electron fraction and entropy per baryon together with the pressure distribution as a function of density to construct the PNS models. However, such distributions can be determined only after the numerical simulation of core-collapse supernovae. Even so, the study of asteroseismology in PNSs is becoming possible with numerical data of simulation.

So far, two different approaches have been proposed for providing the PNS models; one is that the PNS surface is defined with a specific density around 10^{10-12} g/cm^3 [205–209], and the other is that oscillations inside the shock radius are considered [210,211], where different boundary conditions should be adopted according to the approaches. In contrast to the cold NSs, matter widely exists outside the PNSs, which makes it difficult to treat the boundary of the background models. Anyway, with either approach, it seems that the mode frequencies of GWs are expected to range over wide frequencies and that such frequencies would change with time. If one could identify the frequencies of GWs with a specific mode, it would be very helpful for understanding the physics of PNS cooling via understanding of the PNS properties. In practice, the time evolution of the identified frequencies is considered as a result of the changing of the PNS mass and radius, i.e., the mass increases due to accretion and the radius decreases due to both the relativistic effect and neutrino cooling, with

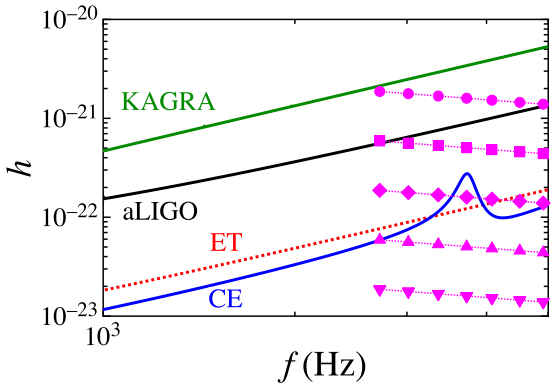

Fig. 8. Effective amplitude of the w_1 mode in GWs from the PNS model constructed with the SFHx EOS is shown in the sensitivity curves of KAGRA, AdVanced LIGO (aLIGO), Einstein Telescope (ET), and Cosmic Explorer (CE). Taken from Ref. [206].

time. So, in the same way as for the cold NSs, if one could simultaneously identify the frequencies with the f- and w_1-modes of GWs from PNSs, one would get the information on the average density and compactness at each time, which enables us to know the evolution of masses and radii of PNSs [206]. That is, unlike cold NSs, in principle one can expect to make a severe constraint on the EOS even with one event of GW detection. It should be emphasized that the frequencies of w_1-mode GWs from the PNSs become typically around a few kHz, because the compactness is smaller than that of cold NSs.

6.3.3. *Future prospects*

We make a comment about the detectability of these modes in GWs. The GW amplitudes have been discussed in Refs. [192,193] for isolated cold NSs, assuming the radiation energy of GWs with each mode. Since the radiation energy with each mode cannot be estimated as long as one examines GW asteroseismology with linear perturbation analysis, one should eventually estimate such radiation energy with numerical simulation to see the detectability. The situation in PNSs born after the core-collapse supernova is the same. Even so, adopting the formula shown in Refs. [192,193], the effective gravitational amplitude of the w_1 mode from the PNSs may be estimated with its energy, E_{w_1}, at each time step as

$$h_{\rm eff}^{(w_1)} \approx 7.7 \times 10^{-23} \left(\frac{E_{w_1}}{10^{-10}{\rm M}_\odot}\right)^{1/2} \left(\frac{4\ {\rm kHz}}{f_{w_1}}\right)^{1/2} \left(\frac{10\ {\rm kpc}}{D}\right), \tag{10}$$

where f_{w_1} and D denote the frequency of considering the w_1 mode and the distance to the source object, respectively [206]. The total radiation energy of the w_1 mode in the GWs from a PNS, $E_{w_1}^T$, may be estimated as $E_{w_1}^T \approx E_{w_1} T_{w_1}/\tau_{w_1}$, where τ_{w_1} denotes the damping time of w_1 mode with the frequency of f_{w_1} at each time step. In this estimation, we assume that w_1-mode GW emission would last for the duration of T_{w_1}, as the frequency of f_{w_1} evolves, where we simply adopt $T_{w_1} = 250$ ms. Then, the effective amplitude is plotted as in Fig. 8, where the circles, squares, diamond, triangles, and upside-down triangles correspond to the expectations with $E_{w_1}^T/{\rm M}_\odot = 10^{-4}, 10^{-5}, 10^{-6}, 10^{-7}$, and 10^{-8}, respectively.

To detect the GW signal due to the NS oscillations, improvements at a higher frequency must be more suitable, although the amount of energy of GWs is unknown at present. If we fix the frequency of the signal to 1 kHz as in Sect. 6.2, the SNR ratios of KAGRA+ to bKAGRA at 1 kHz are 40 kg

1.03, FDSQZ 3.98, HF 7.47, Combined 5.01. Improvements even in the middle-frequency band may be suitable for detecting f-mode GWs from the PNS, but this would only be acceptable in the early phase after core-bounce, because the frequency increases with time and eventually becomes $\sim$ kHz.

7. Supernovae

7.1. The explosion mechanisms and the GW signatures

7.1.1. Scientific objective

Accumulating observational evidence from multi-wavelength EM observations of, e.g., ejecta morphologies and spatial distributions of heavy elements have all pointed toward CCSNe being generally aspherical (see, e.g., Refs. [212,213] and references therein). However, these signals are secondary for probing the multi-dimensionality of the supernova engine because they are only able to provide images of optically thin regions far away from the central core. The GWs from CCSNe are the primary observables, which imprint live information on the central engine.

From a theoretical point of view, understanding the origin of the explosion multi-dimensionality is indispensable for clarifying the as-yet-uncertain CCSN mechanisms. After half a century of continuing effort, theory and neutrino radiation-hydrodynamics simulations are now converging to a point that multi-dimensional (multi-D) hydrodynamics instabilities play a pivotal role in the neutrino mechanism [214], the most favored scenario to trigger explosions. In fact, self-consistent simulations in three spatial dimensions (3D) now report shock revival of the stalled bounce shock into explosion by the multi-D neutrino mechanism (see Refs. [215–218] for recent reviews).

7.1.2. Observations and measurements

The most distinct GW emission process commonly seen in recent self-consistent 3D models is associated with the excitation of core/PNS oscillatory modes (see, e.g., Refs. [219–222]). The dominant modes are quadrupolar ($\ell = 2$) deformations of the PNS excited by non-spherical mass accretion onto it (see also Sect. 6.3). The characteristic GW frequency increases almost monotonically with time due to an accumulating accretion onto the PNS, which ranges from $\sim$ 500 to 1000 Hz (see Ref. [223] for a dedicated scheme to detect the ramp-up GW signature from the noises).

In addition to the prime GW signature, standing accretion shock instability (SASI) (see, e.g., Ref. [224]) has also been considered as a key to generate GW emission in the post-bounce supernova core. It has become apparent [219,220,222] that the predominant GW emission from CCSNe is produced in the same region behind the post-shock region where both SASI and neutrino-driven convection vigorously develop (see, e.g., Ref. [225] for a review). The GW emission from this region—from just above the neutrinospheres at densities of roughly 10^{11} g/cm^3 and inward—is determined by the effects of the super-nuclear EOS, as well as the impact of hydrodynamic instabilities present in the post-shock flow (see, e.g., Ref. [221]). The typical frequency of SASI-induced GWs is in the range of $\sim$100–250 Hz, which is in the best sensitivity range of the currently running interferometers.

Rapid rotation in the iron core leads to significant rotational flattening of the collapsing and bouncing core, which produces a time-dependent quadrupole (or higher) GW emission (see, e.g., Ref. [226] for a review). For bounce signals with a strong and characteristic signature, the iron core must rotate rapidly enough[3]. The GW frequency associated with the rapidly rotating collapse and bounce is in the range of $\sim$ 600–1000 Hz.

[3] Although rapid rotation and the strong magnetic fields in the core are attracting great attention as the key to solving the dynamics of collapsars and magnetars, one should keep in mind that recent stellar evolution

Another feature distinguishing GWs from CCSNe is circular polarization. The importance of detecting circular GW polarization from CCSNe was first discussed in Ref. [228] in the context of rapidly rotating core-collapse. More recently, Ref. [229] presented an analysis of the GW polarization using results from 3D general-relativistic simulations of a non-rotating $15M_\odot$ star [222]. The amplitude of the GW polarization was shown to become larger for the 3D general-relativistic model that exhibits strong SASI activity. The non-axisymmetric flows associated with spiral SASI give rise to the circular polarization. If detected, it will provide us with a new probe into the SASI activity in the pre-explosion supernova core. Note that spiral SASI develops mainly outside of the PNS, so that circular polarization from spiral SASI has different features in the spectrogram compared to the stochastic, weak circular polarization from the PNS oscillations that have no preferential direction of development [229]. By estimating the SNR of the GW polarization, they pointed out the possibility that the detection horizon of circular polarization could extend by more than a factor of several times farther compared to that of the GW amplitude. In order to detect the GW circular polarization with a high SNR, joint GW observation with KAGRA in addition to two LIGOs and Virgo is indispensable.

7.1.3. Future prospects

Each phase of a CCSN has a range of characteristic GW signatures and GW polarization that can provide diagnostic constraints on the evolution and physical parameters of a CCSN and on the explosion hydrodynamics. The GW signatures described in this section commonly appear in the frequency range of 100–1000 Hz in recent simulations of CCSNe. Among them, the PNS oscillatory modes are currently recognized as a model-independent GW signature. The characteristic frequencies of the fundamental (f/g) modes are predominantly dependent on the PNS mass (M) and the radius (R), however, in a non-trivial manner [206]. In order to break the degeneracy, the detection of other eigenmodes (p, w modes) of the PNS oscillations is mandatory. In fact, GW asteroseismology of PNSs has just started [206,207,211] (see also Sect. 6.3). The outcomes of this should reveal the requirement of KAGRA (and the next-generation detectors) to detect the whole of the eigenmodes (presumably extending up to several kHz) for future CCSN events. This could be done in the next five years.

For the detectability of GWs from PNSs, see Sect. 6.3. The GWs due to SASI for a Galactic event may be detected with the SNR of the GW signals predicted in the most recent 3D CCSN models in the range of ∼4–10 for aLIGO [221]. With the third-generation detectors online (e.g., Cosmic Explorer), these signals would never be missed for CCSN events throughout the Milky Way. A current estimate of SNR for GWs from rapidly rotating collapse and bounce based on predictions from a set of 3D models using a coherent network analysis shows that these GW signals could be detectable up to about ∼ 20 kpc for the most rapidly rotating model ([230]; see also Refs. [231,232]). If the spectra of the supernovae are assumed to be flat in the frequency range of 100 Hz–1 kHz, we can quantitatively compare performances of various configurations of possible KAGRA upgrades by defining the SNR ratio $r_{\alpha/\beta} \equiv r_\alpha/r_\beta$ for the configurations α and β where r_α is defined in Eq. (5) and a similar equation holds for the β configuration. For the frequency range between $f_{\rm low} = 100$ Hz and $f_{\rm high} = 1$ kHz, the SNR ratios of KAGRA+ to bKAGRA averaged over relevant frequencies are 40 kg 1.51, FDSQZ 2.35, HF 3.43, Combined 3.55. However, since the spectral evolution of the CCSN GWs has not been completely clarified yet and it does depend upon the details of CCSN modeling (such as on

calculations predict that such an extreme condition can be realized only in a special case [227] ($\lesssim$ 1% of massive star population).

the initial rotation rates and the progenitor masses), it is too early to have a quantitative discussion about the best-suited sensitivity curves for KAGRA+. Because recent CCSN simulations indicate that the important GW frequency to unveil the physics of CCSNe will be $\geq$ 100 Hz, all the candidate upgrades except for LF should help enhance the chance of detection.

8. The early Universe

8.1. GWs from inflation

8.1.1. Scientific objective

Inflation, an accelerated expansion phase of the very early Universe, was proposed in the 1980s to solve problems in the standard model of the Big Bang theory, such as the horizon, flatness, and monopole problems [233–236]. A key feature of inflation is that the rapid expansion stretches quantum fluctuations in a scalar field to classical scales and generates primordial density fluctuations [237–241], which become the seeds of galaxies. The nearly scale-invariant spectrum of scalar perturbations, predicted by the inflationary theory, is strongly supported by cosmological observations of the cosmic microwave background and galaxy surveys. The same mechanism also applies to quantum fluctuations in spacetime, which produce a stochastic background of GWs over a wide range of frequencies with a scale-invariant power spectrum [242–244]. The detection of inflationary GWs is a key to test inflation and distinguish a number of models since the amplitude and spectral index strongly depend on the model.

8.1.2. Observations and measurements

The amplitude of the GWs is typically far below the sensitivity of the ground-based detectors. The dimensionless parameter, $\Omega_{\rm GW}$, which describes the energy density of GWs per logarithmic frequency interval, is roughly given by $\Omega_{\rm GW} \simeq 10^{-15}(H_{\rm inf}/10^{14}\,{\rm GeV})^2$ for a scale-invariant primordial spectrum $\Omega_{\rm GW} \propto f^0$, where $H_{\rm inf}$ is the Hubble expansion rate during inflation. Inflation predicts a slightly red-tilted spectrum, which further reduces the amplitude at high frequency. For example, the model predicts $\Omega_{\rm GW} \sim 10^{-16}$ at 100 Hz for chaotic inflation and $\Omega_{\rm GW} \sim 10^{-17}$ for R^2 inflation, while the cross correlation between LIGO, Virgo, and KAGRA with their final design sensitivities is expected to reach a stochastic background of $\Omega_{\rm GW} \sim 10^{-9}$. For details on the shape of the spectrum, see Refs. [245,246].

Note that a search for a stochastic GW background is performed by cross-correlating data from different detectors over a long time period. The sensitivity is determined by noise curves of the multiple detectors as well as the observation time. Since the two detectors of LIGO have advantages in both sensitivity and observation time, the sensitivity of the four-detector network $\Omega_{\rm GW} \sim 10^{-9}$ will be dominated by LIGO detectors, while KAGRA with the current design sensitivity would not contribute to an increase in the overall sensitivity. Currently LIGO–Virgo O2 data provide an upper limit of $\Omega_{\rm GW} < 6.0 \times 10^{-8}$ for a scale-invariant spectrum [247].

Although the ground-based detectors are not sensitive enough to detect standard inflationary GWs, some models going beyond the standard picture predict a blue-tilted spectrum, e.g., string gas cosmology [248], super-inflation models [249,250], G-inflation [251], non-commutative inflation [252,253], particle production during inflation [254,255], Hawking radiation during inflation [256], a spectator scalar field with small sound speed [257], massive gravity [258], and so on. The amplitude of the inflationary GW spectrum is constrained at low frequencies by the cosmic microwave background

$\Omega_{\rm GW} \lesssim 10^{-15}$, but the amplitude can be large at a frequency of $\sim$ 100 Hz if the spectrum is blue-tilted. There would be a chance for the ground-based detectors to detect inflationary GWs if the spectral index of the spectrum n_T is larger than ~ 0.5.

Another possibility for the ground-based detectors is to probe a non-standard Hubble expansion history of the early Universe [259–264]. Information on the expansion rate, which is determined by the dominant component of the Universe, is imprinted in the spectrum of inflationary GWs. For a scale-invariant primordial spectrum, the spectral dependence of the stochastic background becomes $\Omega_{\rm GW} \propto f^{2(3w-1)/(3w+1)}$, where w is the EOS of the Universe. In the standard cosmological model, the matter-dominated ($w = 0$) and radiation-dominated ($w = 1/3$) phases yield $\Omega_{\rm GW} \propto f^{-2}$ and f^0, respectively. When one considers a kination-dominated phase ($w = 1$) soon after inflation, the spectral amplitude is enhanced at high frequency by the dependence $\Omega_{\rm GW} \propto f$ and peaks at a frequency corresponding to the size of the Universe at the end of inflation, which is typically higher than $\sim$ 100 Hz. Although it is difficult to find a case where GWs are detectable by ground-based experiments satisfying the Big Bang nucleosynthesis (BBN) bound [265,266], $\Omega_{\rm GW} \lesssim 10^{-5}$ for $f \gtrsim 10^{-10}$ Hz, the upper bound on the stochastic background is still helpful to explore early-Universe physics beyond the standard cosmology.

8.1.3. Future prospects

The SNR for a stochastic GW background is computed by taking cross correlation between detector signals [267], and given by

$$\mathrm{SNR}_{IJ} = \frac{3H_0^2}{10\pi^2}\sqrt{2T_{\rm obs}}\left[\int_0^\infty df\, \frac{|\gamma_{IJ}(f)|^2\Omega_{\rm GW}(f)^2}{f^6 S_{n,I}(f)S_{n,J}(f)}\right]^{1/2}, \tag{11}$$

where H_0 is the Hubble constant, $T_{\rm obs}$ is the observation time, and $S_{n,I}(f)$ is the noise spectral density with I and J labeling two different detectors. The overlap reduction function $\gamma_{IJ}(f)$ is given by the detector responses of the two polarization modes F^+ and $F^\times$ as

$$\gamma_{IJ}(f) \equiv \frac{5}{8\pi}\int d\hat{\Omega}(F_I^+F_J^+ + F_I^\times F_J^\times)e^{-2\pi i f\hat{\Omega}\cdot(\mathbf{x}_I-\mathbf{x}_J)}, \tag{12}$$

where $\mathbf{x}$ describes the position of the detector and $\hat{\Omega}$ specifies the propagation direction of GWs. For a network of N detectors, the total SNR is given by

$$\mathrm{SNR} = \left[\sum_{I=1}^{N}\sum_{J<I}^{N}\mathrm{SNR}_{IJ}^2\right]^{1/2}. \tag{13}$$

As seen in the overlap reduction function, the SNR depends on the distance and relative orientation of the detectors. For KAGRA, correlating with AdV+ is better than with A+ because of the relative orientation. Assuming a flat spectrum of $\Omega_{\rm GW}(f)$, the sensitivities of the pair of KAGRA and AdV+ to $\Omega_{\rm GW}$ with SNR $= 5$ are 1.1×10^{-7} for bKAGRA, 3.4×10^{-8} for LF, 8.3×10^{-8} for 40 kg, 1.1×10^{-7} for FDSQZ, 3.3×10^{-7} for HF, and 5.0×10^{-8} for Combined. The lower-frequency upgrades give better sensitivities. However, the sensitivity between two A+ is 4.0×10^{-9}, which is an order of magnitude better than those with KAGRA because of the much closer separation of the detector pair. Therefore, KAGRA is not good for detection but will be able to play an important role in determining the spectral shape and measuring anisotropy, non-Gaussianity, and polarizations, which are discussed in Sect. 8.3.

8.2. GWs from phase transition

8.2.1. Scientific objective

The thermal history of the Universe after BBN, which takes place at a temperature scale on the order of 1 MeV, has been well established thanks to amazing progress made by cosmological observations. On the other hand, our knowledge about the Universe earlier than BBN is quite limited. If we extrapolate our understanding of particle physics, several phase transitions should occur in such early stages of the Universe. These include the QCD phase transition, the electroweak phase transition, the GUT phase transition and some phase transitions of new models beyond the standard model of particle physics. The nature of a phase transition is classified according to the evolution of the order parameter: first order or second order. In addition, the case where the order parameter changes smoothly and no phase transition occurs is referred to as a crossover. For a first-order phase transition, latent heat is released, supercooling occurs, and phases are mixed like boiling water. Non-uniform motion of vacuum bubbles during the first-order phase transition produces GWs. Therefore, one can survey new physics models involving a first-order phase transition by observing GWs [268].

8.2.2. Observations and measurements

GWs produced by the first-order phase transition in the early Universe are stochastic: isotropic, stationary, and unpolarized. They are characterized only by the frequency. There are three known sources for GWs from the first-order phase transition: collisions of vacuum bubble walls, sound waves in the plasma, and plasma turbulence. In general, one has to sum these contributions. For typical non-runaway bubbles, the contribution from sound waves is dominant and the peak energy density[4] is roughly [269]

$$\Omega_{\mathrm{GW,peak}} h^2 \sim 10^{-6}\, \kappa^2 \alpha^2 v \left(\frac{\beta}{H_*}\right)^{-1}; \tag{14}$$

the peak frequency is

$$f_{\mathrm{peak}} \sim 10^{-5} \times v^{-1} \left(\frac{\beta}{H_*}\right) \left(\frac{T_*}{100\ \mathrm{GeV}}\right) \mathrm{Hz}. \tag{15}$$

Here, T_* is the transition temperature, α is the ratio of the released energy (latent heat) to the radiation energy density, β is the inverse of the time duration of the phase transition, H_* is the Hubble expansion parameter at T_*, κ is the ratio of vacuum energy converted into fluid motion, and v is the bubble wall velocity. If one selects a new physics model and chooses a model parameter set, one can compute the finite-temperature effective potential, from which the above quantities are derived. Namely, the above quantities are functions of the underlying model parameters. Therefore, the number of free model parameters can be generally reduced by measuring the stochastic GW spectrum.

8.2.3. Future prospects

Among new physics models that involve phase transitions, models with an extended Higgs sector achieving the electroweak phase transition are of the most importance and should be addressed. Although the Higgs boson has been discovered at the CERN Large Hadron Collider and spontaneous breaking of the electroweak symmetry has been established, the dynamics of the electroweak

[4] The energy density of gravitational waves Ω_{GW} and the power spectral density S_h is related through $\Omega_{\mathrm{GW}} H_0^2 = (2\pi^2/3) f^3 S_h$.

symmetry is still unknown. The baryon asymmetry of the Universe may be accounted for by electroweak baryogenesis, which requires a strongly first-order electroweak phase transition. Since the transition temperature of the electroweak phase transition is of the order of 100 GeV, unfortunately the peak frequency of the predicted GW spectrum falls in the range of 10^{-3}–0.1 Hz, regardless of the details of the extended Higgs models. Therefore, the detection of GWs from the electroweak phase transition and determination of the model parameters of extended Higgs models are challenging for the KAGRA upgrade and need future space-based interferometers, such as LISA and DECIGO [270,271]. Conversely, one can envisage and construct hypothetical models with phase transition temperature of 10^5–10^7 GeV so that the peak frequency matches the KAGRA frequency band [272]. Even in such models, an enormously large latent heat and/or a very long transition duration are necessary for GW signals to hit the sensitivity curves for KAGRA upgrade candidates. Another issue concerns uncertainties in computing the spectrum of generated stochastic GWs at a first-order phase transition. In particular, numerical simulations of the dynamics of nucleated bubbles are rather cumbersome. With the development of computational techniques, the result in Eq. (14) might be revised by one order of magnitude or more. Therefore, although it is difficult to predict the detectability of GWs from a phase transition, KAGRA will play an important role in constraining models of first-order phase transitions that take place at temperatures of around 10^5–10^7 GeV.

8.3. Distinguishing the origins of the GW backgrounds

8.3.1. Scientific objective

GWs generated in the early Universe are typically in the form of a stochastic background, which is a continuous noise-like signal spreading in all directions, while numerous astrophysical GWs also become a stochastic background by overlapping with one another. Even if a stochastic background is detected, it may be difficult to identify its origin among the many cosmological and astrophysical candidates.

8.3.2. Observations and measurements

A standard data analysis provides information only on the amplitude and the tilt of the spectrum. In order to discriminate the origin of the GW background, we need to go beyond conventional data analysis and extract more information, such as the spectral shape [273], anisotropy [274,275], polarization [276,277], and non-Gaussianity (or so-called popcorn background) [278–280]. Anisotropy and non-Gaussianity could arise in a GW background formed by overlapping GW bursts. Typical examples are those originating from astrophysical sources and cosmic strings. Additional GW polarizations appear when the generation process is related to physics beyond general relativity (see Sect. 9.4). Therefore, they can be used as indicators of specific generation mechanisms.

The spectral shape of the stochastic background depends strongly on its origin and can be generally used to distinguish a wide range of generation models. Many models predict a spectral shape spanning a broad range of frequencies. In this case, the ground-based detectors observe part of the spectrum because of the limited sensitivity range of frequency, and multi-band observations are needed to determine the whole spectral shape. However, some models predict a peaky spectral shape; one good example testable by the ground-based detector network itself is a GW background generated by superradiant instabilities [281]. One way to obtain the spectral shape in data analysis is to use broken power-law templates instead of the currently used single power-law templates [273,282]. The uncertainties in the parameter determination decrease in proportion to the inverse of the SNR, and at least SNR $\gtrsim$ 10 is necessary to obtain useful information on the entire spectral shape. If

detection were made with higher SNR, the analysis could be extended to the whole spectral shape reconstruction with multiple frequency bins, which evaluates the spectral index in each bin (see Ref. [283] for a discussion on LISA, which could be applied to ground-based experiments).

8.3.3. Future prospects

In general, a higher SNR is necessary not only to determine the spectral shape but also to obtain the above-mentioned additional properties of the stochastic background. Since inflationary GWs have a red-tilted spectrum in terms of strain amplitude, an improvement of sensitivity at lower frequency would be helpful to test more properties of the stochastic background. On the other hand, as previously mentioned, the sensitivity of the ground-based detectors is not enough to detect a standard inflationary GW background, and a blue-tilted spectrum is necessary to enhance the amplitude for detection. If $n_T > 3$, where we define the spectral tilt as $\Omega_{\rm GW} \propto f^{n_T}$, an improvement of sensitivity at higher frequencies becomes important (see Fig. 1 of Ref. [273]). Astrophysical GWs also have a blue-tilted spectrum $n_T = 2/3$, but when the tilt is not so steep, sensitivity at mid-frequencies (20–50 Hz) is more important.

Apart from sensitivity for the amplitude, multiple detectors facing different directions provide independent information about anisotropy and polarization, and thus the inclusion of KAGRA is essential.

9. Test of gravity

9.1. Test of consistency with general relativity

9.1.1. Scientific objective

There are currently no alternatives to Einstein's GR that are physically viable. As such, one cannot test GR by comparing the data with waveforms in alternative theories. Instead, one can test for the consistency of the signal with GR. In doing so, one must ensure that any deviation from GR cannot be attributed to noise artifacts, but instead are intrinsic to the GW signal itself. However, this must be done without explicitly assuming an alternative model for gravity that governs the morphology of the GW signal.

9.1.2. Observations and measurements

Existing efforts largely focus on comparing different portions or aspects of the signal and require consistency amongst them. For example, one can verify the self-consistency of the post-Newtonian description of the inspiral phase, and from the phenomenological GR model of the merger–ringdown [284–289]. In addition, one can also test the final remnant mass and spin, as determined from the low-frequency (inspiral) and high-frequency (post-inspiral) phases of the signal for mutual consistency [290,291]. Furthermore, one can also compare the residual signal after subtracting the best-fitting GR waveform to the expected statistical properties of the noise. For the first set of BBH detections, no test so far has revealed any significant deviations from GR [292–295]. Instead, constraints on various possible beyond-GR effects have been placed. For example, the fractional deviations to the lowest post-Newtonian parameters have been constrained to tens of %, whereas the higher post-Newtonian orders and the merger–ringdown parameters are constrained to around 100%. Moreover, the possibility of dipolar radiation has been constrained to the % level, and the mass of the graviton has been constrained to $m_g \leq 4.7 \times 10^{-23}\,{\rm eV}/c^2$.

9.1.3. Future prospects

In the future, as the LVK network operates at its full strength, we can anticipate several effects that will improve our ability to constrain general relativity. Firstly, the improved detection rate will allow us see many events for which the different aspects of their dynamics are covered by the network's sensitive frequencies. Secondly, more detections also means that our constraints will be improved statistically. While we do not expect improvements of orders of magnitude, it will help to shrink the parameter space of possible deviations from GR. Thirdly, a full LVK network will greatly enhance tests that require multiple detectors, including tests for alternative polarizations (see Sect. 9.4). These tests are expected to greatly improve as KAGRA, as the fourth detector, improves its sensitivity. Finally, the prospect of observing novel source classes, including highly eccentric systems, highly precessing systems, and even head-on collisions will open up a entirely new suite of tests.

In the era of KAGRA+, we expect more detections of BBHs and BNSs, and anticipate detections of BH–NS systems. The precise way in which KAGRA+'s sensitivity develops will govern the way in which it will contribute to tests of GR. For example, with the focus on low-frequency sensitivity, one improves the insight into the merger and ringdown of heavy BHs, where the gravitational fields are the strongest. In contrast, high-frequency sensitivity allows one to track lower-mass binary mergers for a longer period of time, which improves the precision of the consistency checks. Additionally, by improving the sky coverage and increasing the multiple-detector live time, KAGRA+ will increase the number of detected events and thereby reducing the statistical errors due to detector noise by combining results from multiple events.

9.2. GW generation in modified gravity

9.2.1. Scientific objective

We can raise several motivations to study modified gravity: a) GR is not an ultraviolet (UV) complete theory. It should be modified to describe physics near the Planck scale. b) Cosmology based on GR requires dark components to explain the observed Universe, such as dark matter and dark energy. It is attractive if we can naturally explain the observed Universe by a well motivated modification of gravity without introducing cosmological constant. c) To test GR, it is not enough to know the prediction based on GR when we use GWs as a probe. Since GW data are noisy, an appropriate projection of the data in the direction predicted by the possible modification of gravity is necessary to obtain a meaningful constraint.

As possible modifications of gravity, there are several categories. One is to add a new degree of freedom like a scalar field in scalar–tensor gravity. Such extra degrees of freedom are strongly constrained by existing observations, since they introduce a fifth force. There are various ways, however, to hide the fifth force. 1) Sufficiently small coupling to ordinary matter. 1a) Coupling through higher derivative terms, which only becomes important under strong field environments. 1b) Some non-linear mechanism to reduce the coupling like the chameleon/Vainshtein mechanism [296,297]. 2) Giving a sufficiently large mass to the field that mediates the fifth force.

There is also a possibility to modify gravity without introducing a new degree of freedom. One example is the so-called minimal extension of massive gravity. Phenomenologically, we can give a small mass to the graviton in this kind of model, but the graviton mass at the present epoch is already strongly constrained by the observation of GW170817.

Table 8. List of representative possible modifications in gravitational wave generation. The leading post-Newtonian order of the correction in phase relative to the quadrupole formula is shown.

modification	post-Newtonian order	References
variable Newton's constant	−4PN	[301]
BH evaporation	−4PN	[302]
dipole radiation	−1PN	[303]
non-covariant massive graviton	1PN	[304]
dynamical Chern–Simons gravity	2PN	[305]

9.2.2. Observations and measurements

We focus on compact binary inspirals. In this context, the most probable modification of the generation mechanism of GWs is the one caused by the change in orbital evolution. The orbital evolution is governed by two aspects. One is the conservative part of the gravitational interaction and the other is the dissipative effects of radiation. It is not so obvious which effect is more important even in the weak field regime. Hence, we need a little more careful investigation of each model.

Whichever effect dominates, the main purpose of this study is the same. What we want to clarify is whether or not there exists a new effective propagating degree of freedom that appears only when we consider extremely compact objects like BHs and NSs.

There might be various possibilities. From the observational point of view it is convenient to introduce the parametrized post-Einstein (PPE) framework [298]. The waveform of a quasi-circular inspiral in the Fourier domain will be given in the form of

$$h(f) \approx A(f) f^{-7/6} e^{i\Psi(f)} \tag{16}$$

in GR. The waveform is characterized by the functions $A(f)$ and $\Psi(f)$ and they are modified in the extended theories as

$$A(f) \to \left(1 + \sum_i \alpha_i u^{a_i}\right) A_{\rm GR}(f), \qquad \Psi(f) \to \left(\Psi_{\rm GR}(f) + \sum_i \beta_i u^{b_i}\right), \tag{17}$$

with $u := \pi M f$. Since the test of gravity using GW data is more sensitive to the modification in the phase $\Psi(f)$, we will focus on it.

The smallest non-vanishing value of b_i is related to the leading post-Newtonian order. The nth post-Newtonian correction appears as $b = (2n-5)/3$. Here we list representative possible modifications of gravity with the post-Newtonian order of the leading correction in phase in Table 8. BH evaporation is negligible in the ordinary scenario, but can be accelerated if there are many massless hidden degrees of freedom. For the dipole radiation to be emitted, charge not proportional to the mass of each constituent object is required. One typical example is the scalar–tensor theory. Although BHs are thought not to bear a scalar hair in many cases, they can have a scalar charge in some models like in Einstein–Gauss–Bonnet-dilaton theory [299]. If we naively consider that gravitons have non-vanishing mass, the dispersion relation is also modified to give 1PN-order correction, although this is not the effect in the generation of gravitational waves. However, if we consider covariant theories of massive gravity, we need to consider a bigravity model [300]. As a modification that appears at the 1PN order, one may think of a model in which the mass of each constituent object depends on the Newton potential.

As a typical modification of GR, the scalar–tensor theory is often discussed. If the binary members have some scalar charges coupled to the extra degree of freedom, we have dipolar radiation. Although the overall magnitude also depends on the coupling strength, if we focus only on the frequency dependence, the flux due to dipolar radiation is larger at a low frequency by the factor $(v/c)^{-2} \sim (m\omega)^{-2/3}$ compared with that due to GW radiation. On the other hand, the extra scalar degree of freedom changes the conservative part of the force, but there is no such enhancement in the sense of post-Newtonian order. Hence, at low frequency, where $v/c \ll 1$ the modification to the conservative gravitational interaction can be neglected.

For the modification that predicts negative post-Newtonian order, the deviation from GR is relatively larger at lower frequencies, compared with GR contributions. Therefore, it is not so easy for GW observations to compete with the constraint from the observations at lower frequencies, such as pulsar timing.

There are some more detailed aspects that cannot be expressed by the PPE framework. One possibility is spontaneous scalarization. When we consider BNSs, each NS in isolation may not have a scalar charge. However, there is a region in the model parameter space in which instability occurs as the binary separation decreases and both NSs get charged. Another possibility is that the mediating scalar field is massive. This is quite likely to avoid instability similar to spontaneous scalarization occurring in the whole Universe after the temperature of the Universe becomes 10 MeV or lower. If the instability occurs, the success of the Big Bang nucleosynthesis will be significantly damaged. This gives the constraint on the mass of the mediating field as greater than 10^{-16} eV or so [306], which is comparable to the constraint from pulsar timing (PSRJ0348+0432). On the other hand, ground-based detectors are sensitive to modification if the mass is smaller than 10^{-12} eV. If the mass is in the range between these two, the existence of the extra degree of freedom might be probed only by GWs.

Basically we check the deviation of the observed GW signal from GR templates. For this purpose, it is better to have a better theoretical template based on each candidate of modified gravity. In particular this demand is higher when we consider the models whose leading-order modification appears at the positive post-Newtonian order. In such models, we have more chances to observe the largest deviation at the final stage of inspirals. In many cases, this task remains a challenge for theorists.

9.2.3. Future prospects

As long as we consider BHs with masses larger than a few times the solar mass and NSs, it seems difficult to use a high-frequency band to give constraints on modified gravity. In the case of BHs, we do not have many signals at very high frequencies. In the case of binary NSs, high-frequency signals can be expected but it might be difficult to disentangle the effects of modified gravity from the uncertainty of the complex physics of NSs.

In general, when we wish to give a tighter constraint on the parameters contained in the waveform template, a broader observational sensitivity band is advantageous. A broadband observation is not necessarily realized by a single detector. It would work well if a wider range of the frequency band is covered by plural detectors as a whole. In this sense, it would be necessary to negotiate among the various plans of future upgrade of detectors.

In the near future we will establish a network composed of LIGO, Virgo, and KAGRA. From the point of view of detecting modification in GW generation, the improvement of the constraints

depends on the increase of statistics and finding of some golden events with appropriate binary parameters and a large SNR.

9.3. GW propagation test

9.3.1. Scientific objective

The properties of GW propagation are changed when a gravity theory is modified from GR. In particular, a great deal of attention is paid to such modifications at cosmological distances because the extended theories of gravity may explain the accelerating expansion of the Universe. In other words, testing GW propagation can constrain the possible modification of gravity at cosmological distances and give us an implication about the physical mechanism of the accelerating cosmic expansion [307]. According to Ref. [308], the modifications of GW propagation in the effective field theory are expressed in general as

$$h''_{ij} + (2+\nu)\mathcal{H}h'_{ij} + (c_{\rm T}^2 k^2 + a^2\mu^2)h_{ij} = a^2\Gamma\gamma_{ij} \ , \tag{18}$$

and are characterized by four properties: propagation speed $c_{\rm T}$, amplitude damping rate ν, graviton mass μ, and a source term Γ. Each modification appears differently in a specific theory, but this framework allows us to test many classes of gravity theory at the same time. Among the modifications, the propagation speed is important to test the violation of the Lorentz symmetry and the quantum nature of spacetime (modified dispersion relation). The amplitude damping rate is equivalent to the variation of the gravitational constant for GWs and enables us to test the equivalence principle. The graviton mass is a characteristic quantity in massive gravity. If parity in gravity is violated, it modifies in general the propagation speeds and the amplitude damping rates in Eq. (18) differently for left-handed and right-handed polarizations with opposite signs as shown in Refs. [309,310].

9.3.2. Observations and measurements

The coincidence detection of GW170817/GRB170817A [4] gave us the first opportunity to measure the speed of a GW from the arrival time difference between a GW and an EM radiation[5], as was predicted in Ref. [313], and constrained the deviation from the speed of light at the level of 10^{-15} [143]. Based on this constraint on GW speed, a large class of theories as alternatives to dark energy have already been almost ruled out [314–317]. The graviton mass μ has been tightly constrained from the observation of BBH mergers in the range of $\mu < 5.0 \times 10^{-23}$ eV [295], which is tighter than that obtained in the Solar system [318]. On the other hand, the amplitude damping rate ν was also measured from GW170817/GRB170817A for the first time in Ref. [319], but the constraint is still too weak, $-75.3 \leq \nu \leq 78.4$. However, the anomalous amplitude damping rate is one of the prominent signatures of modified gravity, which is likely to be accompanied by a gravity modification explaining the cosmic acceleration, and plays a crucial role when we test gravity at cosmological distances [320].

In generic parity-violating gravity including recently proposed ghost-free theories with parity violation [321], not only the amplitude damping rate but also the propagation speed are modified, in contrast to Chern–Simons modified gravity in which the GW speed is the speed of light. From GW170817/GRB170817A, since a GW is required to propagate almost at the speed of light, the

[5] Before GW170817/GRB170817A, measurements of the speed of a GW had been done with GWs from BBHs based on the arrival time difference between detectors [311,312].

Table 9. Median SNR, median errors of ν, and median errors of μ in units of 10^{-23} eV. The BBH is at a distance of $z = 0.1$, the $10\,M_\odot$ BH–NS is at $z = 0.06$, and the BNS with masses $1.4\,M_\odot$ is at $z = 0.03$. bKAGRA, LF, HF, 40 kg, FDSQZ, and Combined denote the detector network composed of A+, AdV+, and bKAGRA or KAGRA+ (one of LF, HF, 40 kg, FDSQZ, and Combined).

source	quantile	bKAGRA	LF	HF	40 kg	FDSQZ	Combined
SNR	$30\,M_\odot$ BBH	77.4	73.9	76.6	78.0	79.6	84.8
	$10\,M_\odot$ BBH	32.3	32.9	34.2	33.9	32.3	36.6
	$10\,M_\odot$ BH–NS	25.1	23.7	24.8	25.2	26.4	27.2
	BNS	24.3	24.2	24.7	24.7	24.9	27.5
ν	$30\,M_\odot$ BBH	1.47	1.69	1.50	1.27	1.48	1.09
	$10\,M_\odot$ BBH	3.13	3.85	3.56	2.74	3.08	2.56
	$10\,M_\odot$ BH–NS	7.86	9.53	7.96	6.91	7.32	6.24
	BNS	13.8	17.6	14.1	12.6	13.3	11.4
μ	$30\,M_\odot$ BBH	4.76	4.78	4.53	4.86	4.77	4.87
	$10\,M_\odot$ BBH	11.9	11.7	11.6	11.9	11.9	11.6
	$10\,M_\odot$ BH–NS	15.7	15.4	15.9	15.9	15.5	15.4
	BNS	28.0	27.9	28.0	28.1	28.1	27.6

parity violation in the GW sector of the theory has been constrained almost to that in Chern–Simons gravity, allowing only the amplitude damping rate to differ from GR [309].

9.3.3. Future prospects

To forecast the abilities to measure the modified gravity parameters with a future detector network including bKAGRA and KAGRA+, we estimate the measurement errors of the model parameters in the modified GW waveform with the Fisher information matrix (for details of the analysis, see Ref. [322]). For the waveform, we consider the simplest one in which the amplitude damping rate ν and the graviton mass μ are assumed to be constant, taking $c_T = 1$ and $\Gamma = 0$. Setting $c_T = 1$ is motivated by the existing constraint from GW170817/GRB170817A and $\Gamma = 0$ is true in most gravity theories including the Horndeski theory [308]. Under the assumptions above, the GW waveform is [322]

$$h = (1+z)^{-\nu/2} e^{-ik\Delta T} h_{\rm GR}, \qquad \Delta T = -\frac{\mu^2}{2k^2}\int_0^z \frac{dz'}{(1+z')^3\mathcal{H}}\,, \tag{19}$$

where k is the wave number. The waveform $h_{\rm GR}$ is the one in GR. Then the luminosity distance observed by a GW is interpreted as an effective one, $d_L^{\rm gw}(z) = (1+z)^{-\nu/2} d_L(z)$, which differs from the standard one for EM waves, d_L. To break the parameter degeneracy and determine ν separately, one needs to know the source redshift independently of the GW observation. We assume that the source redshift is obtained somehow from EM observations and impose a prior on z with a standard deviation $\Delta z = 10^{-3}$. We will generate 500 binary sources with random sky locations and other angular parameters, having the network SNR $\rho > 8$, for each case with fixed masses and redshifts.

In Table 9, the parameter estimation errors of ν and μ with detector networks including KAGRA are shown. The sensitivities are better for heavier binaries and best for a $30\,M_\odot$ BBH. The upper limits on graviton mass are similar to the current constraint and are not expected to be improved significantly with the ground-based detectors in the future. Since the graviton mass affects the GW phase more at lower frequencies, the constraints from the planned space-based detectors such as LISA [323] and DECIGO [324] will be much stronger down to $\mu \sim 10^{-26}$–10^{-25} eV [325,326]. On the other hand,

there are modest improvements of the sensitivity to ν with the addition of bKAGRA or KAGRA+ to the global detector network. For a measurement of ν with a 30 $M_\odot$ BBH, the improvement factors of the errors are LF 0.87, 40 kg 1.16, FDSQZ 0.99, HF 0.98, Combined 1.35, reaching $\Delta\nu = 1.09$ in the best case.

9.4. GW polarization test

9.4.1. Scientific objective

In GR, GWs have only two tensor polarization modes. However, a general metric theory of gravity allows four non-tensorial polarization modes in addition to two tensor modes [327]. The properties of GW polarization depend on the alternative theories of gravity. Thus, the observations of polarizations can be utilized to test the nature of gravity. The testable degrees of freedom of GWs are related to the number of GW detectors and it is expected that the participation of KAGRA in the network of detectors make it possible to search for more polarizations more accurately [328,329]. Here, we shall consider KAGRA's potential for polarization tests of GWs from the most promising sources, i.e., compact binary coalescences.

9.4.2. Observations and measurements

In general, the Ith detector signal h_I of GWs propagating in the direction $\hat{\Omega}$ can be expressed as

$$h_I(t, \hat{\Omega}) = \sum_A F_I^A(t, \hat{\Omega}) h_A(t). \tag{20}$$

Here F_I^A is the antenna pattern function of the Ith detector for the polarization A and h_A is the GW waveform for the polarization $A = +, \times, x, y, b$, and ℓ modes, called plus, cross, vector-x, vector-y, breathing, and longitudinal modes, respectively. Provided that there are enough detectors, we can test the theory of gravity by solving the inverse problem, separating and evaluating the waveforms of polarization modes directly. Currently there are observational constraints on the non-tensorial polarization modes of GWs from binary systems by Bayesian inference with the simple substitution of the antenna pattern functions and the assumption of the waveform models [294,330]. They found Bayes factors of more than 200 and 1000 for GW170814 and logarithms of the Bayes factors of 20.81 and 23.09 for GW170817 in favor of the pure tensor polarization against pure vector and pure scalar, respectively.

Another method of model-independent searching for non-tensorial polarizations is constructing null streams, in which tensor signals are automatically canceled and only scalar and vector signals remain [331]. From three (four) detectors, one can obtain one (two) null stream(s) to search for one (two) additional polarization(s). However, as proposed in Refs. [329,332,333], a fortunate case in which more polarizations can be searched exists if an EM counterpart pins down the sky direction of a GW source. In this case, one additional polarization signal happens to be canceled and one more polarization can be searched. Even with four detectors including KAGRA, five polarizations can be searched if an EM counterpart is coincidentally detected.

9.4.3. Future prospects

We estimated the additional polarization amplitude parameters $\{A_{V_x}, A_{V_y}\}$, whose fiducial values are unity, in the following polarization model including two additional vector modes:

$$h_I = \{\mathcal{G}_{T,I} + A_{V_x}\mathcal{G}_{V_x,I} + A_{V_y}\mathcal{G}_{V_y,I}\}h_{\rm GR}, \tag{21}$$

Table 10. Medians of parameter estimation errors of additional polarization amplitude parameters for a $10M_\odot$–$10M_\odot$ BBH at $z = 0.05$ and a $1.4M_\odot$–$1.4M_\odot$ BNS at $z = 0.01$ with six global detector networks. The lower cutoff frequency is 10 Hz and the upper one is the twice the innermost stable circular orbit frequency for a point mass in Schwarzschild spacetime.

		bKAGRA	LF	HF	40 kg	FDSQZ	Combined
BBH	ΔA_{Vx}	0.284	0.325	0.353	0.258	0.283	0.236
	ΔA_{Vy}	0.344	0.456	0.434	0.312	0.342	0.281
BNS	ΔA_{Vx}	0.157	0.198	0.161	0.149	0.151	0.127
	ΔA_{Vy}	0.195	0.244	0.193	0.180	0.185	0.158

where $\mathcal{G}$ denotes the geometrical factors for each mode and includes the antenna pattern function, the Doppler phase, and the binary's orbital inclination angle [328]. We assume several detector network configurations: A+, AdV+, and bKAGRA or KAGRA short-term upgrade candidates (LF, HF, 40 kg, or FDSQZ), or the KAGRA longer-term upgrade candidate (Combined). In fact, the accurate waveforms of non-tensorial modes depend on a theory one considers and its specific parameters. However, accurate waveforms in alternative theories, especially in the strong gravity regime, are not yet well known because of the complexity of the field equations. Therefore, we consider only the inspiral phase and assume for the non-tensorial modes the same waveforms and cutoff frequency as the waveform in GR, $h_{\rm GR}$, and the ISCO frequency in GR, $f_{\rm ISCO}$. In other words, we consider the most pessimistic case in which separating polarization modes is most difficult in order to study fundamental separability. Table 10 shows the medians of parameter estimation errors for a $10M_\odot$–$10M_\odot$ BBH at $z = 0.05$ and a $1.4M_\odot$–$1.4M_\odot$ BNS at $z = 0.01$. The choice of network does not affect the amplitude estimation drastically. However, this kind of search is possible only with four detectors including KAGRA. Basically the errors of the additional polarization amplitude parameters are scaled by the network SNR depending on the detector network as long as the degeneracy among the amplitude parameters is broken. Thus, it would be best to separate polarizations with a 40 kg network among networks with KAGRA short-term upgrade candidates. This is because we are assuming promising sources with masses $\sim 1.4M_\odot$ or $\sim 10M_\odot$ whose merging frequencies are around the bottom of the 40 kg noise curve. If we compute the rms errors of two vector modes, the improvement factors (when the better case of BBHs and BNSs is taken) are LF 0.80, 40 kg 1.10, FDSQZ 1.04, HF 1.00, Combined 1.23. Therefore, the differences between the KAGRA short-term upgrade candidates are not large.

On the other hand, as for the polarization search with an EM counterpart, we do not need any information about GW waveforms of additional polarizations and do not have any preference on the KAGRA upgrades other than precise sky localization.

9.5. Black-hole spectroscopy

9.5.1. Scientific objective

When we treat GWs in the inspiral phase of binaries, there are many parameters to specify the binaries and also a variety of modifications of the waveforms (exotic compact objects, modification of gravity, and so on). Therefore, it will be difficult to test GR, especially in a strong gravity regime, because the derivation of the theoretical waveforms relies on the post-Newtonian approximation. The data analysis of quasi-normal modes (QNMs) of BHs observed in the ringdown phase is the best way to identify a compact object with the BH predicted by GR.

Table 11. SNR of the QNM GWs in the cases of $M_{\rm rem} = 60\ {\rm M}_\odot$ and $700\ {\rm M}_\odot$. Here we assume a luminosity distance of $r = 400\,{\rm Mpc}$.

$M_{\rm rem}$ [$\rm M_\odot$]	bKAGRA	LF	HF	40 kg	FDSQZ	Combined	AdVLIGO ZDHP	Aplus
				$q = 1$				
60	19.0	0.0844	45.4	26.9	36.6	56.3	22.0	48.6
700	62.4	335	19.2	71.0	56.9	128	253	403
				$q = 2$				
60	17.7	0.0795	40.0	25.3	32.9	50.9	19.8	43.5
700	51.0	307	15.6	57.5	45.9	103	208	332

The current status of the ringdown data analysis is that the least-damped ($n = 0$) QNM of the remnant BH has been observed but the SNR is too weak to determine the BH parameters precisely. We find for GW150914 that the late-time behavior is consistent with the ($\ell = m = 2, n = 0$) QNM [292]. Furthermore, to verify the no-hair theorem in GR, we need to measure not only the loudest mode but also multiple QNMs (see, e.g., Refs. [63,334,335]). It should be noted that the determination of the initial time of the ringdown phase is important in the data analysis because this affects the estimation of BH parameters (see, e.g., Refs. [336,337]). We also note that an analysis of multiple QNMs for GW150914 has been done in Ref. [338] recently. Reference [339] is the latest review on theoretical and experimental challenges in BH spectroscopy.

9.5.2. Observations and measurements

The (single-mode) ringdown waveform is given by

$$h(t) = Ae^{-(t-t_0)/\tau}\cos(2\pi f_{\rm R}(t-t_0) - \phi_0), \tag{22}$$

where A is the amplitude and τ and $f_{\rm R}$ are the damping time and frequency, respectively. t_0 and ϕ_0 denote the initial time and phase, respectively. The damping time is related to the quality factor Q as $\tau = Q/(\pi f_{\rm R})$. We note that it is not necessary to search the initial phase in the matched-filtering method [340]. In Table 11, we show the SNR of the QNM GWs in the cases of $M_{\rm rem} = 60\ {\rm M}_\odot$ and $700\ {\rm M}_\odot$ for various detector configurations. Here we assume a source distance of $r = 400\,{\rm Mpc}$.

In the case where the ringdown waveform is described by the QNMs of a BH predicted by GR, the frequency and quality factor are written in terms of the BH mass M and (non-dimensional) spin χ as

$$f_{\rm R} = \frac{1}{2\pi M}\left[f_1 + f_2(1-\chi)^{f_3}\right], \tag{23}$$

$$Q = q_1 + q_2(1-\chi)^{q_3}\,. \tag{24}$$

These are fitting formulae presented in Ref. [63], and f_i, q_i are the fitting coefficients summarized in Table 12.

In general, it is not clear which QNMs will be excited. Here, we restrict the excitation to that of a merging BBH. In this case, the ($\ell = m = 2$) QNM becomes the least-damped, dominant mode, and the other modes are subdominant modes. Furthermore, the mass ratios ($q = m_1/m_2$) of binaries and the spins of each BH affect the excitation. In the following analysis, we focus only on non-spinning BBHs for simplicity. Then, the next-dominant mode becomes the ($\ell = m = 3$) or ($\ell = m = 4$) mode

Table 12. Fitting coefficients for the QNM frequencies [63]. Here, we focus only on the lowest overtone ($n = 0$).

(ℓ, m)	f_1	f_2	f_3	q_1	q_2	q_3
$(2, 2)$	1.5251	−1.1568	0.1292	0.7000	1.4187	−0.4990
$(3, 3)$	1.8956	−1.3043	0.1818	0.9000	2.3430	−0.4810
$(4, 4)$	2.3000	−1.5056	0.2244	1.1929	3.1191	−0.4825

(see Fig. 4 of Ref. [341]; the $(\ell = 3, m = 2)$ mode arises from mode mixing). As a summary, if we observe at least two different QNMs for an event, we can test the no-hair theorem since the remnant BH mass and spin are estimated from each QNM.

Although we focus only on the $(n = 0)$ QNMs in our analysis, it should also be noted that there is a direction to study overtones ($n > 0$); see, e.g., Refs. [342–345].

9.5.3. Future prospects

Based on Ref. [346], we discuss which noise curve for KAGRA is best for observing multiple QNMs in the ringdown data analysis. First, to estimate the SNR of the QNM GWs, we use Eq. (15) of Ref. [346]:

$$\rho_{\ell m}^2 = \left(\frac{M\mathcal{A}_{\ell m}\Omega_{\ell m}}{r}\right)^2 \frac{\tau_{\ell m}}{2S_h(f_{\ell m})}, \tag{25}$$

where $\mathcal{A}_{\ell m}$ is the QNM amplitude related to the radiation efficiency [341], $\Omega_{\ell m}$ is the sky sensitivity, r is the luminosity distance, and $\tau_{\ell m}$ and $f_{\ell m}$ denote τ and $f_{\rm R}$ of the (ℓ, m) QNM.

To check the possibility of testing the no-hair theorem, we use the generalized likelihood ratio test (GLRT) [335] where the SNR greater than $\rho_{\rm GLRT}$ can be resolved from the dominant $(\ell = m = 2)$ mode [347]:

$$\rho_{\rm GLRT}^{2,3} = 17.687 + \frac{15.4597}{q-1} - \frac{1.652\,42}{q}, \tag{26}$$

$$\rho_{\rm GLRT}^{2,4} = 37.9181 + \frac{83.5778}{q} + \frac{44.1125}{q^2} + \frac{50.1316}{q^3}, \tag{27}$$

for the $(\ell = m = 3)$ and $(\ell = m = 4)$ modes, respectively. Here, $q > 1$ and the $(\ell = m = 3)$ mode is not excited for the equal-mass case. In the following analysis, we treat the cases of $q = 1$ and 2. The remnant BH spin becomes $\chi = 0.6864$ for $q = 1$ (RIT:BBH:0198) and $\chi = 0.6235$ for $q = 2$ (RIT:BBH:0117) [348,349].

In Fig. 9, we show the SNR of the $(\ell = m = 2)$ QNM in terms of f_{22} in the case of $r = 400$ Mpc and $\Omega_{22} = \Omega_{22}^{\rm max}$ by using Eq. (25). We have also plotted the critical SNR evaluated by the GLRT in Eq. (27) (note the caption). It should be noted that the mass ratios of BBH estimated in the current observation are less than 2[6] (the median values) [3], although unequal-mass BBHs give a better opportunity to test the no-hair theorem.

[6] Note that a recent observation, GW190412 [45], has a larger mass ratio of ~ 3.6.

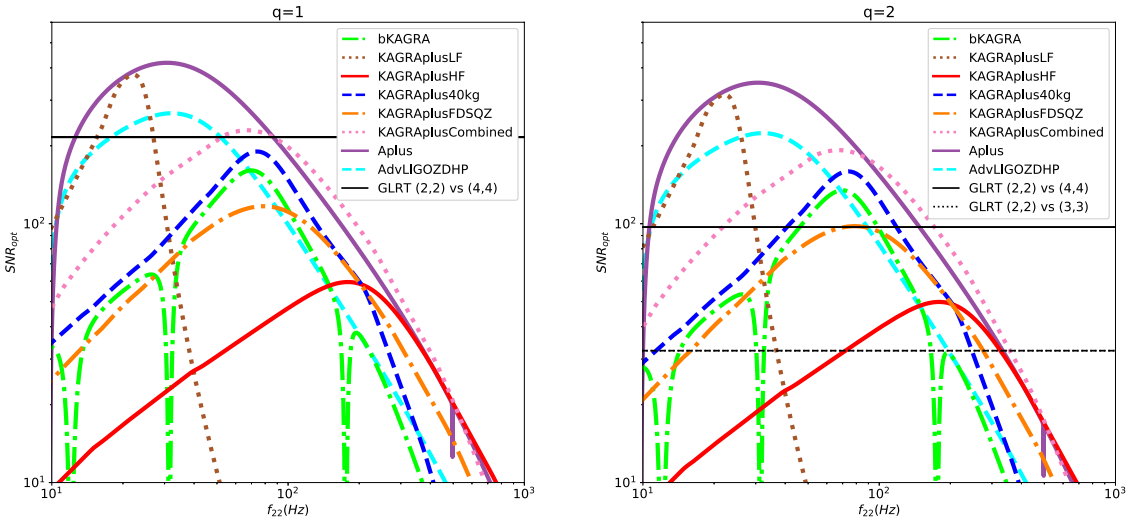

Fig. 9. SNRs versus the real part of the ($\ell = m = 2$) QNM frequency for the mass ratios $q = 1$ (left) and 2 (right), assuming the optimal source direction. Here, the luminosity distance is $r = 400$ Mpc. We have also plotted the critical SNR evaluated by the GLRT with the following assumptions [347]: we have already evaluated the presence of one ringdown signal, and know the parameters for the QNMs and the amplitude of the dominant mode.

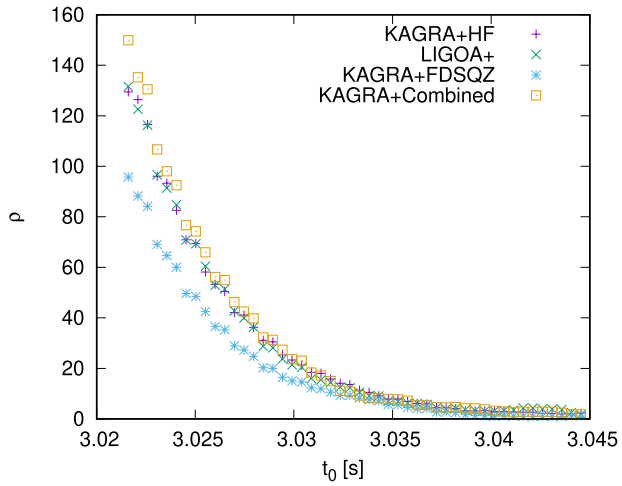

Fig. 10. Evaluated SNRs of the ringdown phase in colored Gaussian noises. The input GW is an SEOBNRv2 (non-precessing) waveform with masses $45M_\odot$ and $15M_\odot$ and spin parameters $\chi_1 = \chi_2 = 0.85$, starting at $t_0 = 0$ s. Note that the peak amplitude of the injected GW is around $t_0 = 3.02$ s.

Next, we discuss the effects of the shape of noise curves on the QNM parameter extraction. Figures 10 and 11 show an example only for the KAGRA+ noise curves, HF, FDSQZ, and Combined, because of the QNM frequency. In the ringdown data analysis, we can reduce the initial phase ϕ_0 for Eq. (22) analytically. Then, we assume that the initial time t_0 is a free parameter and search f_R and Q to maximize the SNR against each t_0. Therefore, we obtain the SNR, f_0, and Q for each t_0. We see that there are some biases that depend on the detector configurations. It is not clear what this means, and we will give a more detailed analysis in the future.

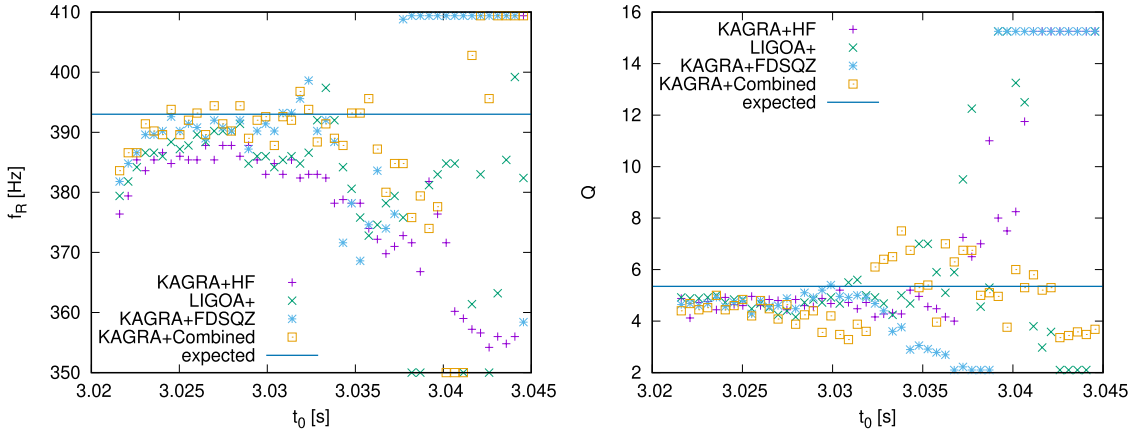

Fig. 11. Same as Fig. 10, but for QNM parameter extraction. The dominant QNM has $f_R = 393$ Hz and $Q = 5.35$.

10. Late-time cosmology

10.1. Measurement of the Hubble constant

10.1.1. Scientific objective

A GW signal from a compact binary provides a unique way to measure the luminosity distance to the source. Given a source redshift, a compact binary can be utilized for measuring the cosmic expansion [350] and is called the *standard siren* in this cosmological context [351]. In particular, the standard siren is expected to play a crucial role in measuring the Hubble constant in the next five years, using relatively nearby ($z \lesssim 0.1$) GW sources, and to resolve the discrepancy problem of the Hubble constants between cosmological measurements such as the cosmic microwave background [352] and baryon acoustic oscillation [353,354] and local measurements with Cepheid variables applied to supernovae [355,356] at the 7–10% level, while measurements by gravitational lensing time delay have given values consistent with those from local measurements [357–359]. Recently the local measurement calibrated by the red giant branch gave a value consistent with that from the cosmological measurements [360]. Therefore, pinning down the Hubble constant is an urgent issue to be solved in order to understand the standard model of cosmology and could be a smoking gun of new physics.

10.1.2. Observations and measurements

The availability of the standard siren essentially depends on whether a source redshift is obtained or not. There are two ways to obtain a source redshift for an individual GW event observed by the current GW detectors: observing an EM counterpart [361] or identifying a unique host galaxy without an EM counterpart [362]. If compact binaries are BNSs or BH–NS binaries, one can obtain the source redshift by observing an EM counterpart that occurs coincidentally with the GW event and identifying a unique host galaxy from the sky position of the EM counterpart. For BBHs, since an EM counterpart cannot be expected, redshift information needs to be obtained by identifying its host galaxy and following up with EM spectroscopic observations. To do that, the sources must be located at lower redshifts $z \lesssim 0.1$, have high SNRs, and must be measured with good determinations of distance and sky localization [363]. Even if a unique host galaxy is not identified, information about the source redshift distribution based on galaxy catalogs is useful. By combining multiple BBH events, it is possible to select out a statistically consistent set of cosmological parameters [364].

Table 13. Top 1% and median errors of the sky localization volume in units of 10^3 Mpc^3. The mass of an NS is 1.4 $M_\odot$. The BBH is at a distance of $z = 0.1$, the 10 $M_\odot$ BH–NS is at $z = 0.06$, and the BNS is at $z = 0.03$. bKAGRA, LF, HF, 40 kg, FDSQZ, and Combined denote the detector network composed of A+, AdV+, and bKAGRA or KAGRA+ (low frequency, high frequency, 40 kg, frequency-dependent squeezing, and combined, respectively).

source	quantile	bKAGRA	LF	HF	40 kg	FDSQZ	Combined
30 $M_\odot$ BBH	top 1%	0.661	0.778	0.600	0.454	0.483	0.335
	median	3.70	10.8	3.37	2.65	2.75	1.63
10 $M_\odot$ BBH	top 1%	3.47	3.61	1.89	2.62	2.15	1.59
	median	21.8	52.6	11.6	15.4	12.5	8.53
10 $M_\odot$ BH–NS	top 1%	8.31	10.2	6.52	5.68	5.74	3.71
	median	44.2	115	40.0	31.2	31.6	22.8
BNS	top 1%	0.261	0.315	0.148	0.222	0.205	0.120
	median	1.79	3.76	0.967	1.33	0.995	0.743

Current observational constraints from one BNS merger (GW170817) and several BBH mergers with statistical redshifts are at the precisions of 17% [365] and 53% [366], respectively. As the luminosity distance error is a dominant error in the measurement of the Hubble constant and degenerates with the inclination angle of a compact binary, the error in the Hubble constant can be improved by determining the inclination angle independently of the GW observation. With the help of the radio imaging observation of the superluminal jet, the inclination angle of the BNS has been constrained and the Hubble constant has been measured at the precision of $\sim$ 7% [367]. However, these constraints are still too weak to resolve the discrepancy problem and need to be improved further. To realize such a precision in the future, the modeling uncertainty of a jet, which is currently estimated to be a few % [367], also needs to be addressed.

10.1.3. Future prospects

In all methods above, a good measurement of sky localization volume is essential for the identification of source redshifts and the use of the compact binaries as a cosmological probe. We estimate the measurement errors of the sky localization volume with the Fisher information matrix [322]. The sky localization volume for each compact binary is defined by [363]

$$\Delta V \equiv \left[V(d_{\rm L,max}) - V(d_{\rm L,min})\right] \frac{\Delta\Omega_{\rm S}}{4\pi} \,. \tag{28}$$

Here $V(d_{\rm L})$ is the comoving volume of a sphere with the radius $d_{\rm L}$. The maximum and minimum luminosity distances are determined by $d_{\rm L,max} = d_{\rm L}(z_{\rm f}) + \Delta d_{\rm L}$ and $d_{\rm L,min} = \max\left[d_{\rm L}(z_{\rm f}) - \Delta d_{\rm L}, 0\right]$, where $z_{\rm f}$ is a fiducial source redshift and $\Delta d_{\rm L}$ is a 2σ-parameter estimation error of luminosity distance. In Table 13, the sky localization volumes for various GW sources with different masses and detector networks are shown.

- BNS and BH–NS
  Based on our results of the sky localization volume, BNSs are much better than BH–NS binaries. Even considering the merger rate uncertainty of the BH–NS and the effect of spin precession on parameter estimation, a typical error in the Hubble constant only with BH–NS binaries is still worse than that with BNSs [368]. Using N BNSs observed by a detector network of two aLIGO and one AdV with redshift information from EM counterparts, the Hubble constant

error is estimated to be $\Delta H_0/H_0 \sim 2\sqrt{50/N}\%$ [369,370]. With the network of KAGRA+ short-term upgrades, the network SNR is larger by about 1.5 times and the Hubble constant error is $\Delta H_0/H_0 \sim 1.5\sqrt{50/N}\%$. However, the number of sources accompanied by EM counterparts is still significantly uncertain and 50 sources roughly correspond to $\sim 10\%$ redshift identification, which is an intermediate value of theoretical predictions [371–373]. Based on the comparison of the sky localization volume in Table 13, the improvement factors for BNSs (median) are LF 0.476, 40 kg 1.35, FDSQZ 1.80, HF 1.85, and Combined 2.41. The upgrades at higher frequencies lead to a smaller localization volume and better sensitivity to the Hubble constant.

- BBH
  As seen from our results of the sky localization volume, $30\,M_\odot$ BBHs are better than $10\,M_\odot$ BBHs and it is easier to identify a unique host galaxy (the number density of galaxies that covers roughly 90% of the total luminosity in the B band [374] is $n_{\rm gal} = 0.01\,{\rm Mpc}^{-3}$) and then obtain redshift information. Assuming the number density of galaxies, the top 1% events of $30\,M_\odot$ BBHs at distances closer than $z \lesssim 0.03$ can marginally identify a unique host galaxy. Extrapolating the result obtained for the bKAGRA detector network [363] to the KAGRA+ short-term upgrade networks, the Hubble constant error is $\Delta H_0/H_0 \sim 0.8\sqrt{10/N}\%$. Based on the comparison of the sky localization volume in Table 13, the improvement factors for $30\,M_\odot$ BBHs (top 1%) are LF 0.85, 40 kg 1.46, FDSQZ 1.37, HF 1.10, Combined 1.97. For BBHs, the upgrades at middle frequencies lead to a smaller localization volume and better sensitivity to the Hubble constant.

In conclusion, we cannot tell which source gives better determination of the Hubble constant because of uncertainties in the merger rates of BNSs and BBHs, the success fraction of redshift identification, and the mass function of BBHs. In addition, there would be potential contributions from systematic errors, e.g., the modeling of the EM counterparts and the calibration errors of GW detectors. Although all of these uncertainties must be reduced or improved, the standard siren has the potential to achieve a 1% precision measurement of the Hubble constant in the future and resolve the discrepancy problem, to which KAGRA can contribute mainly by better sky localization.

10.2. GW lensing

10.2.1. Scientific objective

Gravitational lensing is a well established subject in the EM observation of the Universe [375,376]. For GWs, there are controversial claims that lensing was also already observed from LIGO–Virgo O1/O2 detections [377,378], while the LIGO–Virgo Collaboration claimed that the observed events are fully consistent with unlensed GWs [3]. From an astrophysical viewpoint on the lensing rate, it is unlikely that the observed events are multiple-imaged by stellar-mass objects [379], intervening galaxy population [380], or massive galaxy clusters [381]. However, for the second-generation ground-based GW detectors, it is possible to observe several lensing events at design sensitivity [380–382], and it is almost certain that the third-generation detectors can detect lensed events [379, 382]. The scientific rewards from lensing of GWs are huge [383–385], ranging from probing small structures such as compact dark matter or primordial BHs with mass $M \approx 10$–$10^5\,M_\odot$ [386], to discovering intermediate-mass BHs [387], to testing gravity theories and cosmography [350,383], to name but a few.

10.2.2. Observations and measurements

The detection of possible lensing events has multiple implications for measurement. First, the lensed event is magnified in its SNR by $\sqrt{\mu}$ where μ is the magnification [384]; thus, if the possibility for lensing is not considered, one will underestimate its luminosity distance by $\sqrt{\mu}$, and overestimate the masses in the source frame with a relevant redshift rescaling thereof [381,384,385,388]. Second, because of the magnification effect, for events at large z whose unlensed SNR is below the detection threshold, lensing might increase it to be detectable [384]. Therefore, lensing affects the inference on the event rate and underlying mass distributions (and stellar evolution) of coalescing binaries. Third, if the size of the lens is comparable to or smaller than the GW wavelength, diffraction introduces frequency-dependent time delays and modulation of the waveform [379,385,388], thus reducing the matched-filter capability if unlensed waveforms are used as templates. Fourth, for GW events with observable EM counterparts, it is important to associate them with each other in a convincing manner that enables tests of the speed of gravity and inference of cosmological parameters [350,383,389,390]. A precise localization with multiple detectors helps with such statistical association.

10.2.3. Future prospects

For KAGRA, it will help in localizing GW events significantly together with LIGO and Virgo observations, thus increasing the possibility of detecting lensed events. No specific hardware requirement is additionally requested to achieve the gravitational lensing science goal. However, advanced data analysis including the possibility of lensing events is required. For the operation, coincident observation with LIGO and Virgo detectors would be advantageous. The contribution of KAGRA data to the cooperative parameter estimation with lensing effects encoded in the waveform template will benefit the overall science output. Therefore, the same suggestion as for the measurement of the Hubble constant with BBHs in Sect. 10.1 is applied here.

11. Multi-messenger observations

11.1. Kilonovae/macronovae

11.1.1. Scientific objective

A kilonova (also known as a macronova) is the emission that is expected to be associated with an NS–NS or BH–NS merger as a consequence of mass ejection from the system; see, e.g., Refs. [391,392]. Since the ejected material is composed of neutron-rich matter, heavy radioactive nuclei would be synthesized in the ejecta by the so-called *r-process* nucleosynthesis [393–396], and EM emission could occur by radioactive decays of heavy elements [397–401]. Kilonova emission is expected to be bright in the optical and near-infrared wavelengths and lasts for 1–10 days after the merger. We note that the event rate is currently highly uncertain; it could be $\sim 10^3\ \mathrm{Gpc}^{-3}\ \mathrm{yr}^{-1}$ if kilonovae are associated with all NS–NS mergers.

The light curves of kilonovae reflect the merger process and the late-time evolution of the merger remnant [397,400,402–406]. The presence of kilonova emission suggests that a substantial amount of material is ejected from the system, and this gives constraints on the binary parameters by combining with a theoretical prediction obtained by numerical simulations. Furthermore, detailed properties of kilonova light curves, such as their brightness and color evolution, provide information on the mass and composition of the ejected material; see, e.g., Refs. [407–413]. Such information is useful to understand the merger process of binaries and the late-time evolution of merger remnants as well as the chemical evolution of the Universe.

11.1.2. Observations and measurements

An improvement in the source localization is important to identify the host galaxy of a GW event. Source localization from GW data analysis alone will not be tight enough to uniquely identify the host galaxy even after KAGRA has joined the observation [361] (see Tables 4 and 5). Thus, detection of the EM counterparts will play an important role in identifying the host galaxy. In particular, searching for kilonovae could have an advantage for this purpose because their emission is expected to be approximately isotropic (cf. short GRBs). However, detection of kilonovae will be more challenging at large distances because a kilonova will be dimmer as the distance to the event increases and the number of galaxies in the localized area significantly increases. For example, assuming the same intrinsic brightness as in GW170817, the peak r-band brightness of the kilonova would be fainter than $\approx$ 21 mag at $d_{\rm L}$ $\geq$200 Mpc, which is dimmer than the typical 5σ limiting magnitude of 1-m class telescopes with 60 s exposure [414]. Thus, improvement of the source localization via GW detection is still a key point to restrict the number of host candidates and to achieve simultaneous detection of the kilonova of an event.

Low-latency GW alerts are also a key point for the follow-up of EM counterparts. They help us to find kilonovae because the light curves, in particular at wavelengths shorter than optical bands, are brightest within a few days. Moreover, the light curves of the EM counterparts at $<$ 1 day are of particular interest. For example, in addition to the kilonova emission, the so-called cocoon emission, which is powered by internal energy deposited by relativistic jets, can contribute to the early part of the light curve in the optical and UV wavelengths [415]. It is pointed out that the observed data of light curves in $<$ 1 day can be used to distinguish between these different components of emission [416,417].

Tighter constraints on the inclination angle have a great impact on maximizing the scientific return from observations of kilonovae. Light curves of kilonovae are expected to depend on the observation angle [402,404,411,413]. Much more information on the properties of the ejecta can be extracted if a tighter constraint on the inclination angle is given. Indeed, for the recent BH–NS-like merger event GW190814 [72], the constraint on the ejecta mass is obtained by the upper limits to the EM signals, while the tightness of the constraint is shown to be strongly dependent on the viewing angle [418,419] (by a factor of $\approx$ 3).

11.1.3. Future prospects

Improvements in the source localization both in speed and accuracy are crucial and would be required as the first priority for kilonova follow-up observations. The detector sensitivity should be broadband because a low-frequency band is important for quick localization (early warning) and a high-frequency band is important for accurate localization. According to Tables 4 and 5, the median localized area is improved by up to a factor of $\approx$ 2 by including KAGRA+ in the detector network (by upgrading bKAGRA to one of the KAGRA+ configurations). This enables us to search the localized fields with deeper limiting magnitudes or with lower latency. For example, deepening the EM search by $\approx$ 1 magnitude is in principle possible if the improvement in the localization area enabled us to have a 10 times longer exposure time. Follow-ups by a 2-m or larger class telescopes, such as Pan-STARRS [420] and CTIO-Dark Energy Camera [421], are crucial for the detection of such a situation [414]. We also note that an increase in the number of detectors with stable operations will enhance the chance of multiple detectors being operated at the same time, which is crucial for the source localization.

Tables 4 and 5 show that the determination of the inclination angle is improved by up to $\approx 23\%$ by including KAGRA+ in the detector network (by upgrading bKAGRA to one of the KAGRA+ configurations. As mentioned above, such improvement will help us to provide tighter constraints on the ejecta properties and provide us with a good opportunity to study the spatial distribution of ejecta. For example, numerical-relativity simulations of an NS–binary merger (e.g., Refs. [411,422–424]) predict that the typical polar opening angle of the lanthanide-rich dynamical ejecta component ($\gtrsim 30°$) is comparable to or larger than the determination error of the inclination angle for $\Delta \cos \iota \approx 0.15$ (see Tables 4 and 5). Since the presence of lanthanide-rich material in the line of sight strongly affects the light curves [402], observations of kilonovae with improved measurement of the inclination angle would enable us to examine the presence of such ejecta components.

11.2. Short gamma-ray bursts

11.2.1. Scientific objective

The origin of sGRBs has been a long-standing problem for more than 40 years [425,426]. A BNS merger was thought to be the most promising candidate [394,427,428], although unequivocal evidence was missing. Although it is widely accepted that a GRB is produced by a relativistic jet with a Lorentz factor larger than ~ 100, there remain unresolved issues. (1) The central engine is most likely a spinning BH surrounded by an accretion disk, while a millisecond magnetar remains a candidate. (2) The jet formation mechanism is one of the central subjects in astrophysics. It could be the Blandford–Znajek mechanism or the neutrino annihilation mechanism. For the former case, it is not known how to realize the large-scale, poloidal configuration of the magnetic field. (3) The jet composition is unknown. It is likely dominated by baryon kinetic energy or magnetic energy. (4) The emission mechanism is a puzzle. The emission radius still has uncertainty of approximately four orders of magnitude. A popular mechanism is synchrotron emission, while there is no consensus on how to realize the observed spectral relations such as the Amati and Yonetoku relations [429,430]. (5) The jet structure is unknown in both the radial and polar directions. The long-lasting emission following the main prompt emission such as extended emission ($\sim 10^2$ s) and plateau emission ($\sim 10^4$ s) suggests long-lived central engine activity [431].

The detection of the GW event GW170817 [4] and the associated EM counterparts [361] revolutionized the situation. In particular, sGRB 170817A detected two seconds (~ 1.7 s) after GW170817 [137,143,432] and the following afterglows in radio to X-ray [433–438] give the first direct clues to the origin of sGRBs. However, the situation is not so simple because sGRB 170817A was very weak with an isotropic-equivalent energy $E_{\gamma,\mathrm{iso}} \sim 5.35 \times 10^{46}$ erg, which is many orders of magnitude smaller than ordinary values. On the other hand, the afterglow observations, in particular of superluminal motion in radio [139,439] and the consistency between the spectral index and the light curve slope after the luminosity peak [440–442], strongly suggest that a relativistic jet is launched and successfully breaks out of the merger ejecta in this event [443]. The jet power should be similar to those in other normal sGRBs, otherwise the jet cannot penetrate the merger ejecta [444]. The most likely scenario is that the jet is off-axis to our line of sight and therefore faint in this event [143,445,446], although the emission mechanism is controversial [407,447–449]. The afterglow observation, in particular the slowly rising light curve, is not consistent with a top-hat jet [138], but for the first time strongly suggests a structured jet [438–440,442,450–454]. The angular structure is also important for solving the spectral puzzles of GRB 170817A [447,455–457].

11.2.2. Observations and measurements

The GW signal is basically the same as that of NS mergers with the dimensionless amplitude $h_c \propto f^{-1/6}$ and $f_{\rm max} \sim$ a few kHz (see Sect. 4.1). The mass and mass ratio are important for revealing the jet formation mechanism since they determine the BH and disk masses after the merger.

Sky localization is essential for following up EM counterparts [7]. In GW170817, the error region shrinks from 190 deg^2 to 31 deg^2 by adding Virgo data even though the SNR was 2.0. The survey with Subaru/Hyper Suprime-Cam (one of the most powerful telescope in the world) covered 23.6 deg^2 and reached a 50% completeness magnitude of 20.6 mag [458]. At the design sensitivities of aLIGO, AdV, and KAGRA, the typical source distance is further (or events closer than 40 Mpc are rare given the estimated event rate 1×10^2–4×10^3 Gpc^{-3} yr^{-1} [3]). Thus the localization error should ideally be less than ~ 30 deg^2; this is achievable with detector networks including KAGRA, as shown in Tables 4 and 5. Low latency should also be mandatory. In GW170817, the alert with the localization error ~ 31 deg^2 was sent ~ 5 hours after the merger, although the actual observations started ~ 10 hours after the merger because of the interruption of the sea. In a couple of years, at least minutes or even lower latency will be realized. Ground-based detectors should try localization before the merger [459] to allow other messengers (in particular those with small fields of view) to observe the source at the merger time as well as possible precursor emissions.

The inclination (or viewing angle) of the merging binary is also a crucial parameter for sGRB studies. It affects all the prompt, afterglow, and kilonova emissions.

Post-merger signals are also worth searching to reveal the central engines of sGRBs [154]. They include GW emission from a hypermassive NS (or supramassive NS) and BH (see Sect. 4.3). There are many possibilities for GW emission mechanisms, such as BH ringdown, NS quadrupolar f-mode, magnetic-field-induced ellipticities, unstable bar modes, unstable r-modes, and so on. The possible range of GW duration is broad, from $\sim 10^{-3}$–$\sim 10^4$ s or even longer, as implied by the long-lasting activity of sGRBs.

A magnetar giant flare is also observed as an sGRB. Some GWs are expected from giant flares (see Sect. 6.2) [185]. Currently there is no evidence of GWs associated with giant flares [460], although the f mode may not be the correct target [461]. Possible candidates for giant flares include GRB 070201 [462], GRB 051103 [463], and GRB 150906B [464].

11.2.3. Future prospects

In summary, the frequency band is required to be broadband, where the low-frequency band is important for quick localization (early warning) and the high-frequency band is important for the merger time and the post-merger signals. In addition, inclination measurements are crucial. These are the same as those for a kilonova. See Sect. 11.1. As the typical distance to GW sources increases, only sGRBs remain as detectable EM counterparts. Collaboration with X- and gamma-ray observatories such as SVOM, Einstein Probe, HiZ-GUNDAM, and CTA will become more important.

11.3. Long gamma-ray bursts

11.3.1. Scientific objective

Long GRBs, whose duration is longer than about 2 s, originate in the collapse of a massive star [465,466]. Prompt gamma-ray emissions and subsequent afterglows are emitted at the head of a relativistically moving, narrowly collimated jet toward us. The Lorentz factor of the jet is typically larger than $\sim 10^2$. Currently the jet launch mechanism as well as the radiation process is not yet fully understood. The central engine of the relativistic jet is also unclear, but is most likely to be

massive accretion disk around a newly formed BH. An attempt has been to extract information on the dynamics and/or structure of the jet from the observed EM emissions to tackle this problem. However, the EM emission occurs far from the central engine, so that previous EM observations provided little direct information to solve the problem.

11.3.2. Observations and measurements

In the collapsar model for long GRBs [467], the highly spinning core of a massive star collapses into a rotating BH with an accretion disk, or sometimes an NS, producing a relativistic jet along the rotation axis. Then, the rotating compact objects themselves emit GWs [468,469]. These are the cases of supernovae and hypernovae, so we refer the reader to Sect. 7.1 for a more quantitative discussion. The accretion disk around the BH is massive ($\sim \mathrm{M}_\odot$), so that asymmetrical blobs arise via gravitational instabilities and may be responsible for GWs [469] as well as the observed gamma-ray variability. The characteristic amplitude of the GW emitted by the blob with a mass m_b is estimated as

$$h_c(f) \sim 1 \times 10^{-22} \left(\frac{M_c}{\mathrm{M}_\odot}\right)^{5/6} \left(\frac{d}{100\ \mathrm{Mpc}}\right)^{-1} \left(\frac{f}{f_{\max}}\right)^{-1/6} \tag{29}$$

and the maximum frequency $f_{\max} \sim 300(M_{\mathrm{BH}}/10\mathrm{M}_\odot)^{-1}$ Hz, where d is the distance to the source, M_{BH} is the BH mass, and the chirp mass $M_c \sim 0.6\mathrm{M}_\odot(m_b/0.1\mathrm{M}_\odot)^{3/5}(M_{\mathrm{BH}}/10\mathrm{M}_\odot)^{2/5}$.

In order to understand the jet launch mechanism, it should be clarified when and how the jet departs at the central engine. GW emission also takes place while the jet is accelerating. Such gravitational radiation has a "memory"; i.e., the metric perturbation does not return to its original value at the end of the jet acceleration [470]. Suppose that the mass M is accelerated to a Lorentz factor γ. The memory GW is antibeamed (nearly isotropic) except for the on-axis direction within the angle γ^{-1} around the jet axis [471,472]. The characteristic amplitude is given by

$$h_c(f) \sim 1 \times 10^{-24} \left(\frac{Mc^2}{10^{52}\ \mathrm{erg}}\right) \left(\frac{d}{100\ \mathrm{Mpc}}\right)^{-1} \left(\frac{f}{f_c}\right)^{-1}, \tag{30}$$

where $f_c \sim T_{\mathrm{dur}}^{-1} \sim 0.1(T_{\mathrm{dur}}/10\ \mathrm{s})^{-1}$ Hz, and T_{dur} is the total duration of the burst. When the acceleration takes over a time δt, the maximum frequency $f_{\max}$ is given by $f_{\max} \sim \delta t^{-1} \sim 1\ \mathrm{kHz}\ (\delta t/10^{-3}\ \mathrm{s})^{-1}$. Thus, the expected amplitude looks too small to detect. However, the amplitude may become much larger. First, the energy source is not only limited to the rest mass energy of the jet matter Mc^2 but also other candidates such as neutrino annihilation and magnetic field [473], which can potentially be $E_s \sim 10^{54}$ erg. Second, the amplitude in the high-frequency range ($\sim f_{\max}$) is greatly enhanced if multiple ($\sim 10^2$) short bursts are taken into account [472]. Then, the signal is about two orders of magnitude larger than that estimated in Eq. (30):

$$h_c(f = 100\ \mathrm{Hz}) \sim 1 \times 10^{-23} \left(\frac{E_s}{10^{54}\ \mathrm{erg}}\right) \left(\frac{d}{100\ \mathrm{Mpc}}\right)^{-1}. \tag{31}$$

Once such gravitational radiation is detected, we can extract important information on the time variability and active time of the central engine as well as the jet structure.

Despite extensive searches for GWs from long GRBs, so far firm detection has not yet been obtained [474–477].

11.3.3. Future prospects

For GWs from massive accretion disks or relativistic jet acceleration, observations with frequency less than 1 kHz are important, so the candidates of KAGRA+ (LF, 40 kg, FDSQZ) have better sensitivities for the study of long GRBs. The local rate density of the usual high-luminosity long GRBs that are detectable by gamma-ray instruments has been estimated as $\sim 1\,\mathrm{Gpc}^{-3}\,\mathrm{yr}^{-1}$ [478]. This number is for events with GRB jets toward us to emit bright gamma-rays. If the beaming factor of the jet, i.e., the fraction of solid angle of the gamma-ray emission to the full sky, is $f_b = 1/200$, then the intrinsic rate density is $\sim 200\,\mathrm{Gpc}^{-3}\,\mathrm{yr}^{-1}$. On the other hand, the GW emission is almost isotropic. Hence the all-sky rate of the GW events within 100 Mpc is $\sim 0.8\ \mathrm{yr}^{-1}$. Indeed, more frequent events in the local Universe are low-luminosity long GRBs, a subclass of long GRBs [478]. Their local rate density is two or three orders of magnitude higher than the usual high-luminosity long GRBs, so that the all-sky rate of nearby (< 100 Mpc) low-luminosity long GRBs is estimated as ~ 0.4–$4\ \mathrm{yr}^{-1}$. The beaming factor for this subclass is uncertain. However, if we roughly assume $f_b \sim 1/10$, the unbeamed GW event rate is 4–40 yr^{-1}.

The event rates of GWs sound promising for the current GW detectors even with bKAGRA at design sensitivity. However, the memory GW is more difficult to detect out to 100 Mpc because a matched-filtering technique for a chirp signal is not available and the memory signal is more like a burst signal. In this sense, observations with more detectors are crucial and KAGRA will be able to help veto fake signals and to enhance the network sensitivity.

11.4. Fast radio bursts

11.4.1. Scientific objective

Fast radio bursts (FRBs) are coherent radio transients with a duration of milliseconds. The most outstanding characteristic of FRBs is the dispersion measure (DM); they are as large as DM $\sim 1000\,\mathrm{pc\,cm}^{-3}$, indicating that the sources are at cosmological distances. FRBs were originally discovered by Lorimer et al. in 2007 [479]. The number has been significantly increased by wide-field-survey facilities like ASKAP and CHIME. See FRBCAT [480] for an updated catalog.

It is now known that a fraction (roughly 10%) of FRBs are repeating. The differences between repeating and non-repeating FRBs are still under debate. Host galaxies have been reported for a few FRBs, both for repeating and non-repeating ones. There is a diversity in the host galaxies; the host of FRB 121102 is a dwarf star-forming galaxy while other host galaxies are medium-sized less-active galaxies. No multi-messenger counterpart has been reported.

The origin of FRBs is still not known, and the emission mechanism is rather uncertain. Given the similarities between FRBs and some transient phenomena from Galactic young NSs, e.g., giant radio pulses from the Crab pulsar and magnetar giant flares, the young NS models have been most intensively investigated; see, e.g., Ref. [481] and references therein. For a GW from a young NS, see Sects. 6.2 and 6.3. On the other hand, the most testable and interesting possibility for KAGRA and other ground-based interferometers would be the coalescing BNS model [482]; FRBs could be produced just before the merger, a fraction of the orbital energy being extracted by magnetic braking. Simultaneous detection of a GW and an FRB is a straightforward way to test this scenario.

11.4.2. Observations and measurements

If an FRB is observed with a GW, the source will be determined. In general, arrival timing of the FRB relative to the GW is useful; the FRB will be emitted, say, milliseconds after the the GWs. The

timing of the FRB emission should be closely connected to the emission mechanism; information on the physical condition of the NS magnetosphere can be obtained.

11.4.3. Future prospects

Ongoing and upcoming radio surveys could detect $O(1000)$ FRBs per year (see, e.g., Ref. [483]), providing more opportunities to conduct multi-messenger observations. One can search the GW counterparts of known FRBs; in addition to Galactic young NSs, we can select relatively close extragalactic targets based on their DMs. Conversely, GW detectors could in principle give an alert to radio telescopes. Since the field of view of radio telescopes is relatively small (e.g., $\sim$0.1 deg for Parkes), a better sky localization with KAGRA is, as always, crucial.

12. Others

12.1. Cosmic strings

12.1.1. Scientific objective

Cosmic strings are 1D cosmological defects that are predicted to form under phase transitions in the early Universe [484]. More recently, it has been recognized that cosmological models based on the string theory also result in strings forming and growing to cosmic scales [485,486]. A cosmic string is characterized by its tension, which is linked to the energy scale of the Universe when it is formed. Searching for cosmic strings will thus allow us to investigate the early time of the Universe, which has never been probed before.

12.1.2. Observations and measurements

A promising observational signature of cosmic strings is their gravitational radiation from loops [487–489]. Loops can form through a process called intercommutation, in which two strings change partners upon encounter. An intercommutation of a loop by itself or of two strings on two points creates a loop, which oscillates and radiates their energy by GWs. Special points that are occasionally formed on loops, called cusps and kinks, are the important targets for GW detectors. Cusps are points on a loop that accompany large Lorentz boosts, and kinks are discontinuities on the tangent vectors of a loop [490]. Another interesting GW source is kinks on infinitely long cosmic strings [491,492], which are produced when two strings intersect. As the string network evolves with continuous intersections, a number of small kinks accumulate on infinite strings and their propagation and collisions generate GW bursts. Although the strain amplitude of each GW burst is small, a number of overlapping bursts due to the high event rate generate a GW background with a large amplitude, enough to be tested by ground-based experiments.

Searches for cosmic strings have been conducted in the past, using data from the LIGO and Virgo detectors [493–495]. These works have done two searches, a template-based matched-filtering search for individual burst signals (from cusps and kinks), and a search for the stochastic background generated by an overlapping population of these bursts. These searches have given constraints on the string parameters (e.g., tension) and models on the distribution of these loops in the Universe. The constraints depend on models of the probability distribution on the loop size. The searches using aLIGO's O1 data [495] yielded a constraint of $G\mu < 5 \times 10^{-8}$ for a simple loop model first developed in Refs. [488,490].

GW emission from these features is predicted to be linearly polarized, and have a power-law frequency spectrum of index $-4/3$ for cusps and $-5/3$ for kinks [488]. The amplitude depends on the tension and size of the loop, as well as the distance to the loop. The spectrum also is considered to

have a high-frequency cutoff due to the beamed nature of the signal. The high-frequency cutoff can take arbitrary values, but as bursts with higher-frequency cutoffs are more beamed [488], bursts with lower high-frequency cutoffs can be seen more frequently than those with higher high-frequency cutoffs.

12.1.3. Future prospects

Due to the power-law nature, the signals from cosmic string bursts generally have higher amplitudes in low frequencies. Hence the sensitivity to string signals will be most enhanced by improving the lower-frequency band [495]. By defining the SNR ratio $r_{\alpha/\beta} \equiv r_\alpha/r_\beta$ for the configurations α and β where r_α is defined in Eq. (5) and a similar equation holds for the β configuration, we can quantitatively compare the performances of various configurations of possible KAGRA upgrades. For a cosmic string cusp, the amplitude is proportional to $f^{-4/3}$. If we take the high-frequency cutoff at $f_{\rm high} = 30$ Hz, the SNR ratios from bKAGRA to KAGRA+ for a GW burst from a cosmic string cusp are LF 5.46, 40 kg 1.54, FDSQZ 1.19, HF 0.39, Combined 2.82. Also, significant sensitivity improvements in low frequencies are anticipated in the upgrades of aLIGO and AdV or the Einstein Telescope. Furthermore, because the string bursts are linearly polarized, using the information on polarization can be crucial for differentiating these signals from noise. This can be sufficiently done with a KAGRA detector in collaboration with the LIGO and Virgo detectors.

12.2. Black-hole echoes

12.2.1. Scientific objective

The BH information loss paradox is a long-standing problem. The problem looks complicated, but the rough idea can be captured in the following way. Our assumptions are the following:

(1) Hawking evaporation can be described by a semi-classical picture. Namely, it can be described by the standard field theory in curved spacetime. This means that BHs radiate like a black body at the Hawking temperature $T_{\rm H} = \kappa/2\pi$, where κ is the surface gravity. In the case of a Schwarzschild BH, the surface gravity is given by $1/2r_g$ with r_g being the horizon radius. This emitted radiation is perfectly entangled with the internal state of the BH. It would not be so difficult to convince yourself that this argument is likely. If we simply consider the evolution of an initially pure quantum state, it remains so in the ordinary field theory. So, if the emitted radiation looks thermal, this thermal nature is obtained as a result of integrating out some unobserved degrees of freedom. In the case of a BH spacetime, these hidden degrees of freedom are inside the BH horizon.
(2) BH entropy is bounded by the area of the BH, i.e., $S_{\rm BH} < S_{\rm Bekenstein–Hawking} := A/4G_{\rm N}$, where A is the area of the BH and G_N is Newton's constant. Under the assumption that this bound is saturated, the BH thermodynamics holds.

These assumptions can be easily seen to be inconsistent. Let us consider a stationary process containing a BH emitting Hawking radiation. To make it stationary, we keep throwing some matter continuously down into the BH. Then, in a mean time the total entropy of the emitted radiation exceeds $S_{\rm Bekenstein–Hawking}$. However, the internal state entangled with the emitted radiation should also have the same amount of entropy. Since the spacetime is stationary with an apparent horizon, no information can go out from the inside. This would contradict with the claim that the BH entropy is bounded by $S_{\rm Bekenstein–Hawking}$.

To resolve the contradiction mentioned above, some of our assumptions must be violated. An easy way is to abandon assumption (2). However, many people believe that the BH entropy identified with its area is not just a theoretical illusion but has a deep physical meaning. If we wish to keep assumption (2), we would be required to abandon assumption (1). One possibility is that the Hawking radiation is wrong. However, this is unlikely, although it is true that the explicit calculation of the Hawking radiation based on the field theory in curved spacetime is given only in weak coupling perturbative calculations. Thus, one way, at first glance radical but in a certain sense most conservative, to resolve the contradiction would be to abandon the semi-classical picture. From the point of view of relativity, the horizon is not a special surface at all, unless we care about the global structure of the spacetime. Therefore it is difficult to imagine that something unusual happens particularly on the horizon. However, if we trace back the quanta emitted as the Hawking radiation, they infinitely blue-shift in the near-horizon limit. Hence, field theoretically the horizon might be somehow special, although the argument sounds a little acausal.

From the discussion mentioned above, it would be understandable to doubt if the physics describing the region close to the BH horizon might be significantly modified from our familiar low-energy physics. One simple but radical possibility is that the BH horizon is covered by a wall that reflects all the low-energy excitations including GWs. Ordinary matter whose energy scale is much higher than the energy of the typical gravitons excited in the binary system will be absorbed by BHs, while the quanta whose energy is comparable to or lower than $T_{\rm H}$, i.e., whose wavelength is as long as the BH size, are selectively reflected by the wall. Interestingly, this critical energy scale also follows if we assume that the BH area is quantized by the Planck length squared [496–498].

12.2.2. Observations and measurements

It is difficult to predict the exact waveform of the expected echoes, since the theoretical background is not so sound. What we can expect generically is a repetition of signals similar to the ringdown signal after merger with an equal time interval. Here, the uncertainties are in the boundary condition at the wall and the wall location. One possible ansatz about the properties of the wall is that the reflection rate at the wall is unity and the wall is placed at about a Planck distance from the horizon. Furthermore, we also need to make an assumption about the phase shift at the reflection. One simple assumption is that the phase shift is frequency independent or the frequency dependence is sufficiently weak. Under such an assumption, we could construct a template by solving the master equation for BH perturbation [499].

There was a claim that some echo signal has already been detected [500]. However, a very simple repetition of the same waveform was assumed in that analysis. Such an analysis is an interesting trial, but it is difficult to invent a theoretical model that supports that simple-minded assumption. In fact, our reanalysis indicates that the significance of the echo signal does not survive once we replace the template with a slightly more realistic one [501]; i.e., the reflection rate at the angular momentum barrier calculated by using the BH perturbation theory is employed. However, it is also true that the signal claimed in Ref. [500] does not disappear just by increasing the number of BH merger events including the events from the LIGO/Virgo O2 observing run.

12.2.3. Future prospects

As the number of events increases, the nature of the signal that seems to exist will definitely be uncovered in the near future. In order to discriminate the real signal coming from the sky from the unidentified noise of detectors correlated with GW events, it would be better to analyze the data

from completely different detectors that have a similar sensitivity. In this sense it is quite interesting to analyze the data obtained by Virgo and KAGRA in the same manner.

13. Conclusion

In this article we have reviewed the scientific cases available with second-generation ground-based detectors, including aLIGO, AdV, and the baseline KAGRA (bKAGRA), and their future upgrades, A+, AdV+, and KAGRA+, respectively, and discuss KAGRA's scientific contributions to the global detector networks composed of the detectors above. For compact binaries composed of stellar-mass BHs and/or NSs, at least three detectors are necessary to localize sources and more detectors including KAGRA are preferable to obtain smaller sky areas to be searched. This is also true for science based on these binaries such as tests of gravity (except for BH ringdown), measurement of the Hubble constant, GW lensing, the measurement of the EOS of an NS, and multi-messenger observations of sGRBs and kilonovae. On the other hand, the discovery of new GW sources such as binary IMBHs, supernovae, magnetors, isolated pulsars, and low-mass X-ray binaries can be done with a single detector, though multiple detectors are preferable for events detected only by GWs. Therefore, for these sources, the higher duty cycle of a detector network is more important not to miss signals during detector down times. In summary, KAGRA will be able to contribute to broad science topics and play an important role in joint observations by the global detector networks.

Acknowledgements

This work was supported by MEXT, the Japan Society for the Promotion of Science (JSPS) Leading-edge Research Infrastructure Program, a JSPS Grant-in-Aid for Specially Promoted Research 26000005, JSPS Grants-in-Aid for Scientific Research on Innovative Areas 2905: JP17H06358, JP17H06361, and JP17H06364, JSPS Core-to-Core Program A. Advanced Research Networks, a JSPS Grant-in-Aid for Scientific Research (S) 17H06133, the joint research program of the Institute for Cosmic Ray Research, University of Tokyo, the National Research Foundation (NRF) and Computing Infrastructure Project of KISTI-GSDC in Korea, Academia Sinica (AS), AS Grid Center (ASGC) and the Ministry of Science and Technology (MoST) in Taiwan under grants including AS-CDA-105-M06, the Advanced Technology Center (ATC) of NAOJ, the Mechanical Engineering Center of KEK, the LIGO project, and the Virgo project.

References

[1] J. Aasi et al. [LIGO Scientific and Advanced VIRGO Collaborations], Class. Quantum Grav. **32**, 074001 (2015).
[2] F. Acernese et al., Class. Quantum Grav. **32**, 024001 (2015).
[3] B. P. Abbott et al. [LIGO Scientific and Virgo Collaborations], Phys. Rev. X **9**, 031040 (2019).
[4] B. P. Abbott et al. [LIGO Scientific and Virgo Collaborations], Phys. Rev. Lett. **119**, 161101 (2017).
[5] J. Miller, L. Barsotti, S. Vitale, P. Fritschel, M. Evans, and D. Sigg, Phys. Rev. D **91**, 062005 (2015).
[6] J. Degallaix for the Virgo Collaboration, Advanced Virgo+ preliminary studies, VIR-0300A-18 (2018).
[7] B. P. Abbot et al. [KAGRA, LIGO Scientific and Virgo Collaborations], Living Rev. Relat. **21**, 3 (2018).
[8] T. Akutsu et al. [KAGRA Collaboration], Nat. Astron. **3**, 35 (2019).
[9] T. Akutsu et al. [KAGRA Collaboration], in preparation as the series of article. *Overview of KAGRA: Future plans*.
[10] Y. Michimura et al., Phys. Rev. D **102**, 022008 (2020).
[11] B. P. Abbott et al. [LIGO Scientific and Virgo Collaborations], Phys. Rev. Lett. **116**, 061102 (2016).
[12] B. P. Abbott et al. [LIGO Scientific and Virgo Collaborations], Phys. Rev. Lett. **116**, 241103 (2016).
[13] B. P. Abbott et al. [LIGO Scientific and Virgo Collaborations], Astrophys. J. Lett. **818**, L22 (2016).
[14] K. Belczynski, T. Bulik, and B. Rudak, Astrophys. J. Lett. **608**, L45 (2004).
[15] M. Dominik, K. Belczynski, C. Fryer, D. E. Holz, E. Berti, T. Bulik, I. Mandel, and R. O'Shaughnessy, Astrophys. J. **759**, 52 (2012).

[16] K. Belczynski, D. E. Holz, T. Bulik, and R. O'Shaughnessy, Nature **534**, 512 (2016).
[17] M. Mapelli, Mon. Not. R. Astron. Soc. **459**, 3432 (2016).
[18] S. F. Portegies Zwart and S. L. W. McMillan, Astrophys. J. Lett. **528**, L17 (2000).
[19] R. M. O'Leary, B. Kocsis, and A. Loeb, Mon. Not. R. Astron. Soc. **395**, 2127 (2009).
[20] C. L. Rodriguez, C.-J. Haster, S. Chatterjee, V. Kalogera, and F. A. Rasio, Astrophys. J. Lett. **824**, L8 (2016).
[21] F. Antonini and F. A. Rasio, Astrophys. J. **831**, 187 (2016).
[22] N. C. Stone, B. D. Metzger, and Z. Haiman, Mon. Not. R. Astron. Soc. **464**, 946 (2017).
[23] Y.-B. Bae, C. Kim, and H. M. Lee, Mon. Not. R. Astron. Soc. **440**, 2714 (2014).
[24] D. Park, C. Kim, H. M. Lee, Y.-B. Bae, and K. Belczynski, Mon. Not. R. Astron. Soc. **469**, 4665 (2017).
[25] T. Kinugawa, K. Inayoshi, K. Hotokezaka, D. Nakauchi, and T. Nakamura, Mon. Not. R. Astron. Soc. **442**, 2963 (2014).
[26] T. Hartwig, M. Volonteri, V. Bromm, R. S. Klessen, E. Barausse, M. Magg, and A. Stacy, Mon. Not. R. Astron. Soc. **460**, L74 (2016).
[27] K. Inayoshi, K. Kashiyama, E. Visbal, and Z. Haiman, Mon. Not. R. Astron. Soc. **461**, 2722 (2016).
[28] K. Inayoshi, R. Hirai, T. Kinugawa, and K. Hotokezaka, Mon. Not. R. Astron. Soc. **468**, 5020 (2017).
[29] B. Carr, F. Kühnel, and M. Sandstad, Phys. Rev. Lett. **94**, 083504 (2016).
[30] M. Sasaki, T. Suyama, T. Tanaka, and S. Yokoyama, Phys. Rev. Lett. **117**, 061101 (2016); **121**, 059901 (2018) [erratum].
[31] M. Sasaki, T. Suyama, T. Tanaka, and S. Yokoyama, Class. Quantum Grav. **35**, 063001 (2018).
[32] D. Kushnir, M. Zaldarriaga, J. A. Kollmeier, and R. Waldman, Mon. Not. R. Astron. Soc. **462**, 844 (2016).
[33] C. L. Rodriguez, M. Zevin, C. Pankow, V. Kalogera, and F. A. Rasio, Astrophys. J. Lett. **832**, L2 (2016).
[34] K. Hotokezaka and T. Piran, Astrophys. J. **842**, 111 (2017).
[35] H.-T. Janka, Mon. Not. R. Astron. Soc. **434**, 1355 (2013).
[36] I. Mandel, Mon. Not. R. Astron. Soc. **456**, 578 (2016).
[37] T. Chiba and S. Yokoyama, Prog. Theor. Exp. Phys. **2017**, 083E01 (2017).
[38] V. De Luca, V. Desjacques, A. Malhotra, and A. Riotto, J. Cosmol. Astropart. Phys. **1905**, 018 (2019).
[39] T. Harada, Y. Chul-Moon, K. Kohri, and K.-I. Nakao, Phys. Rev. D **96**, 083517 (2017); **99**, 069904 (2019) [erratum].
[40] E. S. Phinney, arXiv:astro-ph/0108028 [Search INSPIRE].
[41] B. P. Abbott et al. [LIGO Scientific and Virgo Collaborations], Phys. Rev. Lett. **116**, 131102 (2016).
[42] K. A. Postnov and L. R. Yungelson, Living Rev. Relat. **17**, 3 (2014).
[43] M. J. Benacquista, Living Rev. Relat. **5**, 2 (2002).
[44] L. Pekowsky, J. Healy, D. Shoemaker, and P. Laguna, Phys. Rev. D **87**, 084008 (2013).
[45] B. P. Abbott et al. [LIGO Scientific and Virgo Collaborations], Phys. Rev. D **102**, 043015 (2020) [arXiv:2004.08342 [astro-ph.HE]] [Search INSPIRE].
[46] J. M. Bardeen, W. H. Press, and S. A. Teukolsky, Astrophys. J. **178**, 347 (1972).
[47] S. F. Portegies Zwart and S. L. W. McMillan, Astrophys. J. **576**, 899 (2002).
[48] M. Freitag, M. A. Gürkan, and F. A. Rasio, Mon. Not. R. Astron. Soc. **368**, 141 (2006).
[49] P. Amaro-Seoane and L. Santamaría, Astrophys. J. **722**, 1197 (2010).
[50] G. Fragione, I. Ginsburg, and B. Kocsis, Astrophys. J. **856**, 92 (2018).
[51] H.-a. Shinkai, N. Kanda, and T. Ebisuzaki, Astrophys. J. **835**, 276 (2017).
[52] P. Amaro-Seoane, Phys. Rev. D **98**, 063018 (2018).
[53] M. A. Gürkan, J. M. Fregeau, and F. A. Rasio, Astrophys. J. Lett. **640**, L39 (2006).
[54] S. Hirano, T. Hosokawa, N. Yoshida, H. Umeda, K. Omukai, G. Chiaki, and H. W. Yorke, Astrophys. J. **781**, 60 (2014).
[55] A. Stacy and V. Bromm, Mon. Not. R. Astron. Soc. **433**, 1094 (2013).
[56] H. Susa, K. Hasegawa, and N. Tominaga, Astrophys. J. **792**, 32 (2014).
[57] K. Inayoshi and Z. Haiman, Mon. Not. R. Astron. Soc. **445**, 1549 (2014).
[58] M. C. Miller and E. J. M. Colbert, Int. J. Mod. Phys. D **13**, 1 (2004).
[59] D. A. Brown, J. Brink, H. Fang, J. R. Gair, C. Li, G. Lovelace, I. Mandel, and K. S. Thorne, Phys. Rev. Lett. **99**, 201102 (2007).
[60] E. Berti, A. Buonanno, and C. M. Will, Phys. Rev. D **71**, 084025 (2005).

[61] S. Isoyama, H. Nakano, and T. Nakamura, Prog. Theor. Exp. Phys. **2018**, 073E01 (2018).
[62] A. Ori and K. S. Thorne, Phys. Rev. D **62**, 124022 (2000).
[63] E. Berti, V. Cardoso, and C. M. Will, Phys. Rev. D **73**, 064030 (2006).
[64] E. A. Huerta and J. R. Gair, Phys. Rev. D **83**, 044020 (2011).
[65] M. C. Miller, Class. Quantum Grav. **26**, 094031 (2009).
[66] T. M. Tauris et al., Astrophys. J. **846**, 170 (2017).
[67] M. Chruslinska, K. Belczynski, J. Klencki, and M. Benacquista, Mon. Not. R. Astron. Soc. **474**, 2937 (2018).
[68] D. Pooley et al., Astrophys. J. Lett. **591**, L131 (2003).
[69] J. M. Weisberg, D. J. Nice, and J. H. Taylor, Astrophys. J. **722**, 1030 (2010).
[70] P. C. Peters, Phys. Rev. **136**, B1224 (1964).
[71] F. Özel and P. Freire, Ann. Rev. Astron. Astrophys. **54**, 401 (2016).
[72] R. Abbott et al. [LIGO Scientific and Virgo Collaborations], Astrophys. J. Lett. **896**, L44 (2020).
[73] N. Pol, M. McLaughlin, and D. R. Lorimer, Astrophys. J. **870**, 71 (2019); **874**, 186 (2019) [erratum].
[74] R. N. Manchester, G. B. Hobbs, A. Teoh, and M. Hobbs, Astrophys. J. **129**, 1993 (2005).
[75] ATNF Pulsar Catalogue webpage, http://www.atnf.csiro.au/research/pulsar/psrcat/
[76] B. P. Abbott et al. [LIGO Scientific and Virgo Collaborations], Phys. Rev. X **9**, 011001 (2019).
[77] B. P. Abbott et al. [LIGO Scientific and Virgo Collaborations], Phys. Rev. Lett. **121**, 161101 (2018).
[78] J. M. Lattimer and M. Prakash, Phys. Rept. **621**, 127 (2016).
[79] E. E. Flanagan and T. Hinderer, Phys. Rev. D **77**, 021502 (2008).
[80] T. Hinderer, Astrophys. J. **677**, 1216 (2008); **697**, 964 (2009) [erratum].
[81] T. Damour, A. Nagar, and L. Villain, Phys. Rev. D **85**, 123007 (2012).
[82] L. Wade, J. D. E. Creighton, E. Ochsner, B. D. Lackey, B. F. Farr, T. B. Littenberg, and V. Raymond, Phys. Rev. D **89**, 103012 (2014).
[83] T. Hinderer, B. D. Lackey, R. N. Lang, and J. S. Read, Phys. Rev. D **81**, 123016 (2010).
[84] K. Hotokezaka, K. Kyutoku, H. Okawa, M. Shibata, and K. Kiuchi, Phys. Rev. D **83**, 124008 (2011).
[85] A. Buonanno, B. R. Iyer, E. Ochsner, Y. Pan, and B. S. Sathyaprakash, Phys. Rev. D **80**, 084043 (2009).
[86] L. Blanchet, Living Rev. Rel. **17**, 2 (2014).
[87] T. Dietrich, S. Bernuzzi, and W. Tichy, Phys. Rev. D **96**, 121501(R) (2017).
[88] K. Yagi and N. Yunes, Phys. Rept. **681**, 1 (2017).
[89] W. Kastaun and F. Ohme, Phys. Rev. D **100**, 103023 (2019).
[90] B. P. Abbott et al. [LIGO Scientific and Virgo Collaborations], Class. Quantum Grav. **37**, 045006 (2020).
[91] H. Müeller and B. D. Serot, Nucl. Phys. A **606**, 508 (1996).
[92] S. De, D. Finstad, J. M. Lattimer, D. A. Brown, E. Berger, and C. M. Biwer, Phys. Rev. Lett. **121**, 091102 (2018); **121**, 259902 (2018) [erratum].
[93] C. D. Capano, I. Tews, S. M. Brown, B. Margalit, S. De, S. Kumar, D. A. Brown, B. Krishnan, and S. Reddy, Nat. Astron. **4**, 625 (2020).
[94] T. Narikawa, N. Uchikata, K. Kawaguchi, K. Kiuchi, K. Kyutoku, M. Shibata, and H. Tagoshi, arXiv:1910.08971 [gr-qc] [Search INSPIRE].
[95] K. Kiuchi, K. Kawaguchi, K. Kyutoku, Y. Sekiguchi, M. Shibata, and K. Taniguchi, Phys. Rev. D **96**, 084060 (2017).
[96] K. Kawaguchi, K. Kiuchi, K. Kyutoku, Y. Sekiguchi, M. Shibata, and K. Taniguchi, Phys. Rev. D **97**, 044044 (2018).
[97] T. Dietrich, A. Samajdar, S. Khan, N. K. Johnson-McDaniel, R. Dudi, and W. Tichy, Phys. Rev. D **100**, 044003 (2019).
[98] B. Margalit and B. D. Metzger, Astrophys. J. Lett. **850**, L19 (2017).
[99] A. Bauswein, O. Just, H.-T. Janka, and N. Stergioulas, Astrophys. J. Lett. **850**, L34 (2017).
[100] M. Ruiz, S. L. Shapiro, and A. Tsokaros, Phys. Rev. D **97**, 021501(R) (2018).
[101] E. Annala, T. Gorda, A. Kurkela, and A. Vuorinen, Phys. Rev. Lett. **120**, 172703 (2018).
[102] E.-P. Zhou, X. Zhou, and A. Li, Phys. Rev. D **97**, 083015 (2018).
[103] F. J. Fattoyev, J. Piekarewicz, and C. J. Horowitz, Phys. Rev. Lett. **120**, 172702 (2018).
[104] V. Paschalidis, K. Yagi, D. Alvarez-Castillo, D. B. Blaschke, and A. Sedrakian, Phys. Rev. D **97**, 084038 (2018).
[105] R. Nandi and P. Char, Astrophys. J. **857**, 12 (2018).

[106] E. R. Most, L. R. Weih, L. Rezzolla, and J. Schaffner-Bielich, Phys. Rev. Lett. **120**, 261103 (2018).
[107] C. Raithel, F. Özel, and D. Psaltis, Astrophys. J. Lett. **857**, L23 (2018).
[108] P. Landry and R. Essick, Phys. Rev. D **99**, 084049 (2019).
[109] L. Baiotti, Prog. Part. Nucl. Phys. **109**, 103714 (2019).
[110] K. Takami, L. Rezzolla, and L. Baiotti, Phys. Rev. D **91**, 064001 (2015).
[111] A. Akmal, V. R. Pandharipande, and D. G. Ravenhall, Phys. Rev. C **58**, 1804 (1998).
[112] F. Douchin and P. Haensel, Astron. Astrophys. **380**, 151 (2001).
[113] T. Narikawa, N. Uchikata, K. Kawaguchi, K. Kiuchi, K. Kyutoku, M. Shibata, and H. Tagoshi, Phys. Rev. Res. **1**, 033055 (2019).
[114] L. Baiotti and L. Rezzolla, Rep. Prog. Phys. **80**, 096901 (2017).
[115] M. D. Duez and Y. Zlochower, Rep. Prog. Phys. **82**, 016902 (2019).
[116] M. H. P. M. van Putten, M. Della Valle, and A. Levinson, Astrophys. J. Lett. **876**, L2 (2019).
[117] V. Paschalidis and N. Stergioulas, Living Rev. Relat. **20**, 7 (2017).
[118] K. Takami, L. Rezzolla, and L. Baiotti, Phys. Rev. Lett. **113**, 091104 (2014).
[119] F. Maione, R. De Pietri, A. Feo, and F. Löffler, Phys. Rev. D **96**, 063011 (2017).
[120] M. Breschi, S. Bernuzzi, F. Zappa, M. Agathos, A. Perego, D. Radice, and A. Nagar, Phys. Rev. D **100**, 104029 (2019).
[121] A. Bauswein and H.-T. Janka, Phys. Rev. Lett. **108**, 011101 (2012).
[122] S. Bose, K. Chakravarti, L. Rezzolla, B. S. Sathyaprakash, and K. Takami, Phys. Rev. Lett. **120**, 031102 (2018).
[123] K. Chatziioannou, J. A. Clark, A. Bauswein, M. Millhouse, T. B. Littenberg, and N. Cornish, Phys. Rev. D **96**, 124035 (2017).
[124] A. Torres-Rivas, K. Chatziioannou, A. Bauswein, and J. A. Clark, Phys. Rev. D **99**, 044014 (2019).
[125] L. R. Weih, M. Hanauske, and L. Rezzolla, Phys. Rev. Lett. **124**, 171103 (2020).
[126] A. Bauswein, S. Blacker, V. Vijayan, N. Stergioulas, K. Chatziioannou, J. A. Clark, N.-U. Bastian, D. B. Blaschke, M. Cierniak, and T. Fischer, arXiv:2004.00846 [astro-ph.HE] [Search INSPIRE].
[127] L. Baiotti, B. Giacomazzo, and L. Rezzolla, Phys. Rev. D **78**, 084033 (2008).
[128] L. Rezzolla, B. Giacomazzo, L. Baiotti, J. Granot, C. Kouveliotou, and M. A. Aloy, Astrophys. J. Lett. **732**, L6 (2011).
[129] K. Kiuchi, Y. Sekiguchi, K. Kyutoku, M. Shibata, K. Taniguchi, and T. Wada, Phys. Rev. D **92**, 064034 (2015).
[130] D. Radice, A. Perego, K. Hotokezaka, S. A. Fromm, S. Bernuzzi, and L. F. Roberts, Astrophys. J. **869**, 130 (2018).
[131] R. P. Kerr, Phys. Rev. Lett. **11**, 237 (1963).
[132] M. H. P. M. van Putten, Science **284**, 115 (1999).
[133] R. De Pietri, A. Drago, A. Feo, G. Pagliara, M. Pasquali, S. Traversi, and G. Wiktorowicz, Astrophys. J. **881**, 122 (2019).
[134] J. Klimo, M. Veselsky, G. A. Souliotis, and A. Bonasera, Nucl. Phys. A **992**, 121640 (2019).
[135] P. Haensel, J. L. Zdunik, M. Bejger, and J. M. Lattimer, Astron. Astrophys. **502**, 605 (2009).
[136] V. Connaughton, GCN 21505 (2017) (available at: https://gcn.gsfc.nasa.gov/gcn3/21505.gcn3).
[137] V. Savchenko et al., Astrophys. J. Lett. **848**, L15 (2017).
[138] K. P. Mooley et al., Nature **554**, 207 (2018).
[139] K. P. Mooley, A. T. Deller, O. Gottlieb, E. Nakar, G. Hallinan, S. Bourke, D. A. Frail, A. Horesh, A. Corsi, and K. Hotokezaka, Nature **561**, 355 (2018).
[140] C. Cutler and K. S. Thorne, arXiv:gr-qc/0204090 [Search INSPIRE].
[141] R. A. Hulse and J. H. Taylor, Astrophys. J. **195**, L51 (1975).
[142] K. W. Weiler and N. Panagia, Astron. Astrophys. **70**, 419 (1978).
[143] B. P. Abbott et al. [INTEGRAL], Astrophys. J. Lett. **848**, L13 (2017).
[144] B. P. Abbott et al., Astrophys. J. **875**, 160 (2019).
[145] L. Sun and A. Melatos, Phys. Rev. D **99**, 123003 (2019).
[146] R. Gill, A. Nathanail, and L. Rezzolla, Astrophys. J. **876**, 139 (2019).
[147] S. J. Smartt et al., Nature **551**, 75 (2017).
[148] E. Pian et al., Nature **551**, 67 (2017).
[149] M. Lucca and L. Sagunski, J. High Energy Astrophys. **27**, 33 (2020).
[150] D. Pooley, P. Kumar, J. C. Wheeler, and B. Grossan, Astrophys. J. Lett. **859**, L23 (2018).
[151] M. H. P. M. van Putten, C. Guidorzi, and F. Frontera, Astrophys. J. **786**, 146 (2014).

[152] M. H. P. M. van Putten, Prog. Theor. Exp. Phys. **2017**, 093F01 (2017).
[153] M. H. P. M. van Putten and M. Della Valle, Mon. Not. R. Astron. Soc. **482**, L46 (2019).
[154] B. P. Abbott et al. [LIGO Scientific and Virgo Collaborations], Astrophys. J. Lett. **851**, L16 (2017).
[155] M. H. P. M. van Putten, A. Levinson, F. Frontera, C. Guidorzi, L. Amati, and M. Della Valle, Eur. Phys. J. Plus **134**, 537 (2019).
[156] J.-E. Heo, S. Yoon, D.-S. Lee, I.-t. Kong, S.-H. Lee, M. H. P. M. van Putten, and M. D. Valle, New Astron. **42**, 24 (2016).
[157] S. Ando et al., Rev. Mod. Phys. **85**, 1401 (2013).
[158] J. Aasi et al. [LIGO Scientific and Virgo Collaborations], Phys. Rev. D **89**, 122004 (2014).
[159] L. Amati et al., Adv. Space Res. **62**, 191 (2018).
[160] G. Stratta et al., Adv. Space Res. **62**, 662 (2018).
[161] K. Riles, Mod. Phys. Lett. A **32**, 1730035 (2017).
[162] G. Ushomirsky, C. Cutler, and L. Bildsten, Mon. Not. R. Astron. Soc. **319**, 902 (2000).
[163] L. Bildsten, Astrophys. J. Lett. **501**, L89 (1998).
[164] A. Mukherjee, C. Messenger, and K. Riles, Phys. Rev. D **97**, 043016 (2018).
[165] G. D. Meadors, E. Goetz, K. Riles, T. Creighton, and F. Robinet, Phys. Rev. D **95**, 042005 (2017).
[166] B. P. Abbott et al., Astrophys. J. **847**, 47 (2017).
[167] B. P. Abbott et al. [LIGO Scientific and Virgo Collaborations], Phys. Rev. D **95**, 122003 (2017).
[168] B. P. Abbott et al. [LIGO Scientific and Virgo Collaborations], Phys. Rev. D **100**, 122002 (2019).
[169] L. J. Kaluzienski, S. S. Holt, and J. H. Swank, Astrophys. J. **241**, 779 (1980).
[170] C. Messenger et al., Phys. Rev. D **92**, 023006 (2015).
[171] G. D. Meadors, B. Krishnan, M. A. Papa, J. T. Whelan, and Y. Zhang, Phys. Rev. D **97**, 044017 (2018).
[172] C. Dreissigacker, R. Sharma, C. Messenger, R. Zhao, and R. Prix, Phys. Rev. D **100**, 044009 (2019).
[173] R. Smits, S. J. Tingay, N. Wex, M. Kramer, and B. Stappers, Astron. Astrophys. **528**, A108 (2011).
[174] K. Ono, K. Eda, and Y. Itoh, Phys. Rev. D **91**, 084032 (2015).
[175] L. Rezzolla, P. Pizzochero, D. I. Jones, N. Rea and I. Vidaña. The Physics and Astrophysics of Neutron Stars (Springer, 2018).
[176] M. Sieniawska and M. Bejger, Universe **5**, 217 (2019).
[177] B. P. Abbott et al. [LIGO Scientific and Virgo Collaborations], Astrophys. J. **851**, 71 (2017).
[178] B. P. Abbott et al. [LIGO Scientific and Virgo Collaborations], Astrophys. J. **879**, 10 (2019).
[179] B. P. Abbott et al. [LIGO Scientific and Virgo Collaborations], Astrophys. J. **875**, 122 (2019).
[180] B. P. Abbott et al. [LIGO Scientific and Virgo Collaborations], Phys. Rev. Lett. **120**, 031104 (2018).
[181] N. K. Johnson-McDaniel and B. J. Owen, Phys. Rev. D **88**, 044004 (2013).
[182] N. K. Johnson-McDaniel, Phys. Rev. D **88**, 044016 (2013).
[183] M. Pitkin, Mon. Not. R. Astron. Soc. **415**, 1849 (2011).
[184] G. L. Israel, T. Belloni, L. Stella, Y. Rephaeli, D. E. Gruber, P. Casella, S. Dall'Osso, N. Rea, M. Persic, and R. E. Rothschild, Astrophys. J. Lett. **628**, L53 (2005).
[185] K. Ioka, Mon. Not. R. Astron. Soc. **327**, 639 (2001).
[186] A. Corsi and B. J. Owen, Phys. Rev. D **83**, 104014 (2011).
[187] Y. Levin and M. van Hoven, Mon. Not. R. Astron. Soc. **418**, 659 (2011).
[188] B. Zink, P. D. Lasky, and K. D. Kokkotas, Phys. Rev. D **85**, 024030 (2012).
[189] B. Abbott et al. [LIGO Scientific Collaboration], Phys. Rev. D **76**, 062003 (2007).
[190] B. P. Abbott et al. [LIGO Scientific Collaboration], Astrophys. J. **874**, 163 (2019).
[191] K. Kokkotas and B. G. Schmidt, Living Rev. Relat. **2**, 2 (1999).
[192] N. Andersson and K. D. Kokkotas, Phys. Rev. Lett. **77**, 4134 (1996).
[193] N. Andersson and K. D. Kokkotas, Mon. Not. R. Astron. Soc. **299**, 1059 (1998).
[194] L. S. Finn, Mon. Not. R. Astron. Soc. **227**, 265 (1987).
[195] H. Sotani, K. Tominaga, and K.-i. Maeda, Phys. Rev. D **65**, 024010 (2001).
[196] G. Miniutti, J. A. Pons, E. Berti, L. Gualtieri, and V. Ferrari, Mon. Not. R. Astron. Soc. **338**, 389 (2003).
[197] H. Sotani, N. Yasutake, T. Maruyama, and T. Tatsumi, Phys. Rev. D **83**, 024014 (2011).
[198] A. Reisenegger and P. Goldreich, Astrophys. J. **395**, 240 (1992).
[199] V. Ferrari, L. Gualtieri, and J. A. Pons, Class. Quantum Grav. **24**, 5093 (2007).
[200] A. Passamonti, N. Andersson, and W. C. G. Ho, Mon. Not. R. Astron. Soc. **455**, 1489 (2016).
[201] N. Andersson, Astrophys. J. **502**, 708 (1998).
[202] J. L. Friedman and S. M. Morsink, Astrophys. J. **502**, 714 (1998).

[203] P. Arras, E. E. Flanagan, S. M. Morsink, A. K. Schenk, S. A. Teukolsky, and I. Wasserman, Astrophys. J. **591**, 1129 (2003).
[204] E. Gaertig, K. Glampedakis, K. D. Kokkotas, and B. Zink, Phys. Rev. Lett. **107**, 101102 (2011).
[205] H. Sotani and T. Takiwaki, Phys. Rev. D **94**, 044043 (2016).
[206] H. Sotani, T. Kuroda, T. Takiwaki, and K. Kotake, Phys. Rev. D **96**, 063005 (2017).
[207] V. Morozova, D. Radice, A. Burrows, and D. Vartanyan, Astrophys. J. **861**, 10 (2018).
[208] H. Sotani, T. Kuroda, T. Takiwaki, and K. Kotake, Phys. Rev. D **99**, 123024 (2019).
[209] H. Sotani and K. Sumiyoshi, Phys. Rev. D **100**, 083008 (2019).
[210] A. Torres-Forné, P. Cerdá-Durán, A. Passamonti, and J. A. Font, Mon. Not. R. Astron. Soc. **474**, 5272 (2018).
[211] A. Torres-Forné, P. Cerdá-Durán, A. Passamonti, M. Obergaulinger, and J. A. Font, Mon. Not. R. Astron. Soc. **482**, 3967 (2019).
[212] B. W. Grefenstette et al., Astrophys. J. **802**, 15 (2015).
[213] M. Tanaka, K. Maeda, P. A. Mazzali, K. S. Kawabata, and K. Nomoto, Astrophys. J. **837**, 105 (2017).
[214] H. A. Bethe, Rev. Mod. Phys. **62**, 801 (1990).
[215] B. Müller, Publ. Astron. Soc. Aust. **33**, e048 (2016).
[216] H.-T. Janka, T. Melson, and A. Summa, Ann. Rev. Nucl. Part. Sci. **66**, 341 (2016).
[217] A. Burrows, Rev. Mod. Phys. **85**, 245 (2013).
[218] K. Kotake, K. Sumiyoshi, S. Yamada, T. Takiwaki, T. Kuroda, Y. Suwa, and H. Nagakura, Prog. Theor. Exp. Phys. **2012**, 01A301 (2012).
[219] D. Radice, V. Morozova, A. Burrows, D. Vartanyan, and H. Nagakura, Astrophys. J. Lett. **876**, L9 (2019).
[220] H. Andresen, E. Müller, H.-Th. Janka, A. Summa, K. Gill, and M. Zanolin, Mon. Not. R. Astron. Soc. **486**, 2238 (2019).
[221] H. Andresen, B. Müller, E. Müller, and H.-Th. Janka, Mon. Not. R. Astron. Soc. **468**, 2032 (2017).
[222] T. Kuroda, K. Kotake, and T. Takiwaki, Astrophys. J. Lett. **829**, L14 (2016).
[223] P. Astone, P. Cerdá-Durán, I. Di Palma, M. Drago, F. Muciaccia, C. Palomba, and F. Ricci, Phys. Rev. D **98**, 122002 (2018).
[224] T. Foglizzo et al., Publ. Astron. Soc. Aust. **32**, e009 (2015).
[225] K. Kotake, Compt. Rendus Phys. **14**, 318 (2013).
[226] C. D. Ott, Class. Quantum Grav. **26**, 063001 (2009).
[227] S. E. Woosley and A. Heger, Astrophys. J. **637**, 914 (2006).
[228] K. Hayama, T. Kuroda, K. Nakamura, and S. Yamada, Phys. Rev. Lett. **116**, 151102 (2016).
[229] K. Hayama, T. Kuroda, K. Kotake, and T. Takiwaki, Mon. Not. R. Astron. Soc. **477**, L96 (2018).
[230] K. Hayama, T. Kuroda, K. Kotake, and T. Takiwaki, Phys. Rev. D **92**, 122001 (2015).
[231] S. Suvorova, J. Powell, and A. Melatos, Phys. Rev. D **99**, 123012 (2019).
[232] S. E. Gossan, P. Sutton, A. Stuver, M. Zanolin, K. Gill, and C. D. Ott, Phys. Rev. D **93**, 042002 (2016).
[233] A. A. Starobinsky, Phys. Lett. B **91**, 99 (1980).
[234] K. Sato, Mon. Not. R. Astron. Soc. **195**, 467 (1981).
[235] D. Kazanas, Astrophys. J. **241**, L59 (1980).
[236] A. H. Guth, Phys. Rev. D **23**, 347 (1981).
[237] V. F. Mukhanov and G. V. Chibisov, JETP Lett. **33**, 532 (1981) [Pisma Zh. Eksp. Teor. Fiz. **33**, 532 (1981)].
[238] A. D. Linde, Phys. Lett. B **116**, 335 (1982).
[239] S. W. Hawking, Phys. Lett. B **115**, 295 (1982).
[240] A. A. Starobinsky, Phys. Lett. B **117**, 175 (1982).
[241] A. H. Guth and S.-Y. Pi, Phys. Rev. Lett. **49**, 1110 (1982).
[242] A. A. Starobinsky, JETP Lett. **30**, 682 (1979) [Pisma Zh. Eksp. Teor. Fiz. **30**, 682 (1979)].
[243] V. A. Rubakov, M. V. Sazhin, and A. V. Veryaskin, Phys. Lett. B **115**, 189 (1982).
[244] L. F. Abbott and M. B. Wise, Nucl. Phys. B **244**, 541 (1984).
[245] S. Kuroyanagi, T. Chiba, and N. Sugiyama, Phys. Rev. D **79**, 103501 (2009).
[246] S. Kuroyanagi, S. Tsujikawa, T. Chiba, and N. Sugiyama, Phys. Rev. D **90**, 063513 (2014).
[247] B. P. Abbott et al. [LIGO Scientific/Virgo Collaborations], Phys. Rev. D **100**, 061101(R) (2009).
[248] R. H. Brandenberger, A. Nayeri, S. P. Patil, and C. Vafa, Phys. Rev. Lett. **98**, 231302 (2007).
[249] Y.-S. Piao and Y.-Z. Zhang, Phys. Rev. D **70**, 063513 (2004).
[250] M. Baldi, F. Finelli, and S. Matarrese, Phys. Rev. D **72**, 083504 (2005).

[251] T. Kobayashi, M. Yamaguchi, and J. Yokoyama, Phys. Rev. Lett. **105**, 231302 (2010).
[252] G. Calcagni and S. Tsujikawa, Phys. Rev. D **70**, 103514 (2004).
[253] G. Calcagni, S. Kuroyanagi, J. Ohashi, and S. Tsujikawa, J. Cosmol. Astropart. Phys. **1403**, 052 (2014).
[254] J. L. Cook and L. Sorbo, Phys. Rev. D **85**, 023534 (2012); **86**, 069901 (2012) [erratum].
[255] S. Mukohyama, R. Namba, M. Peloso, and G. Shiu, J. Cosmol. Astropart. Phys. **1408**, 036 (2014).
[256] S. Mohanty and A. Nautiyal, arXiv:1404.2222 [hep-ph] [Search INSPIRE].
[257] M. Biagetti, M. Fasiello, and A. Riotto, Phys. Rev. D **88**, 103518 (2013).
[258] T. Fujita, S. Kuroyanagi, S. Mizuno, and S. Mukohyama, Phys. Lett. B **789**, 215 (2019).
[259] P. J. E. Peebles and A. Vilenkin, Phys. Rev. D **59**, 063505 (1999).
[260] M. Giovannini, Phys. Rev. D **58**, 083504 (1998).
[261] M. Giovannini, Phys. Rev. D **60**, 123511 (1999).
[262] M. Giovannini, Class. Quantum Grav. **16**, 2905 (1999).
[263] H. Tashiro, T. Chiba, and M. Sasaki, Class. Quantum Grav. **21**, 1761 (2004).
[264] M. Giovannini, Class. Quantum Grav. **26**, 045004 (2009).
[265] D. G. Figueroa and E. H. Tanin, J. Cosmol. Astropart. Phys. **1910**, 050 (2019).
[266] S. Ahmad, A. De Felice, N. Jaman, S. Kuroyanagi, and M. Sami, Phys. Rev. D **100**, 103525 (2019).
[267] B. Allen and J. D. Romano, Phys. Rev. D **59**, 102001 (1999).
[268] C. Grojean and G. Servant, Phys. Rev. D **75**, 043507 (2007).
[269] C. Caprini et al., J. Cosmol. Astropart. Phys. **1604**, 001 (2016).
[270] M. Kakizaki, S. Kanemura, and T. Matsui, Phys. Rev. D **92**, 115007 (2015).
[271] K. Hashino, R. Jinno, M. Kakizaki, S. Kanemura, T. Takahashi, and M. Takimoto, Phys. Rev. D **99**, 075011 (2019).
[272] P. S. Bhupal Dev and A. Mazumdar, Phys. Rev. D **93**, 104001 (2016).
[273] S. Kuroyanagi, T. Chiba, and T. Takahashi, J. Cosmol. Astropart. Phys. **1811**, 038 (2018).
[274] B. Allen and A. C. Ottewill, Phys. Rev. D **56**, 545 (1997).
[275] B. P. Abbott et al. [LIGO Scientific and Virgo Collaborations], Phys. Rev. Lett. **118**, 121102 (2017).
[276] A. Nishizawa, A. Taruya, K. Hayama, S. Kawamura, and M.-a. Sakagami, Phys. Rev. D **79**, 082002 (2009).
[277] B. P. Abbott et al. [LIGO Scientific and Virgo Collaborations], Phys. Rev. Lett. **120**, 201102 (2018).
[278] S. Drasco and É. É. Flanagan, Phys. Rev. D **67**, 082003 (2003).
[279] E. Thrane, Phys. Rev. D **87**, 043009 (2013).
[280] L. Martellini and T. Regimbau, Phys. Rev. D **89**, 124009 (2014).
[281] R. Brito, S. Ghosh, E. Barausse, E. Berti, V. Cardoso, I. Dvorkin, A. Klein, and P. Pani, Phys. Rev. Lett. **119**, 131101 (2017).
[282] S. Bose, Phys. Rev. D **71**, 082001 (2005).
[283] D. G. Figueroa, E. Megías, G. Nardini, M. Pieroni, M. Quiros, A. Ricciardone, and G. Tasinato, PoS **GRASS2018**, 036 (2018).
[284] T. G. F. Li, W. Del Pozzo, S. Vitale, C. Van Den Broeck, M. Agathos, J. Veitch, K. Grover, T. Sidery, R. Sturani, and A. Vecchio, Phys. Rev. D **85**, 082003 (2012).
[285] T. G. F. Li, W. Del Pozzo, S. Vitale, C. Van Den Broeck, M. Agathos, J. Veitch, K. Grover, T. Sidery, R. Sturani, and A. Vecchio, J. Phys.: Conf. Ser. **363**, 012028 (2012).
[286] M. Agathos, W. Del Pozzo, T. G. F. Li, C. Van Den Broeck, J. Veitch, and S. Vitale, Phys. Rev. D **89**, 082001 (2014).
[287] N. Cornish, L. Sampson, N. Yunes, and F. Pretorius, Phys. Rev. D **84**, 062003 (2011).
[288] L. Sampson, N. Cornish, and N. Yunes, Phys. Rev. D **89**, 064037 (2014).
[289] J. Meidam et al., Phys. Rev. D **97**, 044033 (2018).
[290] A. Ghosh et al., Phys. Rev. D **94**, 021101(R) (2016).
[291] A. Ghosh, N. K. Johnson-McDaniel, A. Ghosh, C. K. Mishra, P. Ajith, W. Del Pozzo, C. P. L. Berry, A. B. Nielsen and L. London, Class. Quantum Grav. **35**, 014002 (2017).
[292] B. P. Abbott et al. [LIGO Scientific and Virgo Collaborations], Phys. Rev. Lett. **116**, 221101 (2016); **121**, 129902 (2018) [erratum].
[293] B. P. Abbott et al. [LIGO Scientific and Virgo Collaborations], Phys. Rev. X **6**, 041015 (2016); **8**, 039903 (2018) [erratum].
[294] B. P. Abbott et al. [LIGO Scientific and Virgo Collaborations], Phys. Rev. Lett. **123**, 011102 (2019).
[295] B. P. Abbott et al. [LIGO Scientific and Virgo Collaborations], Phys. Rev. D **100**, 104036 (2019).

[296] J. Khoury and A. Weltman, Phys. Rev. D **93**, 171104 (2004).
[297] A. I. Vainshtein, Phys. Lett. B **39**, 393 (1972).
[298] N. Yunes and F. Pretorius, Phys. Rev. D **80**, 122003 (2009).
[299] K. Yagi, L. C. Stein, N. Yunes, and T. Tanaka, Phys. Rev. D **85**, 064022 (2012); **93**, 029902 (2016) [erratum].
[300] S. F. Hassan and R. A. Rosen, J. High Energy Phys. **1202**, 126 (2012).
[301] N. Yunes, F. Pretorius, and D. Spergel, Phys. Rev. D **81**, 064018 (2010).
[302] K. Yagi, N. Tanahashi, and T. Tanaka, Phys. Rev. D **83**, 084036 (2011).
[303] C. M. Will and H. W. Zaglauer, Astrophys. J. **346**, 366 (1989).
[304] C. M. Will, Phys. Rev. D **57**, 2061 (1998).
[305] K. Yagi, N. Yunes, and T. Tanaka, Phys. Rev. Lett. **109**, 251105 (2012); **116**, 169902 (2016); **124**, 029901 (2020) [errata].
[306] F. M. Ramazanoğlu and F. Pretorius, Phys. Rev. D **93**, 064005 (2016).
[307] L. Lombriser and A. Taylor, J. Cosmol. Astropart. Phys. **1603**, 031 (2016).
[308] I. D. Saltas, I. Sawicki, L. Amendola, and M. Kunz, Phys. Rev. Lett. **113**, 191101 (2014).
[309] A. Nishizawa and T. Kobayashi, Phys. Rev. D **98**, 124018 (2018).
[310] W. Zhao, T. Zhu, J. Qiao, and A. Wang, Phys. Rev. D **101**, 024002 (2020).
[311] D. Blas, M. M. Ivanov, I. Sawicki, and S. Sibiryakov, JETP Lett. **103**, 624 (2016).
[312] N. Cornish, D. Blas, and G. Nardini, Phys. Rev. Lett. **119**, 161102 (2017).
[313] A. Nishizawa and T. Nakamura, Phys. Rev. D **90**, 044048 (2014).
[314] T. Baker, E. Bellini, P. G. Ferreira, M. Lagos, J. Noller, and I. Sawicki, Phys. Rev. Lett. **119**, 251301 (2017).
[315] P. Creminelli and F. Vernizzi, Phys. Rev. Lett. **119**, 251302 (2017).
[316] J. Sakstein and B. Jain, Phys. Rev. Lett. **119**, 251303 (2017).
[317] J. M. Ezquiaga and M. Zumalacárregui, Phys. Rev. Lett. **119**, 251304 (2017).
[318] L. Bernus, O. Minazzoli, A. Fienga, M. Gastineau, J. Laskar, and P. Deram, Phys. Rev. Lett. **123**, 161103 (2019).
[319] S. Arai and A. Nishizawa, Phys. Rev. D **97**, 104038 (2018).
[320] A. Nishizawa and S. Arai, Phys. Rev. D **99**, 104038 (2019).
[321] M. Crisostomi, K. Noui, C. Charmousis, and D. Langlois, Phys. Rev. D **97**, 044034 (2018).
[322] A. Nishizawa, Phys. Rev. D **97**, 104037 (2018).
[323] P. Amaro-Seoane et al. [LISA Collaboration], arXiv:1702.00786 [astro-ph.IM] [Search INSPIRE].
[324] S. Sato et al., J. Phys.: Conf. Ser. **840**, 012010 (2017).
[325] K. Yagi and T. Tanaka, Phys. Rev. D **81**, 064008 (2010); **81**, 109902 (2010) [erratum].
[326] K. Yagi and T. Tanaka, Prog. Theor. Phys. **123**, 1069 (2010).
[327] D. M. Eardley, D. L. Lee, A. P. Lightman, R. V. Wagoner, and C. M. Will, Phys. Rev. Lett. **30**, 884 (1973).
[328] H. Takeda, A. Nishizawa, Y. Michimura, K. Nagano, K. Komori, M. Ando, and K. Hayama, Phys. Rev. D **98**, 022008 (2018).
[329] Y. Hagihara, N. Era, D. Iikawa, and H. Asada, Phys. Rev. D **98**, 064035 (2018).
[330] B. P. Abbott et al. [LIGO Scientific and Virgo Collaborations], Phys. Rev. Lett. **119**, 141101 (2017).
[331] K. Chatziioannou, N. Yunes, and N. Cornish, Phys. Rev. D **86**, 022004 (2012); **95**, 129901 (2017) [erratum].
[332] Y. Hagihara, N. Era, D. Iikawa, A. Nishizawa, and H. Asada, Phys. Rev. D **100**, 064010 (2019).
[333] Y. Hagihara, N. Era, D. Iikawa, N. Takeda, and H. Asada, Phys. Rev. D **101**, 041501(R) (2020).
[334] O. Dreyer, B. Kelly, B. Krishnan, L. S. Finn, D. Garrison, and R. Lopez-Aleman, Class. Quantum Grav. **21**, 787 (2004).
[335] E. Berti, J. Cardoso, V. Cardoso, and M. Cavaglià, Phys. Rev. D **76**, 104044 (2007).
[336] K. Sakai, K.-i. Oohara, H. Nakano, M. Kaneyama, and H. Takahashi, Phys. Rev. D **96**, 044047 (2017).
[337] G. Carullo et al., Phys. Rev. D **98**, 104020 (2018).
[338] G. Carullo, W. Del Pozzo, and J. Veitch, Phys. Rev. D **99**, 123029 (2019); **100**, 089903 (2019) [erratum].
[339] E. Berti, K. Yagi, H. Yang, and N. Yunes, Gen. Relat. Gravit. **50**, 49 (2018).
[340] S. D. Mohanty, Phys. Rev. D **57**, 630 (1998).
[341] V. Baibhav, E. Berti, V. Cardoso, and G. Khanna, Phys. Rev. D **97**, 044048 (2018).
[342] M. Giesler, M. Isi, M. A. Scheel, and S. A. Teukolsky, Phys. Rev. X **9**, 041060 (2019).

[343] M. Isi, M. Giesler, W. M. Farr, M. A. Scheel, and S. A. Teukolsky, Phys. Rev. Lett. **123**, 111102 (2019).
[344] S. Bhagwat, X. J. Forteza, P. Pani, and V. Ferrari, Phys. Rev. D **101**, 044033 (2020).
[345] I. Ota and C. Chirenti, Phys. Rev. D **101**, 104005 (2020).
[346] V. Baibhav and E. Berti, Phys. Rev. D **99**, 024005 (2019).
[347] E. Berti, A. Sesana, E. Barausse, V. Cardoso, and K. Belczynski, Phys. Rev. Lett. **117**, 101102 (2016).
[348] J. Healy, C. O. Lousto, Y. Zlochower, and M. Campanelli, Class. Quantum Grav. **34**, 224001 (2017).
[349] RIT Waveform Catalog webpage, https://ccrg.rit.edu/content/data/rit-waveformcatalog.
[350] B. F. Schutz, Nature **323**, 310 (1986).
[351] D. E. Holz and S. A. Hughes, Astrophys. J. **629**, 15 (2005).
[352] N. Aghanim et al. [Planck Collaboration], arXiv:1807.06209 [astro-ph.CO] [Search INSPIRE].
[353] N. Schöneberg, J. Lesgourgues, and D. C. Hooper, J. Cosmol. Astropart. Phys. **1910**, 029 (2019).
[354] A. Cuceu, J. Farr, P. Lemos, and A. Font-Ribera, J. Cosmol. Astropart. Phys. **1910**, 044 (2019).
[355] A. G. Riess et al., Astrophys. J. **861**, 126 (2018).
[356] A. G. Riess, S. Casertano, W. Yuan, L. M. Macri, and D. Scolnic, Astrophys. J. **876**, 85 (2019).
[357] T. Collett, F. Montanari, and S. Räsänen, Phys. Rev. Lett. **123**, 231101 (2019).
[358] K. C. Wong et al., arXiv:1907.04869 [astro-ph.CO] [Search INSPIRE].
[359] G. C.-F. Chen et al., Mon. Not. R. Astron. Soc. **490**, 1743 (2019).
[360] W. L. Freedman et al., Astrophys. J. **882**, 34 (2019).
[361] B. P. Abbott et al., Astrophys. J. Lett. **848**, L12 (2017).
[362] C. Cutler and D. E. Holz, Phys. Rev. D **80**, 104009 (2009).
[363] A. Nishizawa, Phys. Rev. D **96**, 101303(R) (2017).
[364] C. L. MacLeod and C. J. Hogan, Phys. Rev. D **77**, 043512 (2008).
[365] B. P. Abbott et al. [LIGO Scientific, Virgo, 1M2H, Dark Energy Camera GW-E, DES, DLT40, Las Cumbres Observatory, VINROUGE, and MASTER Collaborations], Nature **551**, 85 (2017).
[366] M. Soares-Santos et al. [DES, LIGO Scientific, and Virgo Collaborations], Astrophys. J. Lett. **876**, L7 (2019) [arXiv:1901.01540 [astro-ph.CO]] [Search INSPIRE].
[367] K. Hotokezaka, E. Nakar, O. Gottlieb, S. Nissanke, K. Masuda, G. Hallinan, K. P. Mooley, and A. T. Deller, Nat. Astron. **3**, 940 (2019).
[368] S. Vitale and H.-Y. Chen, Phys. Rev. Lett. **121**, 021303 (2018).
[369] N. Seto and K. Kyutoku, Mon. Not. R. Astron. Soc. **475**, 4133 (2018).
[370] H.-Y. Chen, M. Fishbach, and D. E. Holz, Nature **562**, 545 (2018).
[371] N. Gupte and I. Bartos, arXiv:1808.06238 [astro-ph.HE] [Search INSPIRE].
[372] E. J. Howell, K. Ackley, A. Rowlinson, and D. Coward, Mon. Not. R. Astron. Soc. **485**, 1435 (2019).
[373] K. Mogushi, M. Cavaglià, and K. Siellez, Astrophys. J. **880**, 55 (2019) [arXiv:1811.08542 [astro-ph.HE]] [Search INSPIRE].
[374] N. Gehrels, J. K. Cannizzo, J. Kanner, M. M. Kasliwal, S. Nissanke, and L. P. Singer, Astrophys. J. **820**, 136 (2016).
[375] E. L. Turner, J. P. Ostriker, and J. R. Gott III, Astrophys. J. **284**, 1 (1984).
[376] T. Treu, Ann. Rev. Astron. Astrophys. **48**, 87 (2010).
[377] T. Broadhurst, J. M. Diego, and G. Smoot III, arXiv:1802.05273 [astro-ph.CO] [Search INSPIRE].
[378] T. Broadhurst, J. M. Diego, and G. F. Smoot III, arXiv:1901.03190 [astro-ph.CO] [Search INSPIRE].
[379] P. Christian, S. Vitale, and A. Loeb, Phys. Rev. D **98**, 103022 (2018).
[380] K. K. Y. Ng, K. W. K. Wong, T. Broadhurst, and T. G. F. Li, Phys. Rev. D **97**, 023012 (2018).
[381] G. P. Smith, M. Jauzac, J. Veitch, W. M. Farr, R. Massey, J. Richard, Mon. Not. R. Astron. Soc. **475**, 3823 (2018).
[382] S.-S. Li, S. Mao, Y. Zhao, and Y. Lu, Mon. Not. R. Astron. Soc. **476**, 2220 (2018).
[383] L. S. Finn, Phys. Rev. D **53**, 2878 (1996).
[384] Y. Wang, A. Stebbins, and E. L. Turner, Phys. Rev. Lett. **77**, 2875 (1996).
[385] T. T. Nakamura, Phys. Rev. Lett. **80**, 1138 (1998).
[386] S. Jung and C. S. Shin, Phys. Rev. Lett. **122**, 041103 (2019).
[387] K.-H. Lai, O. A. Hannuksela, A. Herrera-Martín, J. M. Diego, T. Broadhurst, and T. G. F. Li, Phys. Rev. D **98**, 083005 (2018).
[388] R. Takahashi and T. Nakamura, Astrophys. J. **595**, 1039 (2003).
[389] T. E. Collett and D. Bacon, Phys. Rev. Lett. **118**, 091101 (2017).

[390] X.-L. Fan, K. Liao, M. Biesiada, A. Piórkowska-Kurpas, and Z.-H. Zhu, Phys. Rev. Lett. **118**, 091102 (2017).
[391] S. Rosswog, M. Liebendöerfer, F.-K. Thielemann, M. B. Davies, W. Benz, and T. Piran, Astron. Astrophys. **341**, 499 (1999).
[392] K. Hotokezaka, K. Kiuchi, K. Kyutoku, H. Okawa, Y. Sekiguchi, M. Shibata, and K. Taniguchi, Phys. Rev. D **87**, 024001 (2013).
[393] J. M. Lattimer and D. N. Schramm, Astrophys. J. Lett. **192**, L145 (1974).
[394] D. Eichler, M. Livio, T. Piran, and D. N. Schramm, Nature **340**, 126 (1989).
[395] O. Korobkin, S. Rosswog, A. Arcones, and C. Winteler, Mon. Not. R. Astron. Soc. **426**, 1940 (2012).
[396] S. Wanajo, Y. Sekiguchi, N. Nishimura, K. Kiuchi, K. Kyutoku, and M. Shibata, Astrophys. J. Lett. **789**, L39 (2014).
[397] L.-X. Li and B. Paczyński, Astrophys. J. Lett. **507**, L59 (1998).
[398] S. R. Kulkarni, arXiv:astro-ph/0510256 [Search INSPIRE].
[399] B. D. Metzger, G. Martínez-Pinedo, S. Darbha, E. Quataert, A. Arcones, D. Kasen, R. Thomas, P. Nugent, I. V. Panov, and N. T. Zinner, Mon. Not. R. Astron. Soc. **406**, 2650 (2010).
[400] D. Kasen, N. R. Badnell, and J. Barnes, Astrophys. J. **774**, 25 (2013).
[401] M. Tanaka and K. Hotokezaka, Astrophys. J. **775**, 113 (2013).
[402] D. Kasen, R. Fernández, and B. Metzger, Mon. Not. R. Astron. Soc. **450**, 1777 (2015).
[403] J. Barnes, D. Kasen, M.-R. Wu, and G. Martínez-Pinedo, Astrophys. J. **829**, 110 (2016).
[404] R. T. Wollaeger, O. Korobkin, C. J. Fontes, S. K. Rosswog, W. P. Even, C. L. Fryer, J. Sollerman, A. L. Hungerford, D. R. van Rossum, and A. B. Wollaber, Mon. Not. R. Astron. Soc. **478**, 3298 (2018).
[405] M. Tanaka et al., Publ. Astron. Soc. Jpn. **69**, 102 (2017).
[406] M. Tanaka et al., Astrophys. J. **852**, 109 (2018).
[407] M. M. Kasliwal et al., Science **358**, 1559 (2017).
[408] P. S. Cowperthwaite et al., Astrophys. J. Lett. **848**, L17 (2017).
[409] D. Kasen, B. Metzger, J. Barnes, E. Quataert, and E. Ramirez-Ruiz, Nature **551**, 80 (2017).
[410] V. A. Villar et al., Astrophys. J. Lett. **851**, L21 (2017).
[411] A. Perego, D. Radice, and S. Bernuzzi, Astrophys. J. Lett. **850**, L37 (2017).
[412] N. R. Tanvir et al., Astrophys. J. Lett. **848**, L27 (2017).
[413] K. Kawaguchi, M. Shibata, and M. Tanaka, Astrophys. J. Lett. **865**, L21 (2018).
[414] S. Nissanke, M. Kasliwal, and A. Georgieva, Astrophys. J. **767**, 124 (2013).
[415] O. Gottlieb, E. Nakar, and T. Piran, Mon. Not. R. Astron. Soc. **473**, 576 (2018).
[416] I. Arcavi, Astrophys. J. Lett. **855**, L23 (2018).
[417] T. Matsumoto, Mon. Not. R. Astron. Soc. **481**, 1008 (2018).
[418] I. Andreoni et al., Astrophys. J. **890**, 131 (2020).
[419] K. Kawaguchi, M. Shibata, and M. Tanaka, Astrophys. J. **893**, 153 (2020).
[420] Pan-STARRS project webpage, http://pan-starrs.ifa.hawaii.edu.
[421] J. P. Bernstein et al., Astrophys. J. **753**, 152 (2012).
[422] D. Radice, F. Galeazzi, J. Lippuner, L. F. Roberts, C. D. Ott, and L. Rezzolla, Mon. Not. R. Astron. Soc. **460**, 3255 (2016).
[423] Y. Sekiguchi, K. Kiuchi, K. Kyutoku, and M. Shibata, Phys. Rev. D **91**, 064059 (2015).
[424] Y. Sekiguchi, K. Kiuchi, K. Kyutoku, M. Shibata, and K. Taniguchi, Phys. Rev. D **93**, 124046 (2016).
[425] E Nakar, Phys. Rep. **442**, 166 (2007).
[426] E. Berger, Ann. Rev. Astron. Astrophys. **52**, 43 (2014).
[427] B. Paczynski, Astrophys. J. **308**, L43 (1986).
[428] J. Goodman, Astrophys. J. **308**, L47 (1986).
[429] L. Amati et al., Astron. Astrophys. **390**, 81 (2002).
[430] D. Yonetoku, T. Murakami, T. Nakamura, R. Yamazaki, A. K. Inoue, and K. Ioka, Astrophys. J. **609**, 935 (2004).
[431] S. Kisaka, K. Ioka, and T. Sakamoto, Astrophys. J. **846**, 142 (2017).
[432] A. Goldstein et al., Astrophys. J. Lett. **848**, L14 (2017).
[433] E. Troja et al., Nature **551**, 71 (2017).
[434] R. Margutti et al., Astrophys. J. Lett. **848**, L20 (2017).
[435] D. Haggard, M. Nynka, J. J. Ruan, V. Kalogera, S. B. Cenko, P. Evans, and J. A. Kennea, Astrophys. J. Lett. **848**, L25 (2017).
[436] G. Hallinan et al., Science **358**, 1579 (2017).

[437] K. D. Alexander et al., Astrophys. J. Lett. **848**, L21 (2017).
[438] J. D. Lyman et al., Nat. Astron. **2**, 751 (2018).
[439] G. Ghirlanda et al., Science **363**, 968 (2019).
[440] E. Troja, H. van Eerten, G. Ryan, R. Ricci, J. M. Burgess, M. H. Wieringa, L. Piro, S. B. Cenko, and T. Sakamoto, Mon. Not. R. Astron. Soc. **489**, 1919 (2019).
[441] K. P. Mooley et al., Astrophys. J. Lett. **868**, L11 (2018).
[442] G. P. Lamb et al., Astrophys. J. Lett. **870**, L15 (2019).
[443] H. Nagakura, K. Hotokezaka, Y. Sekiguchi, M. Shibata, and K. Ioka, Astrophys. J. Lett. **784**, L28 (2014).
[444] H. Hamidani, K. Kiuchi, and K. Ioka, Mon. Not. R. Astron. Soc. **491**, 3192 (2020).
[445] K. Ioka and T. Nakamura, Prog. Theor. Exp. Phys. **2018**, 043E02 (2018).
[446] J. Granot, D. Guetta, and R. Gill, Astrophys. J. Lett. **850**, L24 (2017).
[447] S. Kisaka, K. Ioka, K. Kashiyama, and T. Nakamura, Astrophys. J. **867**, 39 (2018).
[448] E. Nakar, O. Gottlieb, T. Piran, M. M. Kasliwal, and G. Hallinan, Astrophys. J. **867**, 18 (2018).
[449] E. Nakar, arXiv:1912.05659 [astro-ph.HE] [Search INSPIRE].
[450] E. Troja, L. Piro, G. Ryan, H. van Eerten, R. Ricci, M. H. Wieringa, S. Lotti, T. Sakamoto, and S. B. Cenko, Mon. Not. R. Astron. Soc. **478**, L18 (2018).
[451] J. J. Ruan, M. Nynka, D. Haggard, V. Kalogera, and P. Evans, Astrophys. J. Lett. **853**, L4 (2018).
[452] R. Margutti et al., Astrophys. J. Lett. **856**, L18 (2018).
[453] P. D'Avanzo et al., Astron. Astrophys. **613**, L1 (2018).
[454] D. Lazzati, R. Perna, B. J. Morsony, D. Lopez-Camara, M. Cantiello, R. Ciolfi, B. Giacomazzo, and J. C. Workman, Phys. Rev. Lett. **120**, 241103 (2018).
[455] K. Ioka and T. Nakamura, Mon. Not. R. Astron. Soc. **487**, 4884 (2019).
[456] T. Matsumoto, E. Nakar, and T. Piran, Mon. Not. R. Astron. Soc. **483**, 1247 (2019).
[457] T. Matsumoto, E. Nakar, and T. Piran, Mon. Not. R. Astron. Soc. **486**, 1563 (2019).
[458] N. Tominaga et al., Publ. Astron. Soc. Jpn. **70**, 28 (2018).
[459] K. Cannon et al., Astrophys. J. **748**, 136 (2012).
[460] J. Abadie et al. [LIGO Scientific and Virgo Collaborations], Astrophys. J. Lett. **734**, L35 (2011).
[461] K. Kashiyama and K. Ioka, Phys. Rev. D **83**, 081302(R) (2011).
[462] B. Abbott et al. [LIGO Scientific Collaboration], Astrophys. J. **681**, 1419 (2008).
[463] J. Abadie et al. [LIGO Scientific Collaboration], Astrophys. J. **755**, 2 (2012).
[464] B. P. Abbott et al. [LIGO Scientific and Virgo and IPN Collaborations], Astrophys. J. **841**, 89 (2017).
[465] T. Piran, Rev. Mod. Phys. **76**, 1143 (2005).
[466] P. Kumar and B. Zhang, Phys. Rep. **561**, 1 (2015).
[467] A. I. MacFadyen and S. E. Woosley, Astrophys. J. **524**, 262 (1999).
[468] R. F. Stark and T. Piran, Phys. Rev. Lett. **55**, 891 (1985); **56**, 97 (1986) [erratum].
[469] S. Kobayashi and P. Mészáros, Astrophys. J. **589**, 861 (2003).
[470] V. B. Braginsky and K. S. Thorne, Nature **327**, 123 (1987).
[471] E. B. Segalis and A. Ori, Phys. Rev. D **64**, 064018 (2001).
[472] N. Sago, K. Ioka, T. Nakamura, and R. Yamazaki, Phys. Rev. D **70**, 104012 (2004).
[473] Y. Suwa and K. Murase, Phys. Rev. D **80**, 123008 (2009).
[474] P. Astone et al., Phys. Rev. D **71**, 042001 (2005).
[475] B. Abbott et al. [LIGO Scientific Collaboration], Phys. Rev. D **72**, 042002 (2005).
[476] J. Aasi et al. [LIGO Scientific, Virgo, and IPN Collaborations], Phys. Rev. Lett. **113**, 011102 (2014).
[477] B. P. Abbott et al. [LIGO Scientific and Virgo Collaborations], Astrophys. J. **886**, 75 (2019).
[478] E. Liang, B. Zhang, F. Virgili, and Z. G. Dai, Astrophys. J. **662**, 1111 (2007).
[479] D. R. Lorimer, M. Bailes, M. A. McLaughlin, D. J. Narkevic, and F. Crawford, Science **318**, 777 (2007).
[480] FRBCAT, http://frbcat.org/.
[481] K. Kashiyama and K. Murase, Astrophys. J. Lett. **839**, L3 (2017).
[482] T. Totani, Publ. Astron. Soc. Jpn. **65**, L12 (2013).
[483] P. Chawla et al., Astrophys. J. **844**, 140 (2017).
[484] T. W. B. Kibble, J. Phys. A: Math. Gen **9**, 1387 (1976).
[485] S. Sarangi and S.-H. H. Tye, Phys. Lett. B **536**, 185 (2002).
[486] R. Jeannerot, J. Rocher, and M. Sakellariadou, Phys. Rev. D **68**, 103514 (2003).
[487] T. Damour and A. Vilenkin, Phys. Rev. Lett. **85**, 3761 (2000).

[488] T. Damour and A. Vilenkin, Phys. Rev. D **64**, 064008 (2001).
[489] T. Damour and A. Vilenkin, Phys. Rev. D **71**, 063510 (2005).
[490] A. Vilenkin and E. Shellard, *Cosmic Strings and Other Topological Defects* (Cambridge University Press, Cambridge, UK, 2000).
[491] Y. Matsui, K. Horiguchi, D. Nitta, and S. Kuroyanagi, J. Cosmol. Astropart. Phys. **1611**, 005 (2016).
[492] Y. Matsui and S. Kuroyanagi, Phys. Rev. D **100**, 123515 (2019).
[493] B. P. Abbott et al. [LIGO Scientific Collaboration], Phys. Rev. D **80**, 062002 (2009).
[494] J. Aasi et al. [LIGO Scientific and Virgo Collaborations], Phys. Rev. Lett. **112**, 131101 (2014).
[495] B. P. Abbott et al. [LIGO Scientific and Virgo Collaborations], Phys. Rev. D **97**, 102002 (2018).
[496] J. D. Bekenstein, Lett. Nuovo Cimento **11**, 467 (1974).
[497] V. F. Mukhanov, JETP Lett. **44**, 63 (1986) [Pisma Zh. Eksp. Teor. Fiz. **44**, 63 (1986)].
[498] C. Barceló, R. Carballo-Rubio, and L. J. Garay, J. High Energy Phys. **1705**, 054 (2017).
[499] H. Nakano, N. Sago, H. Tagoshi, and T. Tanaka, Prog. Theor. Exp. Phys. **2017**, 071E01 (2017).
[500] J. Abedi, H. Dykaar, and N. Afshordi, Phys. Rev. D **96**, 082004 (2017).
[501] N. Uchikata, H. Nakano, T. Narikawa, N. Sago, H. Tagoshi, and T. Tanaka, Phys. Rev. D **100**, 062006 (2019).